# Pennsylvanian-Permian Chronostratigraphy of the Eastern Midland Basin: Implications for basin filling evolution and paleogeography

by

Jill Nicole Garcia, B.S.

A Thesis

In

Geosciences

Submitted to the Graduate Faculty
of Texas Tech University in
Partial Fulfillment of
the Requirements for
the Degree of

MASTER OF SCIENCES

Dustin Sweet, Ph.D.
Chairperson of the Committee

Jim Barrick, Ph.D.

George Asquith, Ph.D.

Mark Sheridan
Dean of the Graduate School

May, 2017

# ACKNOWLEDGEMENTS

I would like to thank Dustin Sweet for his guidance, time, and assistance while I've attended Texas Tech. I would also like to thank my committee members, Jim Barrick and George Asquith, for their feedback and support throughout my research. The time that all three of these individuals spent on facilitating my growth as a writer, researcher, and geologist has been greatly appreciated and will not be forgotten.

Additionally, I would like to thank the undergraduate Geosciences students under Dustin Sweet, who paved the way for this report to be possible. Their tireless efforts on cataloging the biostratigraphic reports are appreciated and this thesis would not have been possible without them. I would also like to thank all those that provided feedback on my research through the West Texas Geological Society, and the Abilene Geological Society. Their comments and suggestions assisted in the molding of my thesis and research.

Special thanks should be extended to the Texas Tech Department of Geosciences, for allowing me the opportunity to complete this research with their financial assistance and use of facilities.

Lastly, this project would not have been possible without the enormous support I have received from my parents, my brother, and special friends I've made during my time at Texas Tech. Their emotional and technical support have been astounding, and I have the upmost appreciation for their assistance and patience throughout this endeavor.

# TABLE OF CONTENTS

# ABSTRACT

The Midland Basin of the Permian Basin Province in West Texas has proven to be a lucrative source of petroleum and natural gas since the 1970's. Unfortunately, large-scale sub-surface maps of the region, especially for the eastern shelf of the basin, are not readily available. Fusulinid biostratigraphy has provided an opportunity to construct chronostratigraphic surfaces of several Pennsylvanian-aged and Permian-aged units in the Midland Basin, including the Atoka, Strawn, Canyon, Cisco, Wolfcamp, and Leonard.

A collection of fusulinid occurrence reports compiled by R.V. Hollingsworth catalog fusulinid last appearance datums of genera characteristic of the units above and represent the main data in the Permian Basin Archival of Biostratigraphic Tops (PABZT) project. These datums were used to create paleogeographic maps of the Midland Basin from the Late Pennsylvanian through early Permian. The shelf edge of the eastern Midland Basin is delineated using these maps, through geometric reconstruction of the eastern shelf. Along each cross section a topographic profile was created, which revealed the quantitative position of the shelf edge during each time interval.

The shelf edge position produced through the PABZT data is then compared against maps depicting coeval time frames that were mined from existing Permian Basin literature. The distances were divided against one another, and produced a ratio that determined the accuracy of the constructed shelf edges versus the literature's shelf edges. For example, an accuracy ratio of 1.0 indicates exact shelf positions locations, less or greater than that indicated how much distance existed between the positions. Comparison of accuracy ratios showed a high degree of similarity between the Canyon and Cisco paleogeographic maps and the BEG's picks. Variance from north-to-south along the eastern shelf may be the result of the loss of chronostratigraphic significance when lithologically correlating thicker packages of strata in the south to thinner strata units in the north.

Analysis of the chronostratigraphic surfaces also revealed the progradational and aggradational trends along the eastern shelf. The northern and southern regions displayed dissimilar histories of shelf movement. The maximum amount of progradation observed

between the two regions was an event that began during the Virgilian through the Wolfcampian and exhibited 80 kilometers of landward shelf movement. One aggradation pattern that was correlated between both areas was the Atokan to Missourian/Virgilian event. This event has been correlated to both the northern and southern regions, and indicates a regional transgression event.

The eastern shelf experienced local progradational and aggradational events of similar magnitudes, and two major events were recorded in northern and southern locations. Most likely the significant progradational episodes during the Virgilian to Wolfcampian were the result of sediment supply increasing from the Llano Uplift, and waning tectonic activity. This resulted in the reduction of available accommodation space, especially along the eastern shelf. The aggradational events seen during the Atokan to Missourian/Virgilian are likely driven by a higher rate of basin subsidence in the Pennsylvanian. These results suggest greatly reduced subsidence near the Pennsylvanian-Permian boundary, a relationship observed elsewhere in late Paleozoic basins across western equatorial Pangaea.

# LIST OF TABLES

# LIST OF FIGURES

# CHAPTER I
# INTRODUCTION

## PURPOSE OF STUDY

The Midland Basin is an intracratonic, deep-water basin, located in North West Texas in the Permian "Basin" Province. Basins in this broad region are filled with Early Pennsylvanian to late Permian sediments (Handford, 1981). The Midland Basin is the easternmost basin in the region and is rimmed by shelfal carbonate platforms (Handford, 1981; Blakey, 2011). Structurally higher regions that surround the Midland Basin include the Central Basin Platform to the West, the Northern Shelf and the Eastern Shelf (Fig. 1.1) (Midland Subsurface Library, 2017).

The Pennsylvanian Horseshoe Atoll, a notable topographic feature in the northern part of the Midland Basin, is composed primarily of reefal buildups, with Strawn, Canyon, and Cisco shallow-water carbonate strata overlain by Wolfcampian and Leonardian-aged sandstone and shale (Galley, 1958; Vest, 1970). Water depths projected for the Midland Basin during the late Paleozoic ranged from 500 to 2,000 feet deep, and the margins of the platforms vary from mildly sloping shelves to steeper ramp structures (Hamlin and Baumgardner, 2012).

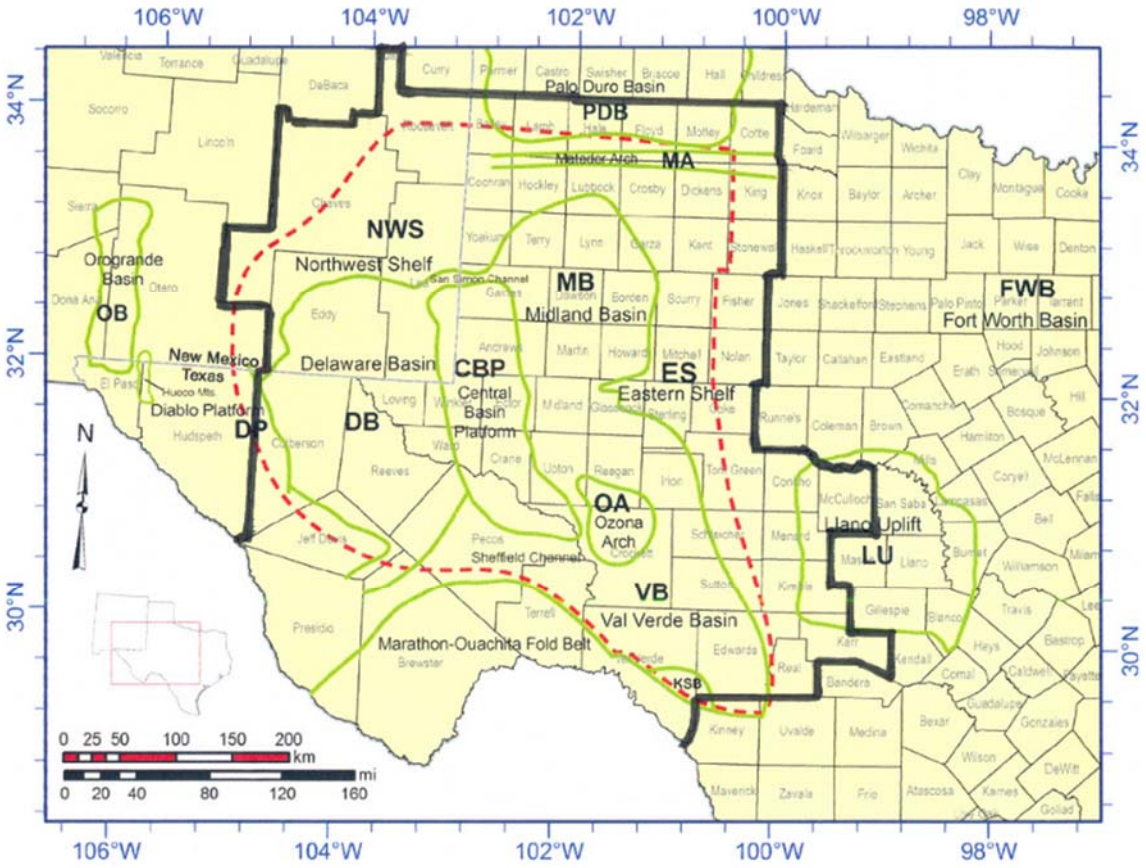


Figure 1.1. The geographic location of the Midland Basin with the Pennsylvanian Period geology in Southwestern Laurentia overlaid in green (Midland Subsurface Library, 2017). The red dotted line indicates the Permian Basin, and the green lines indicate the subsequent sub-basins.

The Midland Basin is a prolific hydrocarbon producing region. Oil production from the basin has been ongoing since the 1940's, and to date has produced over 1.5 billion barrels of oil (Hamlin and Baumgardner, 2012). Research into the depositional history as well as petroleum potential of the basin is still ongoing, but one area that appears to be lacking is regional subsurface maps. The goal of this project is to create chronostratigraphic maps derived from biostratigraphic data found in cores and well cuttings. I hypothesize that the biostratigraphic data can be used to produce subsurface chronostratigraphic maps that will mimic previously published synopses. If the subsurface maps produced in this study do align with prior studies, then these regional subsurface maps can illuminate the basin history of less studied regions of

the Midland and Palo Duro Basins. Conversely, if the hypothesis fails and the maps do not mimic prior synopsis, then assessing the root of the disagreement may lead to new basin history or paleogeographic interpretations for parts of the study area. In summary, the data produced here will 1) confirm previous localized studies and thus provide a "one-stop" regional overlook of the region, 2) disagree with previous portrayals and thus either provide new interpretations to basin history, or require some reassessment if the biostratigraphic data is locally erroneous. Assuming this hypothesis holds, then mapping the shelf edge by noting the point of maximum flexure in the distal shelf region allows a time-step reconstruction of the shelf edge trajectory. With this trajectory, progradational and aggradational trends for the specific chronostratigraphic surfaces are mapped. Thus, the basin-filling history is reconstructed.

Chronostratigraphic surfaces also bear on the structural evolution. The southern Midland Basin has been proposed as a flexural basin due to crustal thickening from the south (e.g., Ward et al., 1986) or a mixture of high angle reverse faults with a significant component of wrenching (e.g., Algeo, 1992). The temporal migration (or lack of it) of the depocenters should bear on the creation of accommodation space, and thus provide insights into these two models.

## GEOLOGICAL BACKGROUND

### *Paleogeographic and Tectonic Setting*

Subsidence of the Midland Basin began in the Early Pennsylvanian from the collision between Laurentia and Gondwanaland that also produced uplifted and depressed structural features in the Southwestern United States, including the Tobosa, Delaware, Anadarko, Orogande, and Midland Basins (Fig.1.1; Midland Subsurface Library, 2017).

The Tobosa Basin was segmented during late Paleozoic deformation, which fragmented the basin into smaller sections (Kluth, 1986). The faults that are found on the edges of the Midland Basin were most likely structural weaknesses that existed before the collision, but were then reactivated after the two continents came into contact (Kluth, 1986). Tectonism caused the uplift between the Midland Basin and the Delaware Basin, resulting in the Central Basin Platform (Kluth, 1986).

The Midland and Delaware Basins are bounded by strike-slip and dip-slip faults (Kluth, 1986; Algeo, 1992). The Midland Basin is bounded on the southwestern margin by strike slip faults (Algeo, 1992). Intracratonic deformation that occurred during the late Paleozoic also produced the Ancestral Rocky Mountains in the craton interior (Kluth and Coney, 1981; Kluth, 1986). Structural studies on the western margin of the Midland Basin reveal NW to SE trending echelon fold sets (Tai and Dorobek, 2000). The anticlinal patterns seen indicate that formation occurred under a convergent strike-slip setting (Tai and Dorobek, 2000).

The following sections will detail the lithological trends observed during each of the chronostratigraphic time intervals, as well as regional facies. The stratigraphic groups are discussed in regions; however, only those regions for which previous work exists are discussed.

## STRATIGRAPHIC CHARACTER AND LITHOLOGY

### *Atokan*

The majority of sediments were accumulated in the Midland and surrounding basins from Late Mississippian to early Permian, when rapid subsidence resulted in the deposition of 500 meters of strata (Algeo, 1992; Saller, 1994). Within the Midland Basin, Atokan-aged sediments are referred to as the Atokan Group (Wright, 2008a). The Atoka group is underlain by Morrowan-aged sediments, and overlain by Desmoinesian-aged strata known as the Strawn Group (Fig. 1.2; Dutton et. al, 2005).

#### *Northern Region Lithology*

Basinal carbonate, slope carbonate, and dark shale strata similar to those found in the Delaware Basin's Smithwick Formation are found on the northern region of the Midland Basin, in Martin, Dawson, and Lynn counties (Wright, 2008a).

*Southern Region Lithology*

Near the Southern boundary of the Midland Basin in Upton County, Atokan sediments are described as mud-matrix conglomerate (Troschinetz and Loucks, 1991; Wright, 2008a). Atokan composition changes from the northern to the southern basinal region from coarse-grained siliciclastic strata to silty, sheet-like shale intervals (Wright, 2008a). The proposed depositional setting for the shale is either basinal margin wedges or submarine fans that deposited the sediments in a sheet-like pattern (Wright, 2008a). Overall thickness patterns of Atokan-aged sediments are fairly consistent within the Midland Basin, thickening only slightly when coming closer to the Central Basin Platform near the western margin. The bulk of siliciclastic sedimentation during the Atokan was sourced from the Ozona Arch, which was funneled to the basin floor likely through turbidity currents (Wright, 2008a).


Figure 1.2. A general stratigraphic column documenting the litho-stratigraphy of the Midland Basin during the Pennsylvanian and Permian (Dutton et. al, 2005). This chart does not reference that some Wolfcampian strata are Leonardian in age, and some Canyon strata fall into the Cisco Series.

*Central Basin Platform Lithology*

Along the Central Basin Platform boundary of the Midland Basin, silty bioclastic carbonate strata and dark shale beds are observed in Andrews and Midland County (Wright, 2008a). The fauna observed in bioclastic carbonate beds near the Central Basin Platform includes crinoids and sponge spicules (Wright, 2008a). These units are ~15 to 20 feet thick, and are interpreted to have been deposited as distal basin floor fans (Candelaria 1990; Wright, 2008a). Basinal shale intervals are observed near the southwestern border of the Central Basin Platform (Wright, 2008a). Small variations in thickness in the Midland Basin have suggested that localized uplift may have influenced deposition during Atokan times (Yang and Dorobek, 1995; Wright, 2008a).

*Fusulinid Biostratigraphy*

Fusulinid biostratigraphy has proved useful in the Permian Basin for characterizing boundaries within litho-stratigraphy, and the Midland Basin facies are no exception. The designated top of the Atokan Series is the genera *Fusulinella*. The primary genus observed in Permian facies before Atokan and Missourian times is *Millerella* and *Eostafella*, primitive forms in the span of fusulinid morphology (Thompson, 1950). *Eoschubertella,* and *Profusulinella,* are common during the lower Atokan (Fig. 1.3) (Wahlman, 2013). *Profusulinella* is also observed as a middle Atokan occurrence, with six different species identified in Permian facies (Fig. 1.3) (Wilde, 2004). *Fusulinella* comprises the middle and upper zones of the Atokan assemblage, with six different species observed (Wilde, 2004).

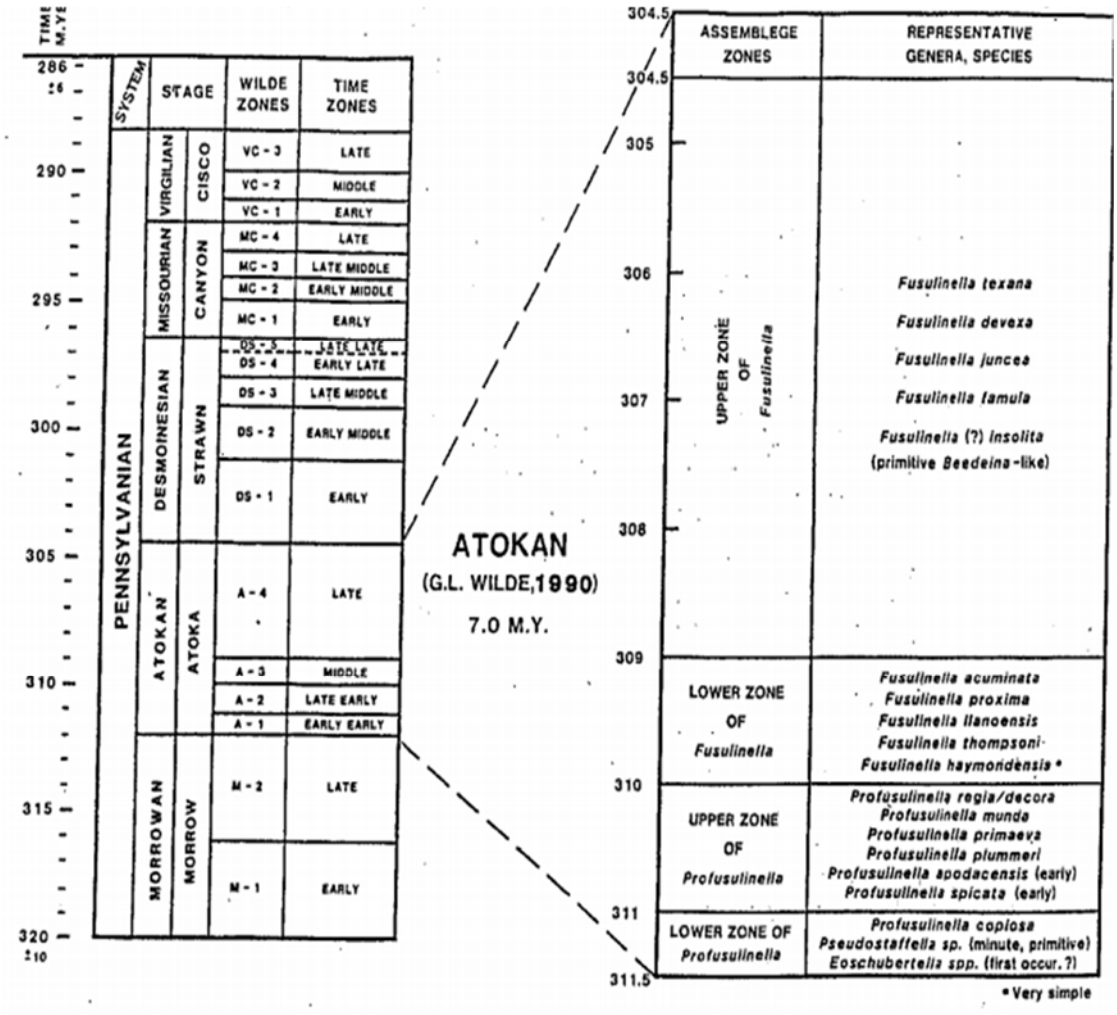


Figure 1.3. Shows the distribution of fusulinids in the Midland Basin during the Atokan as determined by Wilde (2004). This shows the presence of *Profusulinella*, *Fusulinella*, and *Eoschubertella* as present in Atokan sediments. The age of the top of the Atokan series is approximately 304.5 mya (Wilde, 2004).

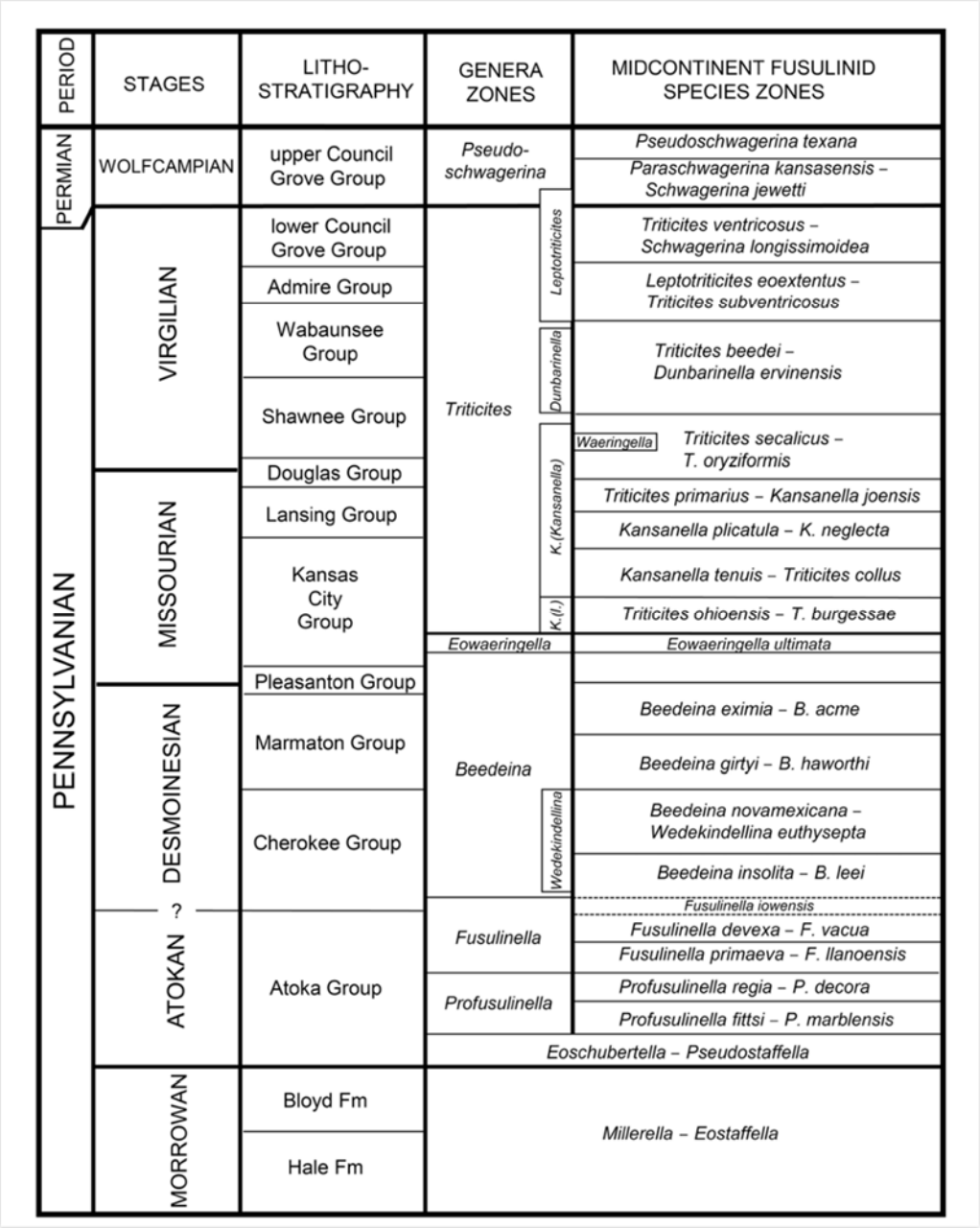


Figure 1.4. A biostratigraphic section of fusulinids found in the Southwestern United States and in Midcontinent America as determined by Wahlman; distinct species are also included (Wahlman, 2013).

*Strawn Group*

Desmoinesian-aged deposits in the Midland Basin are referred to as the Strawn Group, or Strawn Formation (Boring, 1993; Wright, 2008b). The relative thickness of the formation in the Midland Basin is approximately 225 to 275 feet thick (Boring, 1990;

Wright, 2008b). Studies conducted by Yang and Dorobek (1995) observed the thickness of the Strawn to be relatively uniform across the Midland Basin. The Strawn Group has been discussed previously in literature as the Upper Strawn Formation and the Lower Strawn Formation; this report discusses the formations as one collective group (Hillier, 2015). The Strawn Group comprises a major portion of the Pennsylvanian reef complex seen in the Midland Basin (Wright, 2008b). Overall, sedimentation trends during the Desmoinesian include extensive carbonate deposition throughout the entire Midland Basin, and siliciclastic deposition reserved to the eastern shelf and some basinal localities (Boring, 1990; Wright, 2008b).

*Southern Region Lithology*

In Andrews County, near the southern boundary, phylloid-rich algal packstone intervals are observed, overlain by wackestone and grainstone intervals (Wright, 2008b). The carbonate facies by the southern boundary include algal biowackestone, crinoidal wackestone, algal bioclastic grainstone, and crinoidal bryozoan wackestone. Algal foraminiferans and crinoidal beds are also present (Mazzullo and Reid, 1989; Boring, 1993). These carbonate facies are normally found along a platform environment, such as middle and outer platforms, algal mounds, and platform margins (Boring, 1990).

Sedimentological studies have been conducted in the southern portion of the Midland Basin, in Andrews and Midland counties. Four distinct sediment packages compose the Strawn Group. They include a bottom package of spiculitic mudstone, a lower middle package of calcareous algae and bioclastic grainstone package, a phylloid-rich boundstone package 50 m thick, and an upper package of basal spiculitic mudstone, overlain with ooid peloid grainstone, 10-15 m thick (Wright, 2008b). Depositional settings for the lower packages of facies described above are inferred as deep water (i.e. 30 to 100 meters). A sequence boundary separates the Strawn and Canyon groups in the Midland Basin (Wright, 2008b; Wahlman, 1998).

Near the southern Midland Basin, siliciclastic facies including cross-bedded sandstone, intercalated sandstone and shale, and fine-grained mudstone/shale are

observed (Boring, 1993). During Desmoinesian times, sloughed off sediments from higher relief areas surrounding the Midland Basin generated lobate deltas and offshore bars (Boring 1993). Shales have been observed in the southern portion of the Midland Basin, including Reagan, Martin, Howard, and Mitchell counties (Wright, 2008b).

*Eastern Shelf Lithology*

Along the Eastern Shelf of the Midland Basin in Fisher, Nolan, and Coke counties, carbonate strata are observed and divided into three units (Hopkins and Ahr, 1985; Wright, 2008b). The lower unit is composed of cherty limestone and interpreted to have a consistent aerial distribution across the entire basin, whereas, the middle unit is a massive dark limestone with interfingering shale, and the upper unit is back reef facies and shelf facies (Hopkins and Ahr, 1985; Wright, 2008b). The siliciclastic strata observed on the margin of the eastern shelf are coarser-grained siliciclastics inferred as deltaic deposits (Wright, 2008b).

*Central Basin Platform Lithology*

Even distribution of carbonate strata is observed along the Central Basin Platform near the western edge of the Midland Basin (Wright, 2008b). Shelf reef and patch reef facies are observed near Gaines and Yoakum counties. Similar carbonate facies are also observed near Ozona Arch and the eastern Midland shelf (Wright, 2008b).

*Fusulinid Biostratigraphy*

The designated top of the Strawn Series is *Fusulina*, also known later as *Beedeina*. During the early to middle Desmoinesian, *Wedekindellina euthysepta* provides the boundary between Strawn and Atokan groups in the Midland Basin (Fig. 1.5) (Wilde, 2004). The second genera found in Strawn-aged deposits is *Beedeina*, with seven different species observed. *Fusulina* marks the upper boundary between the Strawn and Canyon series, with five species observed (Fig. 1.5) (Wilde, 2004).

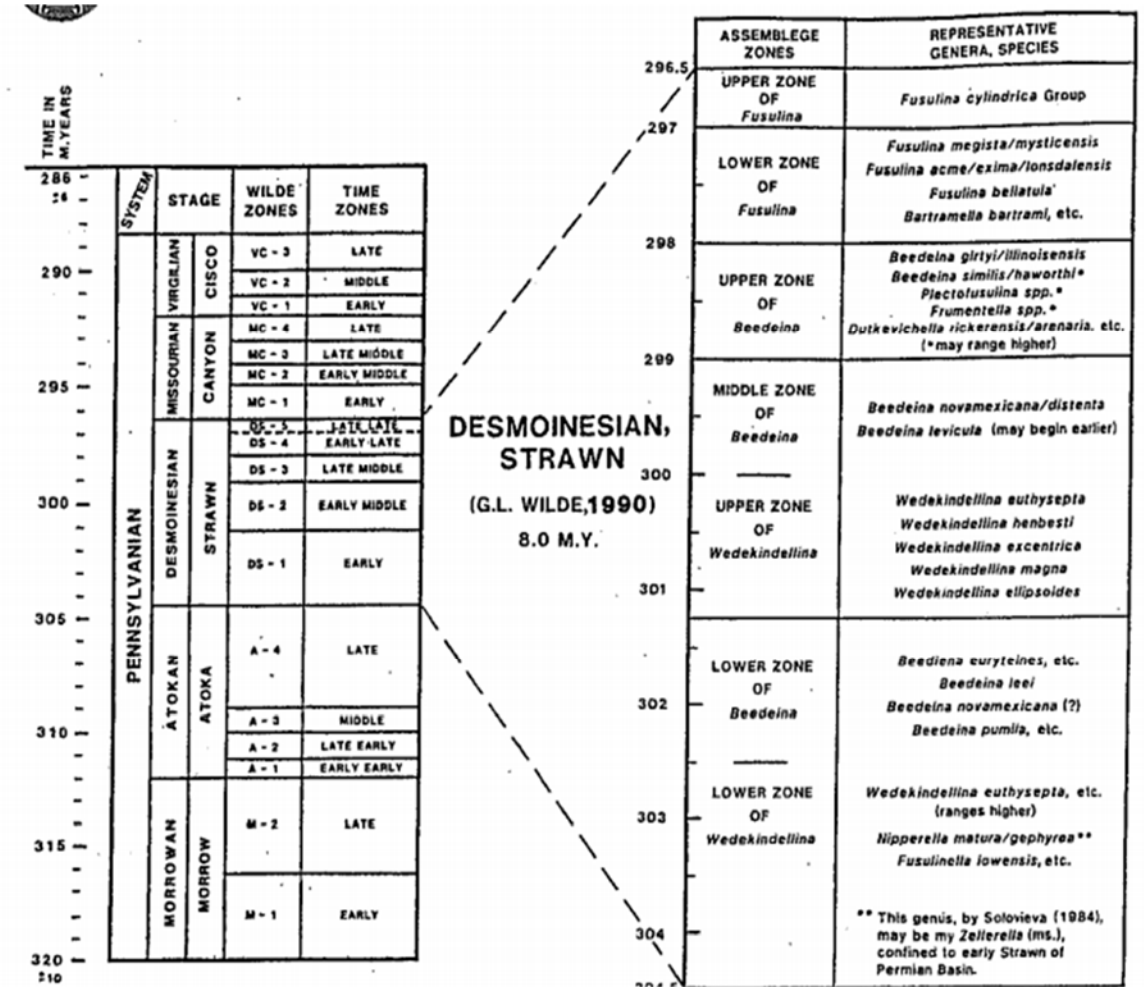


Figure 1.5. Shows the distribution of fusulinids in the Midland Basin during the Desmoinesian. *Beedeina*, *Wedekindellina*, and *Fusulina* are all noted as present in Strawn-aged deposits.

*Canyon Group*

Virgilian-aged sediments found in the Midland Basin are known as the Canyon Group, or sometimes the Canyon Formation (Fig. 1.2; Wright, 2008c; Hentz, 2016). The Canyon Group extends from the base of Palo Pinto Limestone to the top of the Home Creek Limestone (Hentz, 2016). Overall, trends show that many siliciclastic deposits that reached the Midland Basin were basin-floor fan sediments (Wright, 2008c). Thick shale

deposits are also observed across the whole of the Midland Basin during the Missourian and Virgilian (Wright, 2008c).

*Southern Region Lithology*

Along the southern boundary of the Midland Basin in Coke County, carbonate platform successions are approximately 1,530 feet thick (Hentz, 2016). The carbonate deposits in the southern Midland Basin form an irregular platform that has localized pinnacles of algal buildup (Hentz, 2016). Canyon-aged strata in Andrews County are thick limestone sequences (Saller, 2014). The Canyon Group in the southern region is divided up into four facies zones; spiculitic mudstone and ooid grainstone, phylloid-algal wackestone, shale and fossiliferous wackestone, and bioclastic grainstone. (Saller et al., 1994; Wright, 2008c). The Palo Pinto Limestone, the Winchell Formation, the Ranger Formation, and the Home Creek Limestone comprise the carbonate formations found in the Midland Basin. These carbonate formations make up the bulk of the Canyon Group, and provide boundaries between the Strawn and Cisco groups (Wright, 2008c).

*Eastern Shelf Lithology*

Facies seen near the eastern shelf of the Midland Basin include dolomite, dolomitic limestone, and red/green/yellow shale. The latter is inferred as evidence of aerial exposure in the Pennsylvanian (Mazzullo and Reid, 1989; Wright, 2008b). Common trends of carbonate facies in the Midland Basin during the Missourian include limestone atoll bodies that grew along the margin of the basin (Brown and Cleaves, 1973). The center of the Midland Basin exhibits Missourian-aged black shale, which indicates sediment starving and/or anoxia during Missourian times (Mazzullo and Reid, 1989).

Other shelf facies include shallow-water limestone, dolomitic phylloid-algal reefstone and bioclastic grainstone. Porous dolomite is noted along the edge of the Canyon and Cisco platforms as well (Mazzullo and Reid, 1989, 1995; Wright, 2008b).

*Fusulinid Biostratigraphy*

Fusulinids that characterize Missourian-aged deposits within the Permian Basin region are an overlap of three different genera that also are found in the Missourian-aged Canyon deposits. The tentative designated top of the Canyon Series is *Kansanella*, or *Triticites*. *Eowaeringella* is found in lower Canyon deposits with only one species, *Eowaeringella ultimata* (Fig. 1.6). The middle and upper Missourian strata contain *Kansanella and Triticites*, with four and five species, respectively (Wilde, 2004). *Triticites* species are also seen in lower, middle, and upper regions of the Virgilian, while *Kansanella* makes an appearance in early Canyon deposits (Fig. 1.6) (Wilde, 2004).

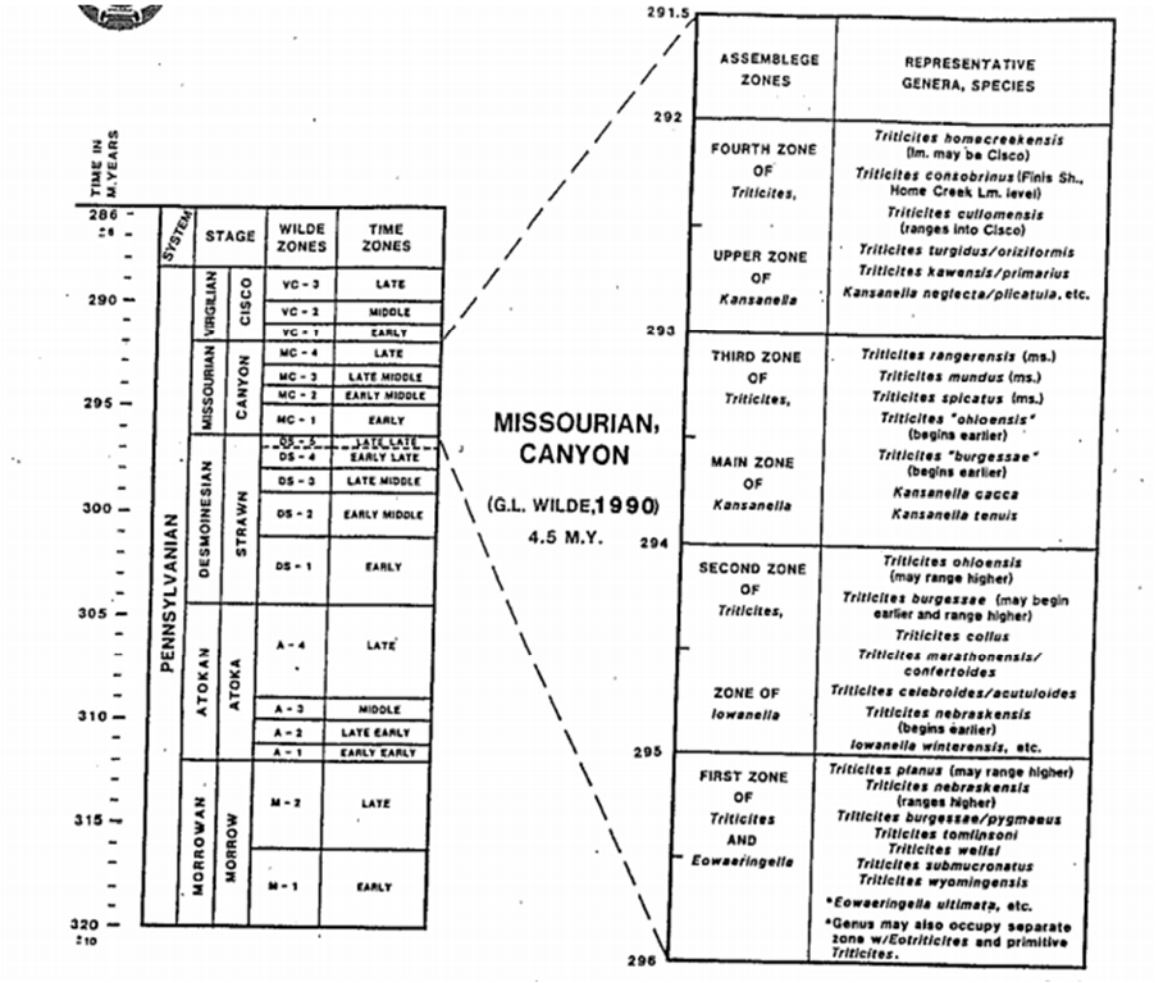


Figure 1.6. Shows the distribution of fusulinid species observed in the Midland Basin during the Missourian. *Eowaeringella*, *Iowanella*, *Kansanella* and *Triticites* are all observed as present in Canyon-aged strata.

*Cisco Group*

Virgilian-aged sediments were deposited atop the Canyon Group. These sediments are referred to as the Cisco Group. The Cisco section in the Midland Basin has 14 cyclical mudrock, sandstone, and carbonate deposits layered throughout (Hentz, 2016). The top of the formation is marked by the Home Creek Limestone, whereas the bottom boundary is the contact between the Coleman Junction Limestone (Hentz, 1995; Mazzullo and Reid, 1989). The time boundary between the Pennsylvanian and the Permian in the Midland Basin is located at the top of the Cline Shale Formation,

otherwise known as "Wolfcamp D" (Hentz, 2016). But, in shelfal localities, the boundary is placed at the top of the Crystal Falls Limestone (Hentz, 2016).

The following facies are identified near Scurry and Mitchell counties, the site of the SACROC project, where since 1972 carbon dioxide has been used as a tool to extract further petroleum from Pennsylvanian reef facies. Mounded crinoidal wackestone, interbedded, crinoidal packestone, grainstone and bioclastic packstone are observed in both counties. These were interpreted as turbidite flows (Schatzinger, 1987; Janson and Kerans, 2007). Large-scale debris beds are also observed covering the entire platform of Missourian-aged strata (Janson and Kerans, 2007).

*Eastern and Western Shelf Lithology*

Slope facies are commonly seen in the Cisco and lower Wolfcampian deposits, and are dominated by siliciclastic mudrock and debris-flow sandstone, that formed as the result of channel-levee complexes along the sides of the basin (Mazzullo and Reid, 1989; Hentz, 2016). Deposition of Cisco-aged carbonate exhibits roughly the same distribution as their Canyon counterparts, but a long term decrease in relative sea level likely modulated by glacial eustacy resulted in decreasing accommodation space, thus stacking patterns are thinner than in Canyon deposits (Wright, 2008c). Nine overall siliciclastic and carbonate sequences are noted in Virgilian-aged strata that barely reach the edges of the Midland Basin (Brown, 1982; Wright, 2008c). The eastern shelf has multiple siliciclastic and carbonate units interfingered together (Wright, 2008c). The carbonate units that compose the Cisco Group include Gonzales, North Leon, Bunger, Gunsight, Ivan, Blach Ranch, Breckenridge, Crystal Falls, and Flippen limestone intervals (Wright, 2008c; Cleaves, 2000).

*Fusulinid Biostratigraphy*

Three different genera of fusulinids are observed during the Virgilian, with some overlap between the Wolfcampian (Wilde, 2004; Wahlman, 2013). The designated top of the Cisco Series is *Dunbarinella*. The lower Cisco is characterized by the appearance

of *Waeringella* and a continuation of *Triticites*, with *Triticites beedei* and *Waeringella spiveyi* (Fig. 1.7). The middle and upper Cisco deposits contain two *Dunbarinella species* and four *Triticites* (Fig. 1.7) (Wilde, 2004).

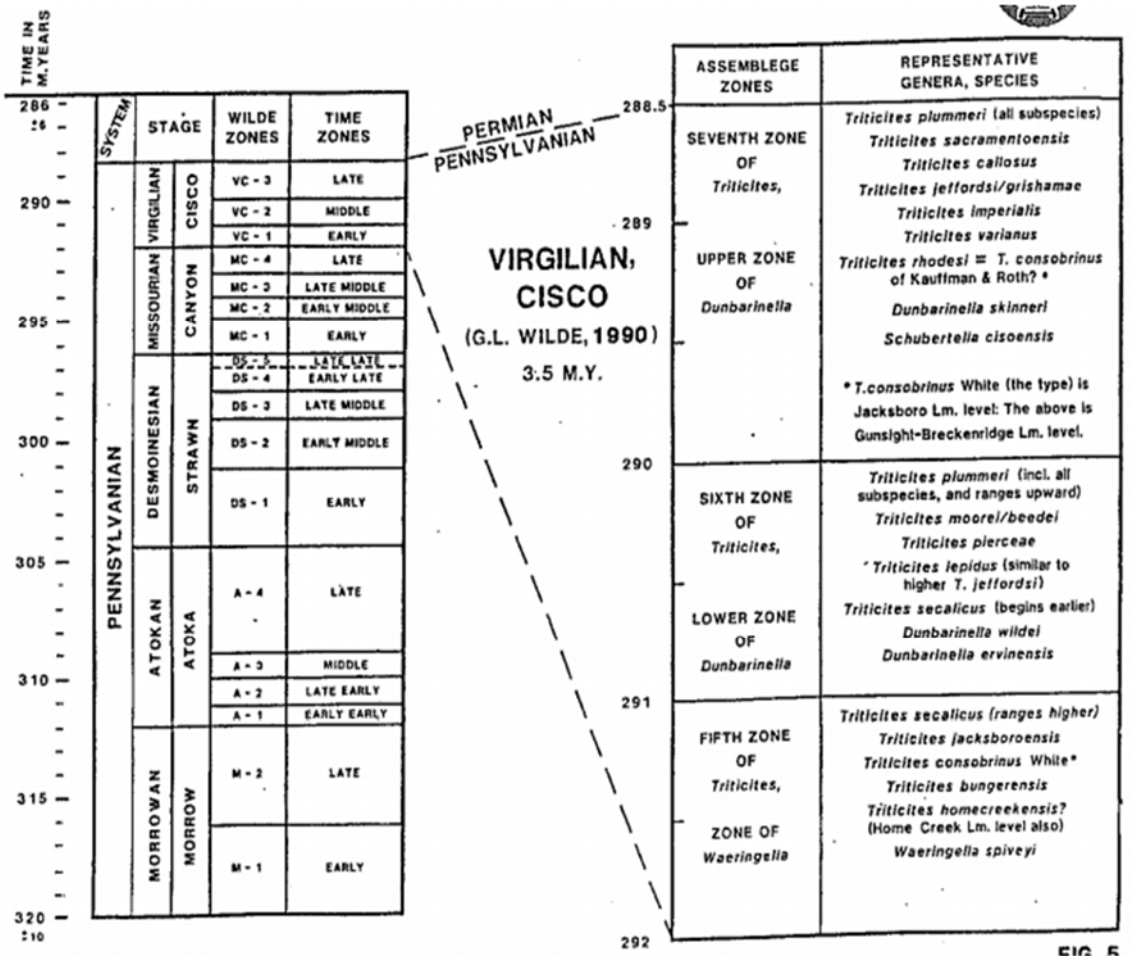


Figure 1.7. Shows the distribution of fusulinids in the Midland Basin during the Virgilian. *Waeringella*, *Dunbarinella*, and *Triticites* are genera of interest, and are marked as present among Cisco-aged strata.

*Wolfcamp Group*

*Southern Boundary*

The Wolfcamp Group within the Permian Basin can be divided into three distinct lithologic groups, separated through fusulinid biostratigraphy and unconformities noted in case studies (Fig. 2; Silver and Todd, 1969). The thickness of the Wolfcamp section around the shelf edges is between 700 and 850 feet thick. On the shelf edge, the thickness near slope systems reaches ~3,500 feet, but in the basin, the thickness decreases to less than 700 feet (Hentz, 2016). The lower facies unit of the Wolfcamp are skeletal rich wackestone and packstone (Baumgardner, 2014). Forams, algae, peloids, and fusulinids are common, while crinoids and brachiopods are less abundant (Ruppell,

2000). Depositional environment is inferred as low-energy, which resulted in strata with lower permeability than other Wolfcampian facies (Ruppel, 2000). The second facies in this region is skeletal grain dominated packestone with abundant ooids, crinoids, fusulinids, forams, and brachiopods (Ruppel, 2000). This facies is well sorted, suggesting a higher energy environment. Other facies include nodular skeletal wackestone and packstone, which are the most abundant of the Wolfcampian facies (Ruppel, 2000). Nodular wackestone and fusulinid packstone are commonly seen at the base of cycles in the Wolfcampian section. The shale interval noted in the Wolfcampian are black and unfossiliferous, and are found above and below the main Wolcampian reservoir section in Andrews County (Ruppel, 2000).

*Western Shelf Margin*

Wolfcampian facies observed on the Western Shelf were strongly influenced by the presence of the Central Basin Platform. Bioclastic grainstone, packstone and wackestone are all observed on the western margin, in Andrews County (Fu, 2011). Fusulinid packstone beds also occur along the edge of the Central Basin Platform. Interpretations along this shelf edge suggest some materials sloughed off the eastern edge of the Central Basin Platform. Towards the center of the basin, east of Ector County, debris flows and black organic shale were sampled for provenance studies (Fu, 2011). Ector County also exhibits shelf-margin shoals, deposited during the early Permian (Fu, 2011). Algal-mound buildups were also recorded in Ector County (Fu, 2011).

*Fusulinid Biostratigraphy*

Early Permian fusulinids are characterized by two major genera, *Pseudoschwagerina* and *Triticites* (Fig. 1.8). The designated top of the Wolfcamp Series is *Monodiexodina*. This group formed the boundary between the Wolfcamp and Cisco groups in the Permian Basin region (Wilde, 2004). *Monodiexodina* and *Schwagerina* genera *are* viewed in the upper assemblage zones seen during the Wolfcampian before major extinction events occurred (Fig. 1.8) (Wilde, 2004).

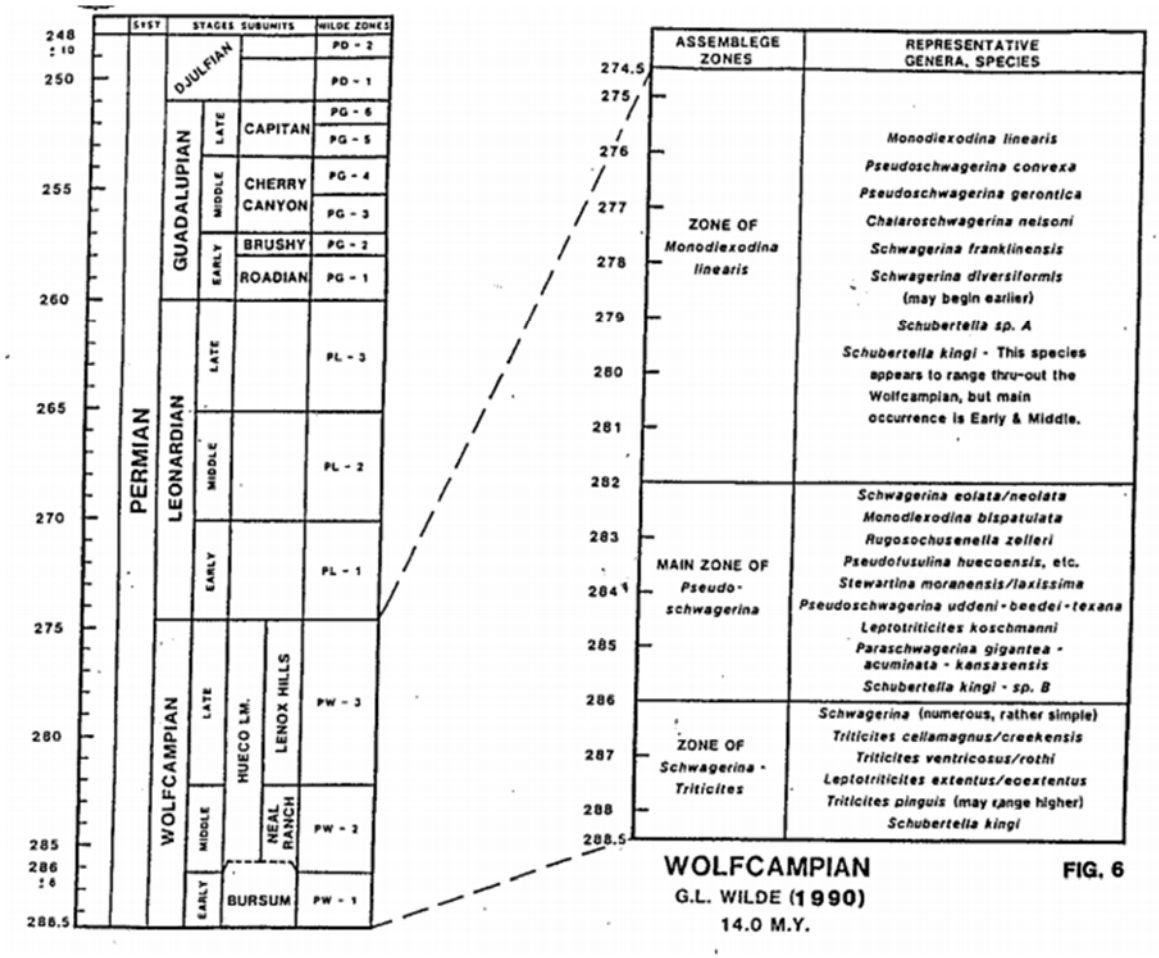


Figure 1.8. shows the distribution of fusulinid species in the Midland Basin during the Wolfcampian/Early Permian. *Schwagerina*, *Triticites*, *Pseudoschwagerina*, and *Monodiexodina* were significant genera observed as present in Wolfcampian-aged strata.

*Leonardian Group*

Wolfcampian and Leonardian strata are occasionally grouped together for petroleum reservoir studies, and are termed the Wolfberry trend (Flamm, 2008). The boundary between Leonardian and Wolfcampian strata within the Midland Basin has been a debatable subject for some years (Flamm, 2008), but fusulinid zonations place the boundary below the Dean Sandstone, which is also referred to as the "Wolfcamp shale marker" (Flamm, 2008). Strata deposited during the Leonardian include some mistakenly assigned to Wolfcampian-aged strata, the Dean Sandstone, the upper and lower Spraberry

Formation, and the Clear Fork Shale. Most facies seen in the Leonardian are shallow-water carbonate and deep-water basinal facies (Ruppel et al., 2004). Platforms formed during this time are up to 2,500 feet thick, and shallow-water peritidal and subtidal facies are seen by these platforms, whereas sandstone turbidities and carbonate debris flows are seen in deeper water deposits (Ruppel et al., 2004). The whole Leonardian stratigraphic section has an average thickness between 2,500 to 3,000 feet (Dutton et al., 2005).

Along the Western and eastern shelf, shallow water carbonate deposits are observed, as well as tidal flat deposits (Dutton et al., 2005). In Andrews County, the Lower Clear Fork Shale is composed of grain-rich packestone, as well as fusulinid-bearing wackestone and packestone (Dutton et al., 2005).

*Spraberry Formation and Dean Sandstone*

The Spraberry Formation is a part of the larger group of Leonardian-aged strata within the Midland Basin. The general composition of the group is siltstone, black organic shale, and argillaceous limestone (Marshall, 1952). The overall thickness of the Spraberry Formation across the Midland Basin is approximately 950 feet thick (Marshall, 1952). The upper 250 feet of the member contains coarse siltstone, while the middle 250 feet of section contains organic brown and black shale. The bottom 400-450 feet of the group contains siltstone and argillaceous mudstone, and these lithologies have been observed on both eastern and western margins of the basin (Marshall, 1952).

*Clear Fork Group*

During the Leonardian, deposition consisted predominately of siliciclastic sediments. A detailed case study of the Clear Fork Group (Landreth, 1977) was conducted in Mitchell County, in the southern region of the Midland Basin. Shelf-margin facies in Andrews County exhibit brown to grey fossiliferous dolostone with some interbedded anhydrite and shale (Landreth, 1977). The depositional environment of carbonate beds in the Clear Fork Group is inferred as supratidal, intertidal, and subtidal (Landreth, 1977). The thicknesses of the Clear Fork is approximately 100 feet

thick (Landreth, 1977). Facies observed along the shelf and platforms of the Midland Basin include fusulinid and oolitic grainstone. The presumed depositional environment for these facies was an outer shelf system due to allochem richness and distribution (Landreth, 1977). The basinal facies are mostly shaly limestone and black shale, but thickness of these strata is not known at this time (Landreth, 1977).

*Fusulinid Biostratigraphy*

The major fusulinid genera that are diagnostic of the Leonardian in the Midland Basin are *Schwagerina* and *Parafusulina* (Fig. 1.9) (Wilde, 2004). The designated top of the Leonardian Series is *Parafusulina*. During this period, fusulinids were growing rapidly in size, from the width of pinheads to the size of rice grains (Thompson, 1950).

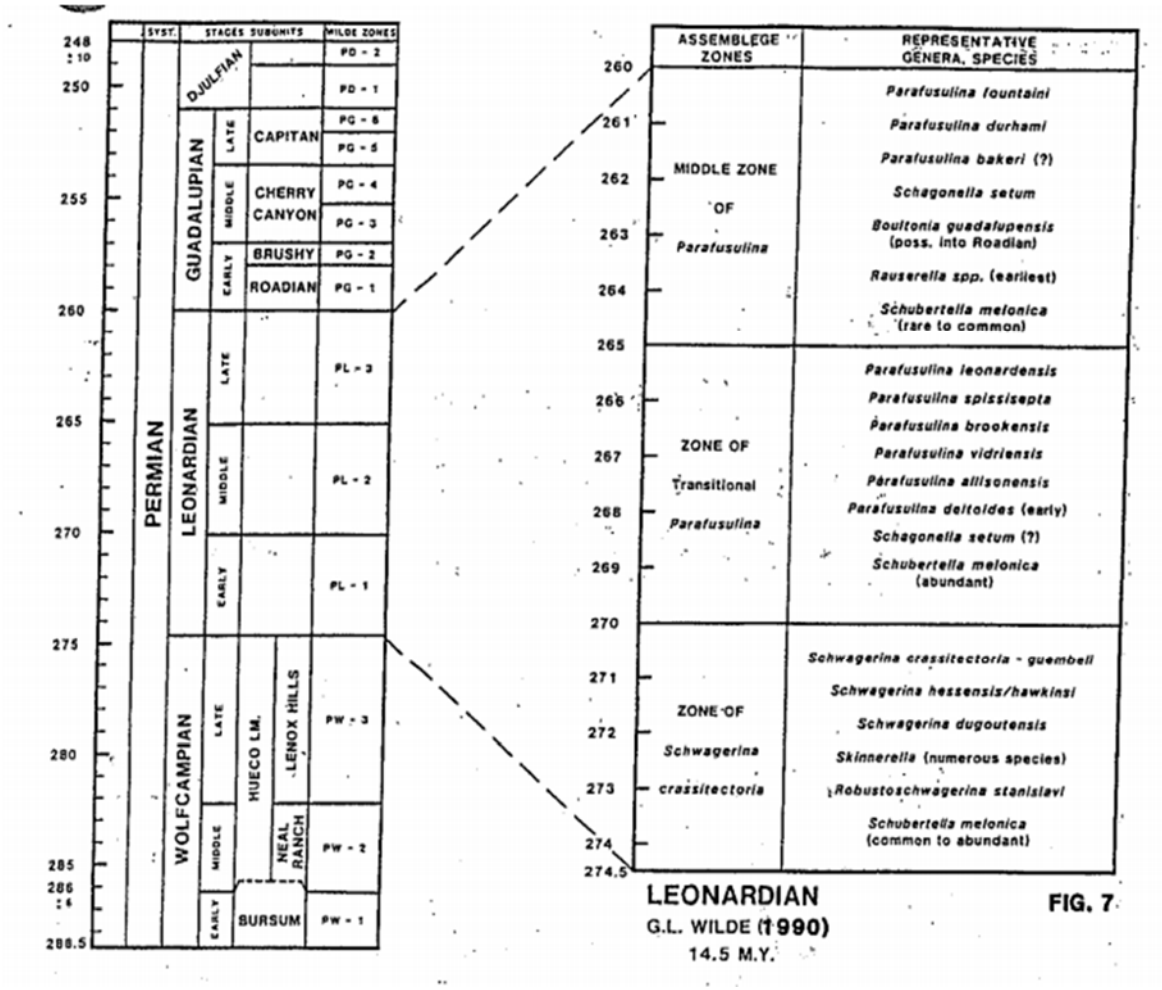


Figure 1.9. The distribution of fusulinid species in the Midland Basin during the Leonardian/Middle Permian. *Schwagerina*, and *Parafusulina* were significant genera observed as present in Leonardian-aged strata.

# CHAPTER II
# METHODOLOGY

## DATA COLLECTION

This thesis report has been a part of a larger undertaking at Texas Tech University, named the PABZT Project. The Permian Basin Archival of Biostratigraphic Zone Tops project seeks to investigate the structural evolution of the Permian Basin. Through utilization of fusulinid biostratigraphy, different chronostratigraphic surfaces in the Permian Province will be mapped with fusulinid LADs, or Last Appearance Datums, allowing the top of the formations to be tracked across a large region (Fig. 2.1). The justification of using LAD's as opposed to FAD's (first appearance datums) of the fusulinids was due to the 10 foot cutting intervals utilized during collection. Utilizing FAD's would be more precise in isolating the top of the formation series, which is what were being mapped during this report (Fig. 10). A large collection of biostratigraphic reports was donated to the university, which contained fusulinid depth information from more than 7,000 well sites in Texas and New Mexico (Fig. 2.2). This set of maps represents Phase One of the project, which includes all counties in the Texas Panhandle. The goal is to archive the fusulinid depth information from cuttings and cores, and after which compare the chronostratigraphic maps with existing literature on shelf progradation by the Bureau of Economic Geology.

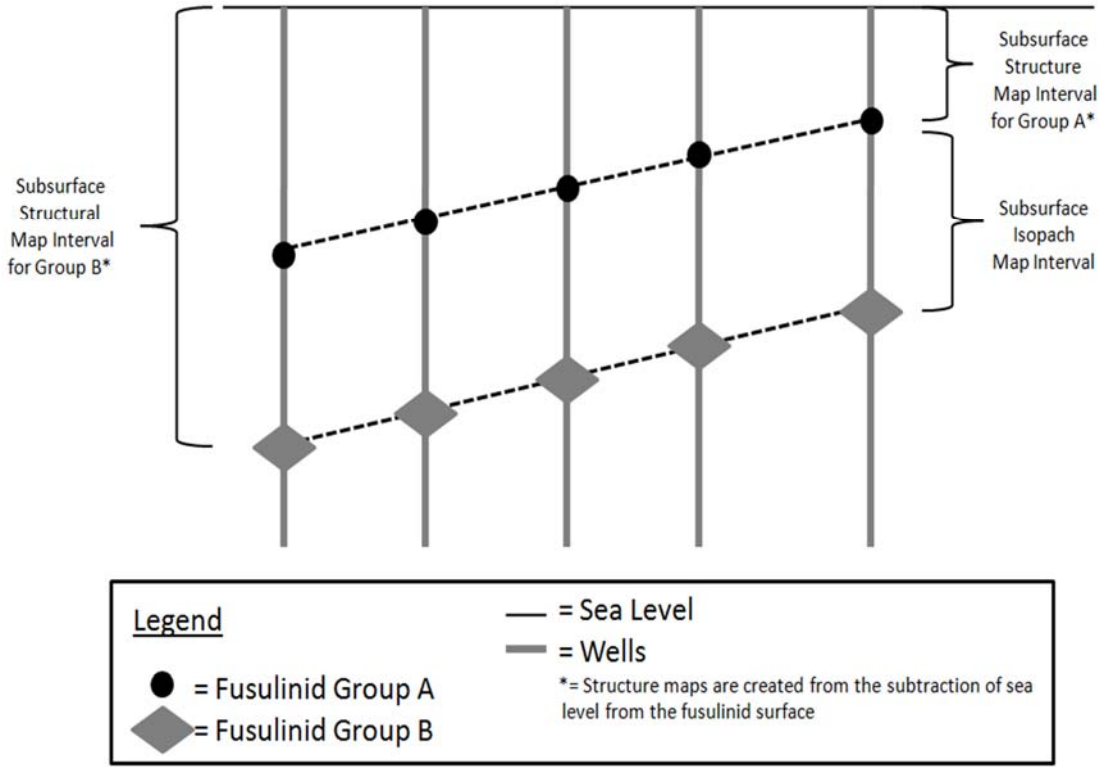


Figure 2.1. A figure explaining the use of fusulinid LAD's, and their presences in creating the subsurface structural maps, as well as the isopach intervals. The grey vertical lines represent well locations where fusulinids were extracted from, and the dotted lines represent the boundaries creating the different intervals determined from fusulinid presences.

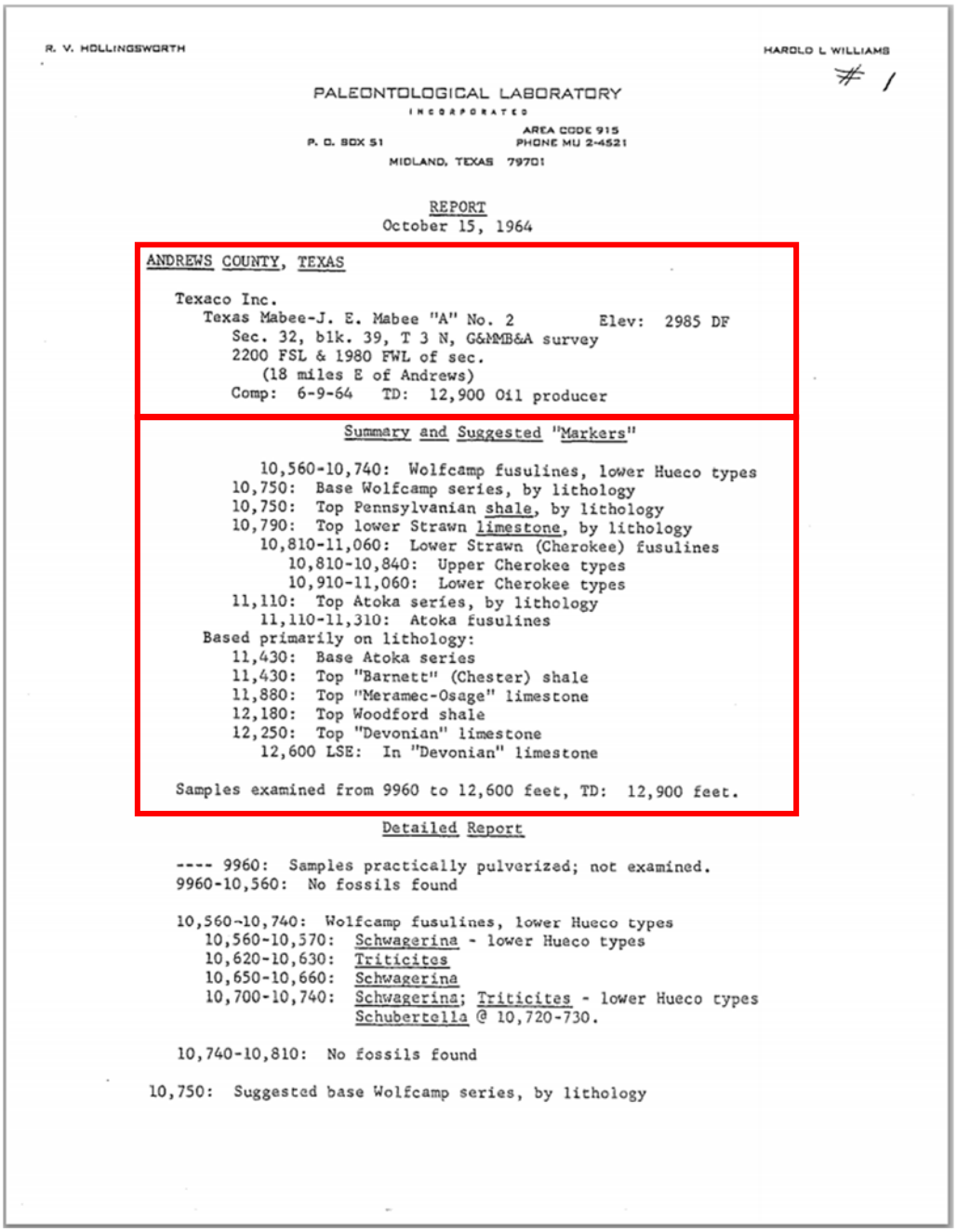

R. V. HOLLINGSWORTH

HAROLD L WILLIAMS

≠ 1

PALEONTOLOGICAL LABORATORY
INCORPORATED

P. O. BOX 51
AREA CODE 915
PHONE MU 2-4521
MIDLAND, TEXAS 79701

REPORT
October 15, 1964

ANDREWS COUNTY, TEXAS

Texaco Inc.
Texas Mabee-J. E. Mabee "A" No. 2 Elev: 2985 DF
Sec. 32, blk. 39, T 3 N, G&MMB&A survey
2200 FSL & 1980 FWL of sec.
(18 miles E of Andrews)
Comp: 6-9-64 TD: 12,900 Oil producer

Summary and Suggested "Markers"

10,560-10,740: Wolfcamp fusulines, lower Hueco types
10,750: Base Wolfcamp series, by lithology
10,750: Top Pennsylvanian shale, by lithology
10,790: Top lower Strawn limestone, by lithology
10,810-11,060: Lower Strawn (Cherokee) fusulines
10,810-10,840: Upper Cherokee types
10,910-11,060: Lower Cherokee types
11,110: Top Atoka series, by lithology
11,110-11,310: Atoka fusulines
Based primarily on lithology:
11,430: Base Atoka series
11,430: Top "Barnett" (Chester) shale
11,880: Top "Meramec-Osage" limestone
12,180: Top Woodford shale
12,250: Top "Devonian" limestone
12,600 LSE: In "Devonian" limestone

Samples examined from 9960 to 12,600 feet, TD: 12,900 feet.

Detailed Report

---- 9960: Samples practically pulverized; not examined.
9960-10,560: No fossils found

10,560-10,740: Wolfcamp fusulines, lower Hueco types
10,560-10,570: Schwagerina - lower Hueco types
10,620-10,630: Triticites
10,650-10,660: Schwagerina
10,700-10,740: Schwagerina; Triticites - lower Hueco types
Schubertella @ 10,720-730.

10,740-10,810: No fossils found

10,750: Suggested base Wolfcamp series, by lithology

Figure 2.2. A sample copy of a biostratigraphic report by James Hollingsworth. Included in the report are the location of the well, fusulinid species, and which groups were identified from microfossils versus lithology. The Texas Land Survey system coordinates are featured in the top red box, while the lower red box highlights the fusulinid depth occurrences.

Data collection progressed in two main phases. Phase one was the collection of various chronostratigraphic horizons in X-Y-Z space (Table 2.1). Latitude and longitude of the well location formed the X-Y components. The Z-component was the depth to

those biostratigraphic zone tops that are inferred in the reports. All the reports were completed by the Paleontological Laboratory in Midland, Texas between the 1920's to the late 1970's, with the majority authored by R.V. Hollingsworth. The data currently resides at Texas Tech University, under the care of the Geosciences Department.

The ultimate goal is to create a searchable database where access to the reports as well as the maps can be rented and purchased. Any inquiries about the reports can be made to that office. No reinterpretation of those biostratigraphic zone tops was undertaken; however, individual fusulinid genera from the reports were checked against more modern assessment (Wilde, 2004) to see if any age reassignment of certain species had recently occurred. No such cases have been found to date. There were also sections of the reports that determined the top of the series based upon lithology, even though fusulinid data was found beneath. Those picks were used to ensure the top of the series was successfully recorded in the database. The difference between the lithological picks and the fusulinid occurrences was between 20-30 feet. The picking of the tops of the series units was based upon the fusulinid picks made by Wilde, as mentioned previously in the fusulinid biostratigraphy sections. The reports explicitly state which series the fusulinids belong to (ie: Wolfcampian fusulinids, or Cisco fusulinids) so those levels were recorded accordingly in the database.

Latitude and longitude of the wells analyzed in each report are not recorded. Instead, these reports utilize original Texas Land Survey locations (Fig. 2.3). Conversion to latitude and longitude was completed by overlaying the survey outline in Google Earth through the Earth Point website, and measuring out the location of the well site (Fig. 2.4). This process only provides a close approximation to the well site, within a several hundred-meter radius. Elevation of the well site from the reports was checked against the location of the approximate latitude and longitude for consistency.

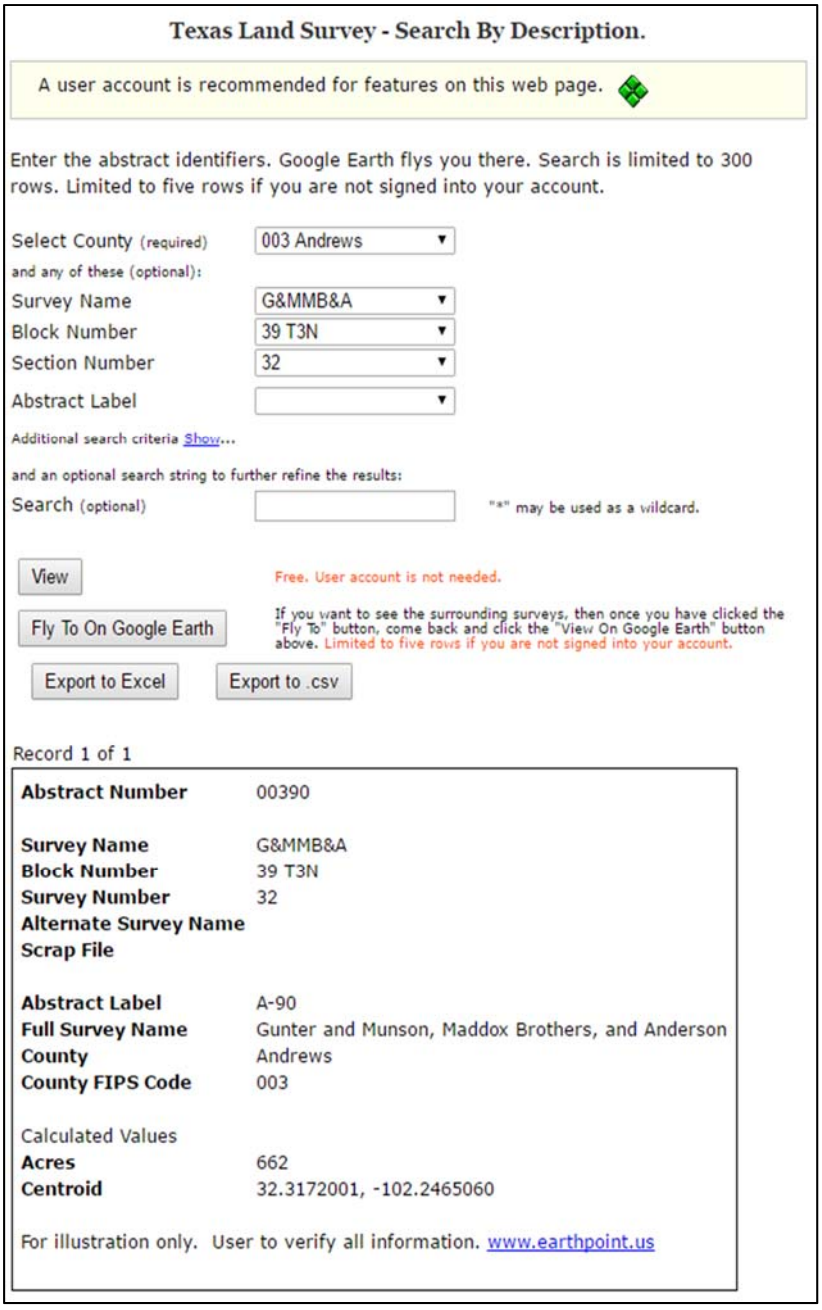


Figure 2.3. A clipping of the Texas Public Land Survey website where the biostratigraphic report information was entered. Once the data was successfully entered, a Google Earth link was generated that zoomed in directly to the tract of land where the samples were taken.

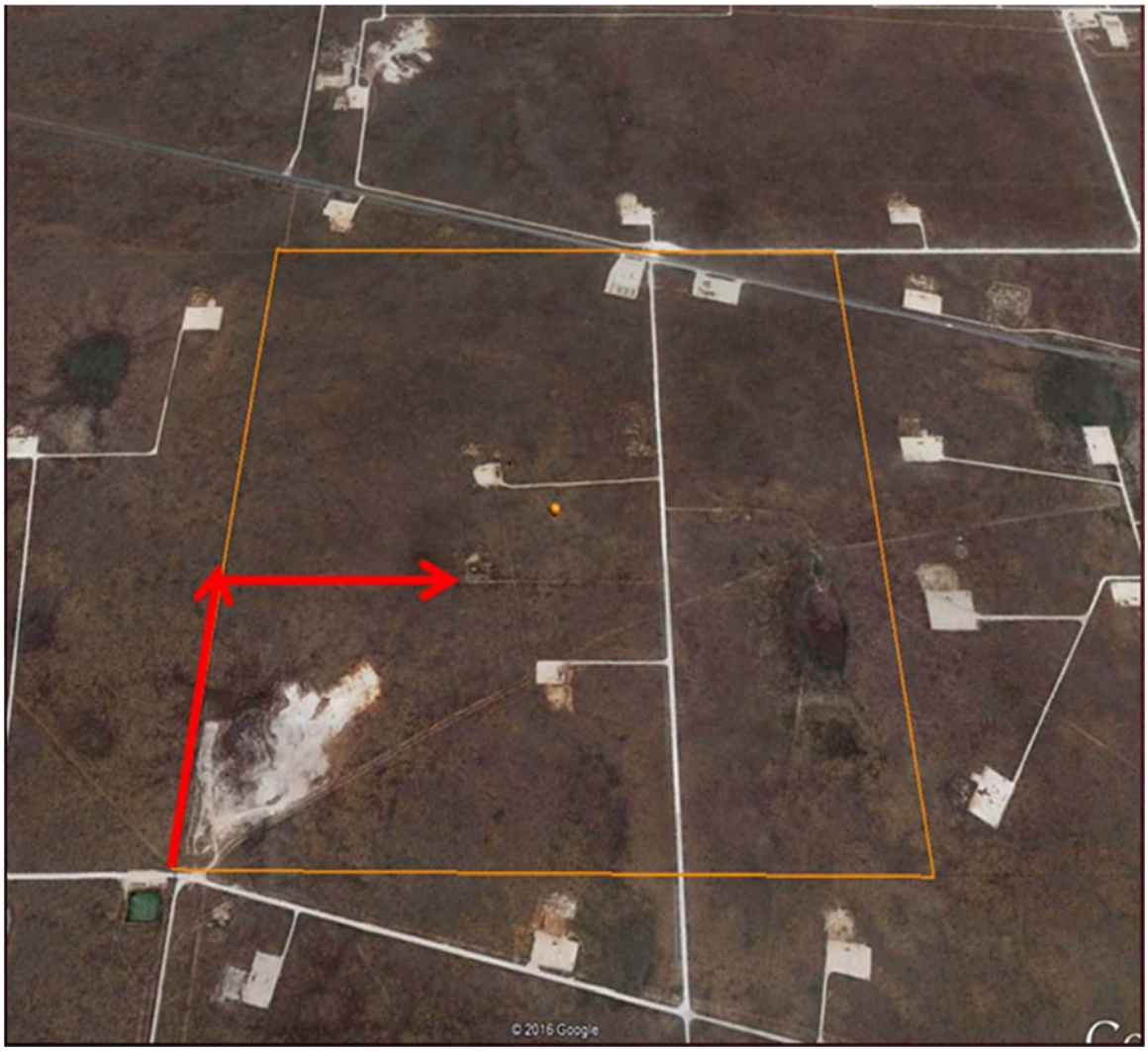


Figure 2.4. An example tract of land that was generated from the data on the biostratigraphic reports, zoomed in on Google Earth. The red arrows depict the location of the fusulinid sampling site as determined from the reports.

The second phase of the project was importation of the data into ArcGIS software. Querrying the database in ArcMap allowed for the production of subsurface chronostratigraphic maps during the Pennsylvanian and the early Permian in West Texas (Fig. 14). Each data point assigned to a specific biostratigraphic top was used to interpolate between regions with a natural neighbor's algorithm to create a continuous surface. These maps are all hung on the sea level datum and thus are reported as depth below sea level.

*Database Construction*

The database was organized into columns of biostratigraphic horizons and the associated depth in feet that the tops of the horizons occurred. Biostratigraphic horizons recorded include the Atokan, Strawn, Canyon, Cisco, Wolfcampian, and Leonardian (Table 1). Depths to the top of certain lithostratigraphic horizons within the middle and lower Paleozoic strata were also recorded.

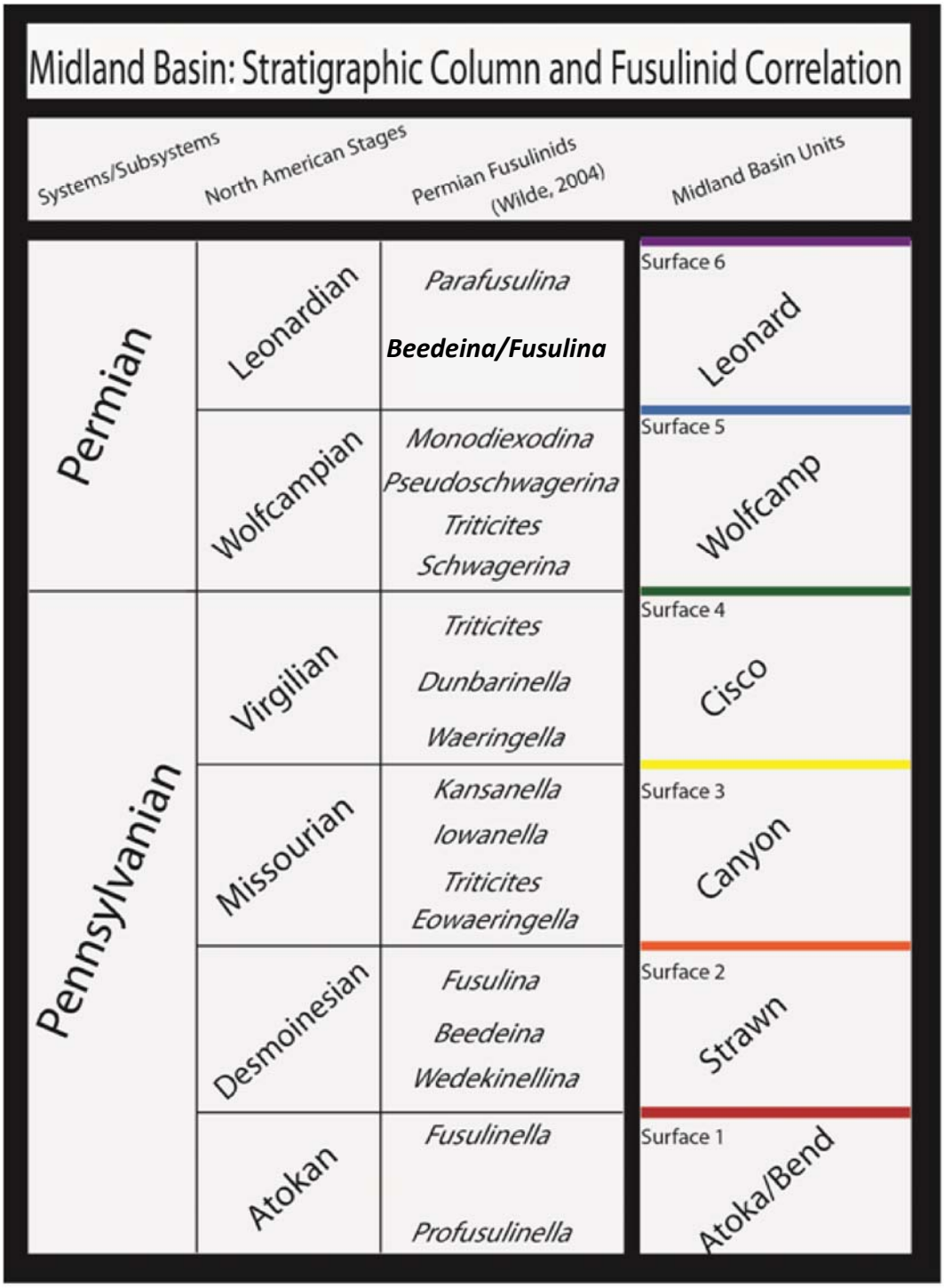


Figure 2.5. The distribution of fusulinid genera observed in the Permian Basin from Wilde (2004) as well as the locations of the surfaces mapped through biostratigraphy, at the top of each of the units. Surfaces 3-6 were compared against existing literature.

| Surface | Modern Equivalent | # of wells in Database |
|---|---|---|
| *Leonardian* | Leonardian | 243 |
| *Wolfcampian* | Wolfcampian | 1490 |
| **Wolfcampian Clastic** | N/A | 100 |
| *Cisco* | Virgilian | 614 |
| *Canyon* | Missourian | 1029 |
| *Upper Strawn* | Upper Desmoinesian | 892 |
| *Lower Strawn* | Lower Desmoinesian | 1059 |
| *Upper Cherokee* | Lower Desmoinesian | 407 |
| *Lower Cherokee* | Lower Desmoinesian | 434 |
| *Atokan* | Atokan | 782 |
| | Total Wells | 2369 |

Table 2.1. Table documenting the number of wells in the database. The italicized names are chronostratigraphic surfaces that were identified through fusulinid occurrences.

*Quality Control*

After the well locations were finalized, quality control measures were implemented to ensure the data entered was accurate. Interpolated surfaces that contained points of obvious erroneous elevation values or nonsensical fusulinid depths that largely occurred due to erroneous entry into the database were re-examined. For Example, in Figure 15, the wells are plotted in their respective counties, and can be cross referenced in the database to ensure they are in the correct location. Furthermore, a surface elevation map of all well points was created and compared to the modern earth

surface. Surface elevations in the database that were entered incorrectly were changed accordingly by either relocating the well and/or entering the correct well elevation.

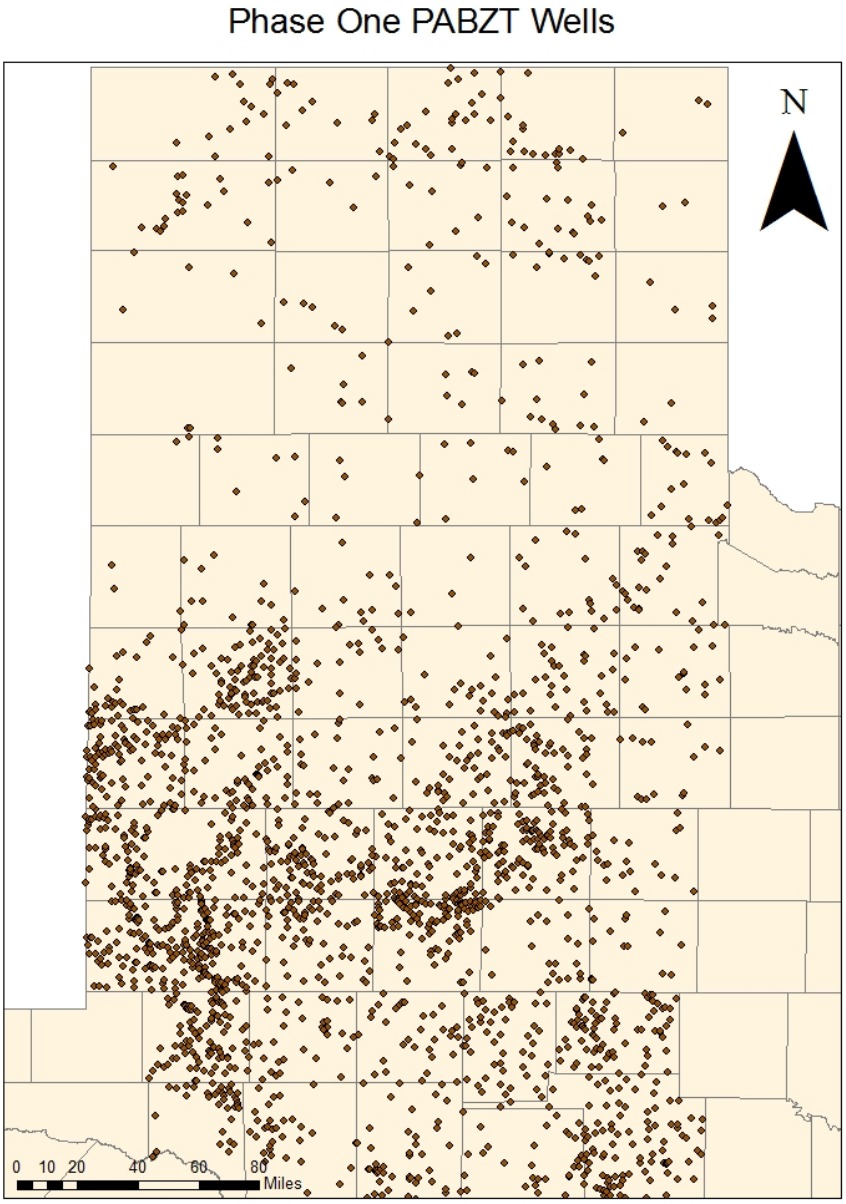


Figure 2.6. The distribution of all recorded well sites in phase one of the PABZT Project. Each dot represents a well site where fusulinid data was present in the PABZT collection for the construction of the chronostratigraphic surfaces.

*Existing Literature Review*

Several prominent papers detailing paleogeographic time periods of the Midland Basin were collected for statistical comparison to contrast against the eastern shelf margin depicted on the six chronostratigraphic surfaces created with the PABZT data. Unfortunately, there was little literature on the shelf development during the

Desmoinesian and the Atokan in the Midland Basin, due to the position of the shelf edge during that time. These time periods are not presented in this part of the analysis. The papers that included comparable maps are publications from the 1980's and later. Each of the maps also used a different set of data, either seismic, core, or a combination of both (Fig. 2.7). The first publication is a presentation by Qilong Fu, presented to the West Texas Geological Society in 2011, titled "A synthesis of the Wolfcampian platform carbonate system in the Permian Basin Region". This paper included maps that detailed the eastern shelf position during the early Permian, and are suitable for comparison against the Wolfcampian shelf edge maps (Fig. 2.10). The second publication selected for comparison is by Robert Baumgardner et al. (2016) titled "An early Permian coastal flora dominated by *Germaopteris martinsii* from basinal sediments in the Midland Basin, West Texas". This paper included a background on the Midland Basin and the eastern shelf during the early Permian, and is suitable for comparison with the Wolfcampian chronostratigraphic surface (Fig. 2.12). The third publication selected for comparison is authored by S.L. Montgomery (1996). The paper is titled "Permian Wolfcamp Limestone Reservoirs: Powell Ranch Field, Eastern Midland Basin", and included a map detailing the position of the eastern shelf during the early Permian, which can be compared against the Wolfcampian chronostratigraphic surface (Fig. 2.11). The fourth publication selected for comparison is a compilation of maps published by the Bureau of Economic Geology (BEG) through the Permian Basin Synthesis Project, which is an undertaking designed to compile large amounts of information on the Permian Basin from multiple sources and produce regional paleogeographic maps (2008). These maps include shelf edges suitable for comparison against the Cisco and Canyon Series (Fig. 2.8, 2.9, 2.13).

The Permian paleogeographic maps from the various authors were derived primarily from lithology data. Several of the publications, including those by Baumgardner et al. (2016) and Fu (2011), based their paleogeographic settings on the literature of Silver and Todd (1969), which used core data to build a lithological map of the Midland Basin (Figure 2.7). The maps produced by the BEG are based upon wireline log correlations and seismic interpretations taken from petroleum companies and independent core data (BEG, 2008). Montgomery (1996) also referenced facies studies of the Delaware and Midland Basins by authors such as Hobson and Loucks (1985). While seismic is suitable

for demonstrating stratal geometry, the reflectors are due to impedance contrasts, which is a function of lithological parameters. None of the literature maps compared against use data that provides a chronostratigraphic framework and, therefore, correlation of data across wide regions likely reflects some degree of age diachroneity.

| Author | Date of Publication | Map Comparison | Data used for Maps |
|---|---|---|---|
| Bureau of Economic Geology | 2008 | Canyon Series | Core Data |
| Bureau of Economic Geology | 2008 | Cisco Series | Core Data |
| Bureau of Economic Geology | 2008 | Leonardian Series | Core Data and Seismic Data |
| Fu | 2011 | Wolfcamp Series | Core Data |
| Baumgardner et al. | 2016 | Wolfcamp Series | Core Data |
| Montgomery | 1996 | Wolfcamp Series | Core Data and Seismic Data |

Figure 2.7. A chart detailing the source of each Permian literature's maps of the Midland Basin. Many maps were based on lithological studies, and included core data from the sites.

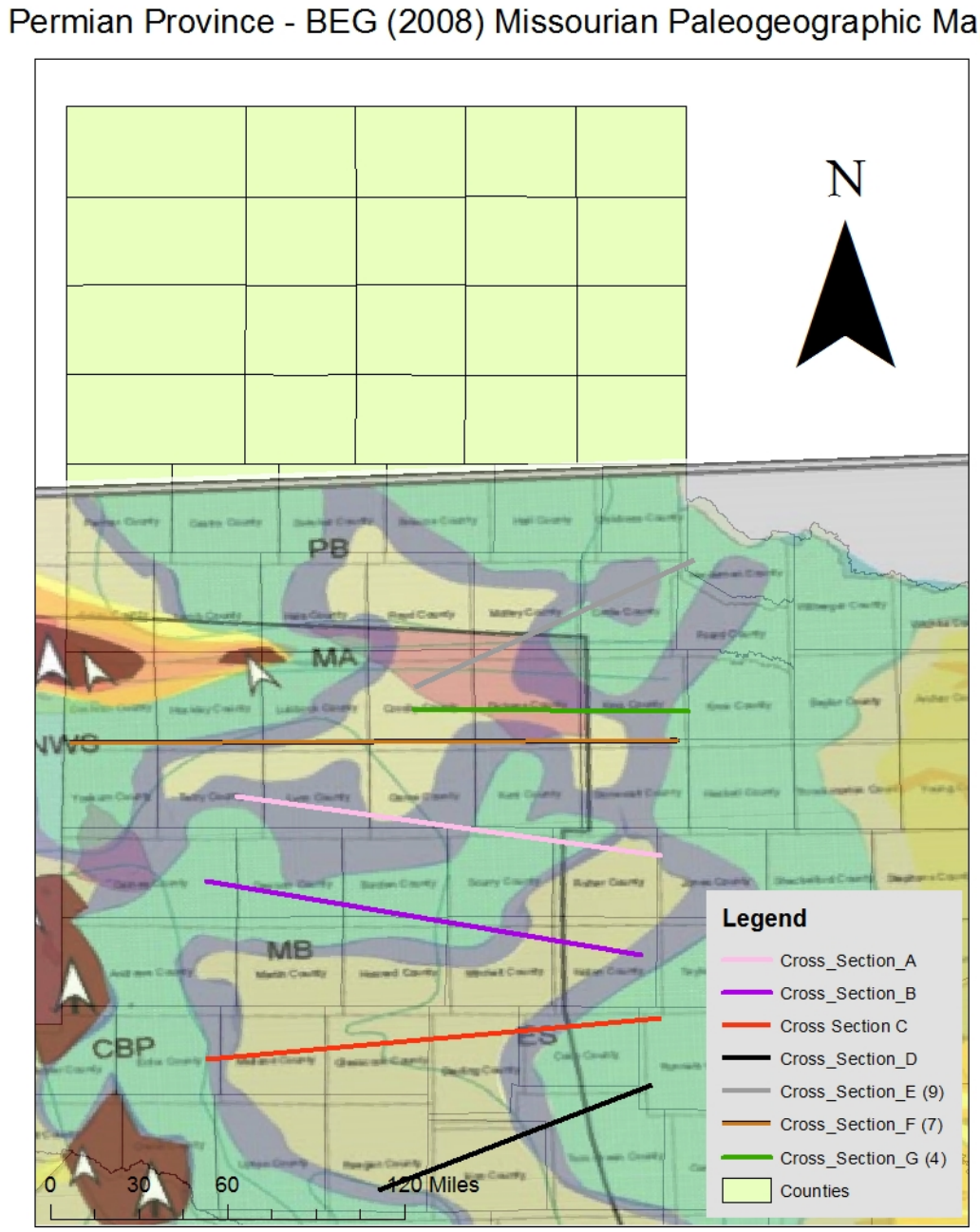


Figure 2.8. The digitized map of the Permian Basin during the Missourian, from the BEG's 2008 project, the Permian Basin Synthesis Project. The map was overlaid on the Texas basemap and transformed to match county boundaries. The shelf edges were then drawn and digitized from the overlaid image.

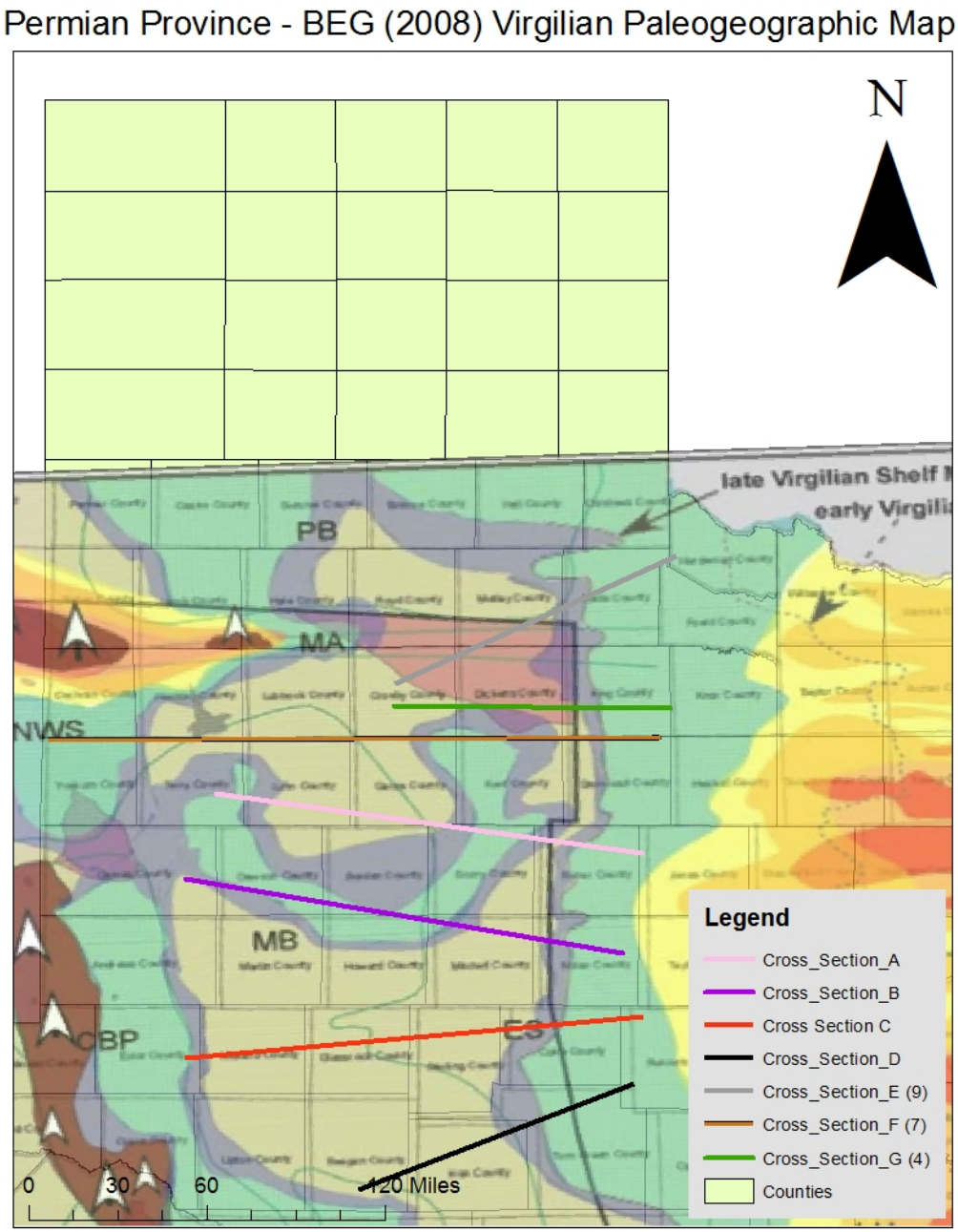


Figure 2.9. The digitized map of the Permian Basin during the Virgilian, from the BEG's 2008 project, the Permian Basin Synthesis Project. The map was overlaid on the Texas basemap and transformed to match county boundaries. The shelf edges were then drawn and digitized from the overlaid image.

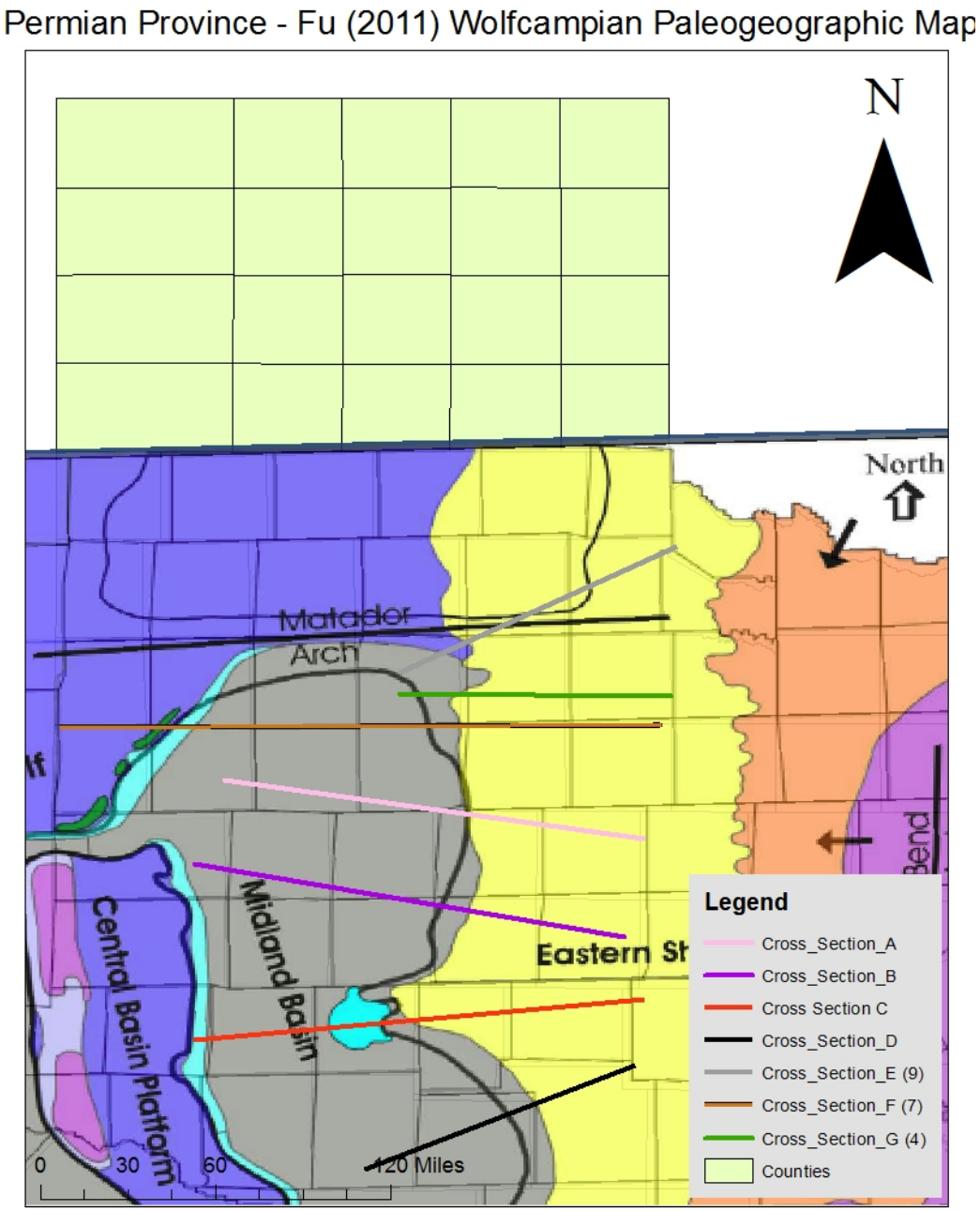


Figure 2.10. The digitized map of the Permian Basin during the Wolfcamp, from Qilong Fu's publication titled A synthesis of the Wolfcampian platform carbonate system in the Permian Basin region (2011). The map was overlaid on the Texas basemap and transformed to match county boundaries. The shelf edges were then drawn and digitized from the overlaid image.

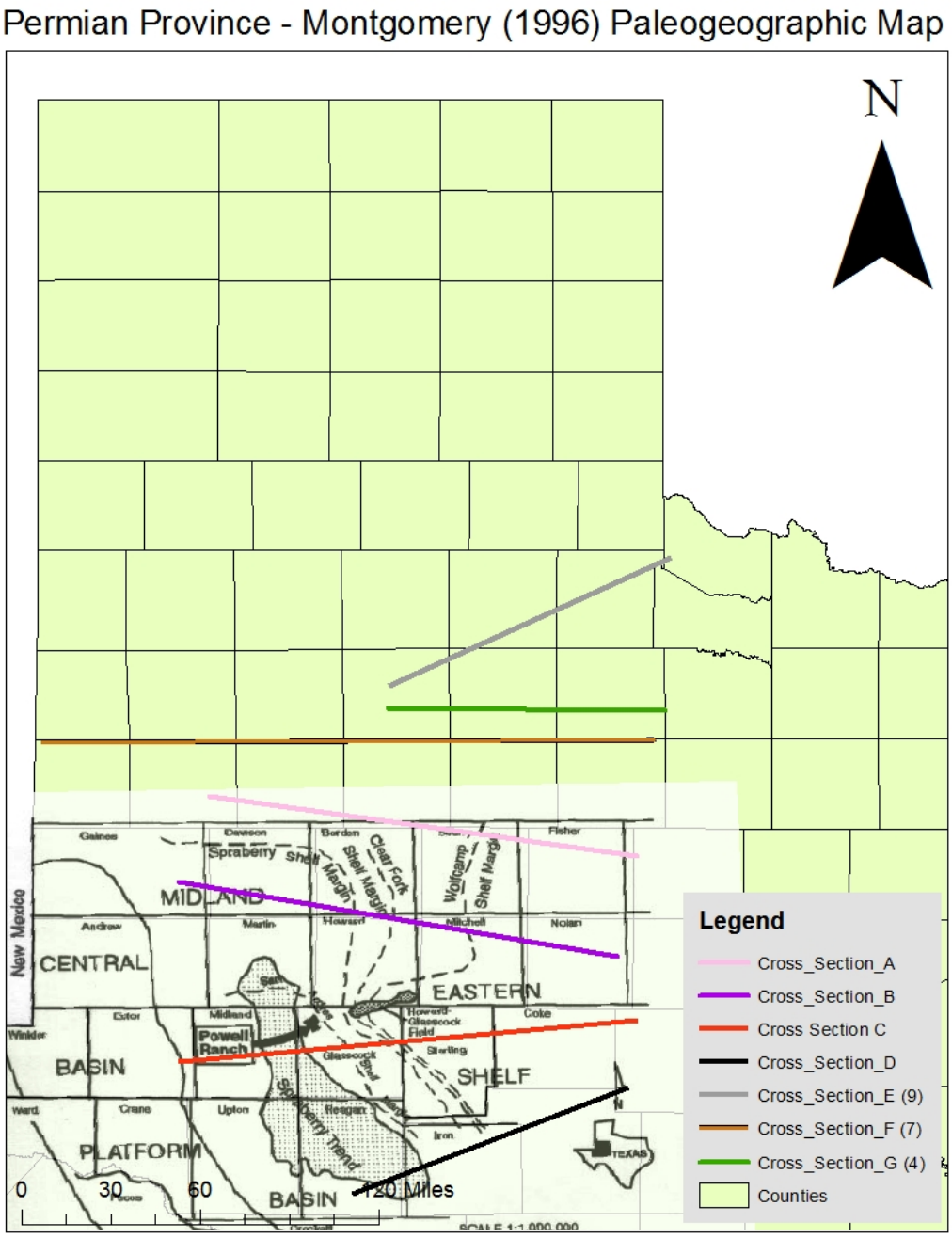


Figure 2.11. The digitized map of the Permian Basin during the Wolfcamp, from Montgomery's 1996 publication, Permian "Wolfcamp" Limestone Reservoirs: Powell Ranch Field, Eastern Midland Basin. The map was overlaid on the Texas basemap and transformed to match county boundaries. The shelf edges were then drawn and digitized from the overlaid image.

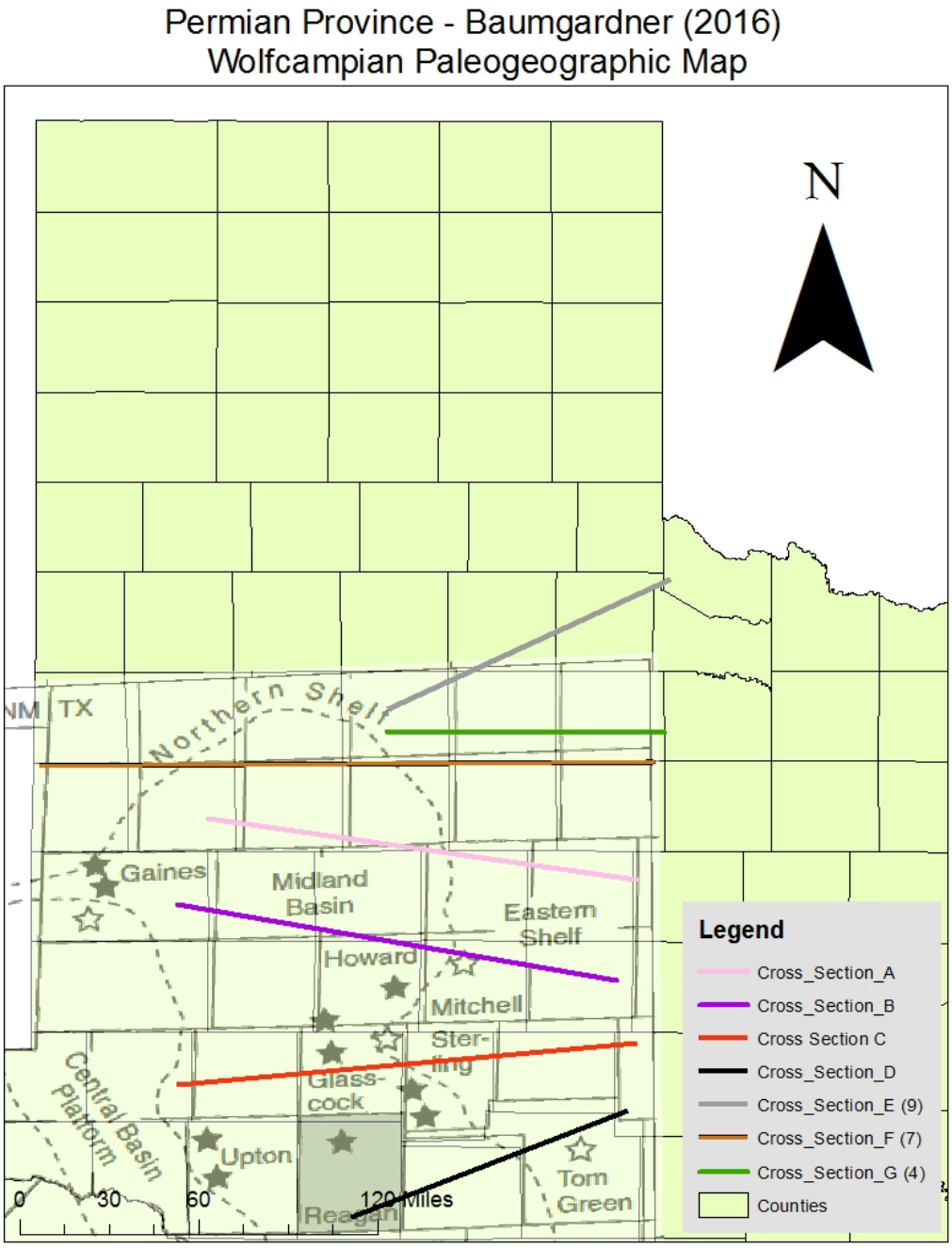


Figure 2.12. The digitized map of the Permian Basin during the Wolfcamp, from Baumgardner's 2016 publication, An early Permian coastal flora dominated by *Germaopteris martinsii* from basinal sediments in the Midland Basin, West Texas. The map was overlaid on the Texas basemap and transformed to match county boundaries. The shelf edges were then drawn and digitized from the overlaid image.

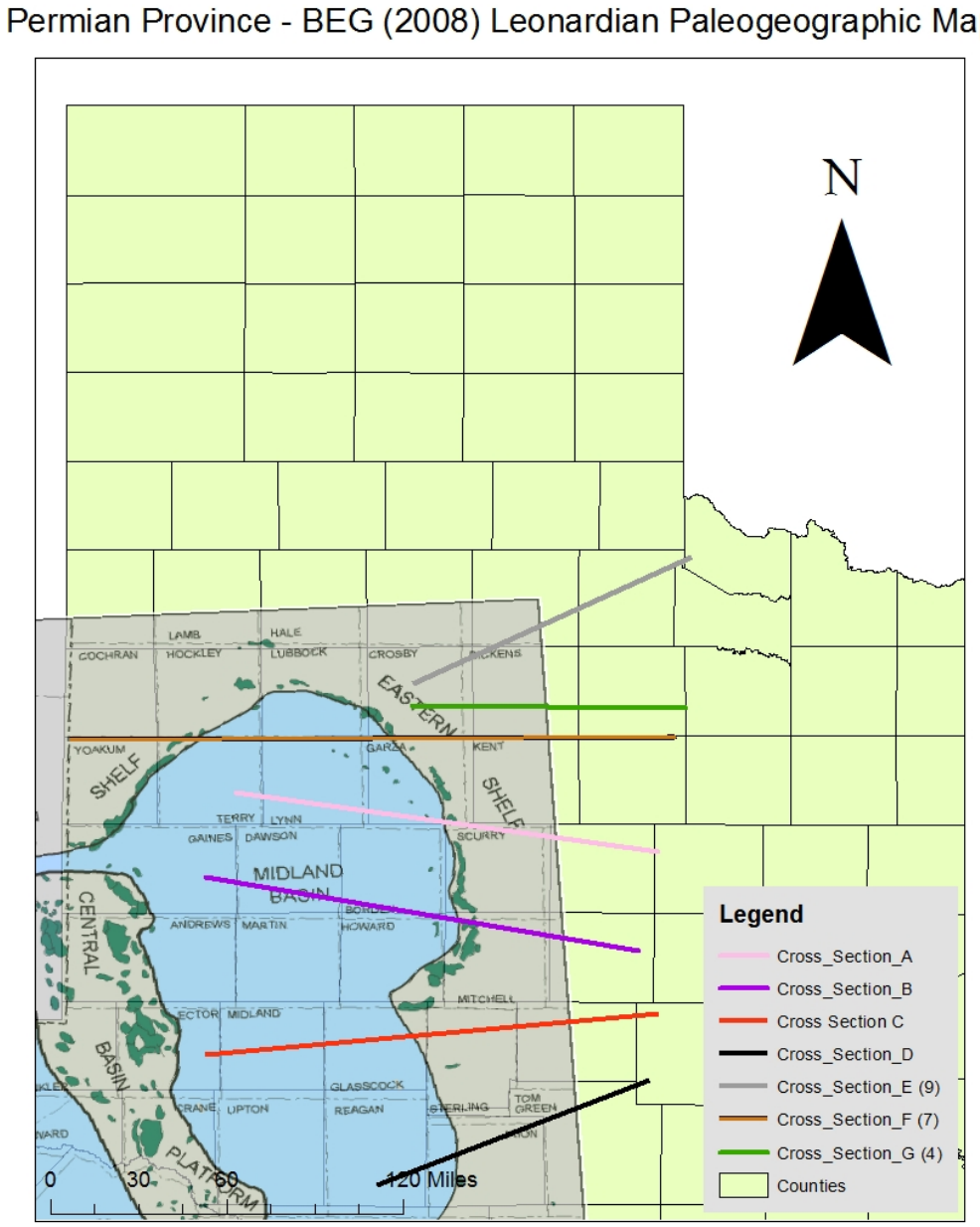


Figure 2.13. The digitized map of the Permian Basin during the Leonardian, from the BEG's 2008 project, the Permian Basin Synthesis Project. The map was overlaid on the Texas basemap and transformed to match county boundaries. The shelf edges were then drawn and digitized from the overlaid image.

# CHAPTER III
# DATA ANALYSIS

There are six chronostratigraphic maps that were constructed using the fusulinid occurrences. Using the topographic profiles from each cross section, the shelf edge was successfully constructed along five of the six maps (Fig. 3.1). The Atokan chronostratigraphic map did not adequately highlight the position of the eastern shelf, and so it not drawn (Fig. 3.2). The maps depict the entirety of the Texas Panhandle, and the eastern shelf of the Midland Basin is located on the southeastern corner of the maps (Fig. 3.2, 3.3, 3.4, 3.5, 3.6 3.7).

*Statistical Analysis and Quantitative Comparisons to literature*

Once the location of the shelf edge is constructed from the biostratigraphic data it is compared to existing maps that delineate the paleogeography of the Midland Basin. The distance between the literature's shelf edge and the shelf edge constructed here is measured from the western edge of the cross section line (i.e. closest to the basin). Dividing the two values produces a dimensionless ratio that allows easy comparison.

$$\frac{[Literature\ Shelf Edge\ Position\ (km)]}{[PABZT\ Edge\ Position\ (km)]} = Comparison\ ratio\ (dimensionless)$$

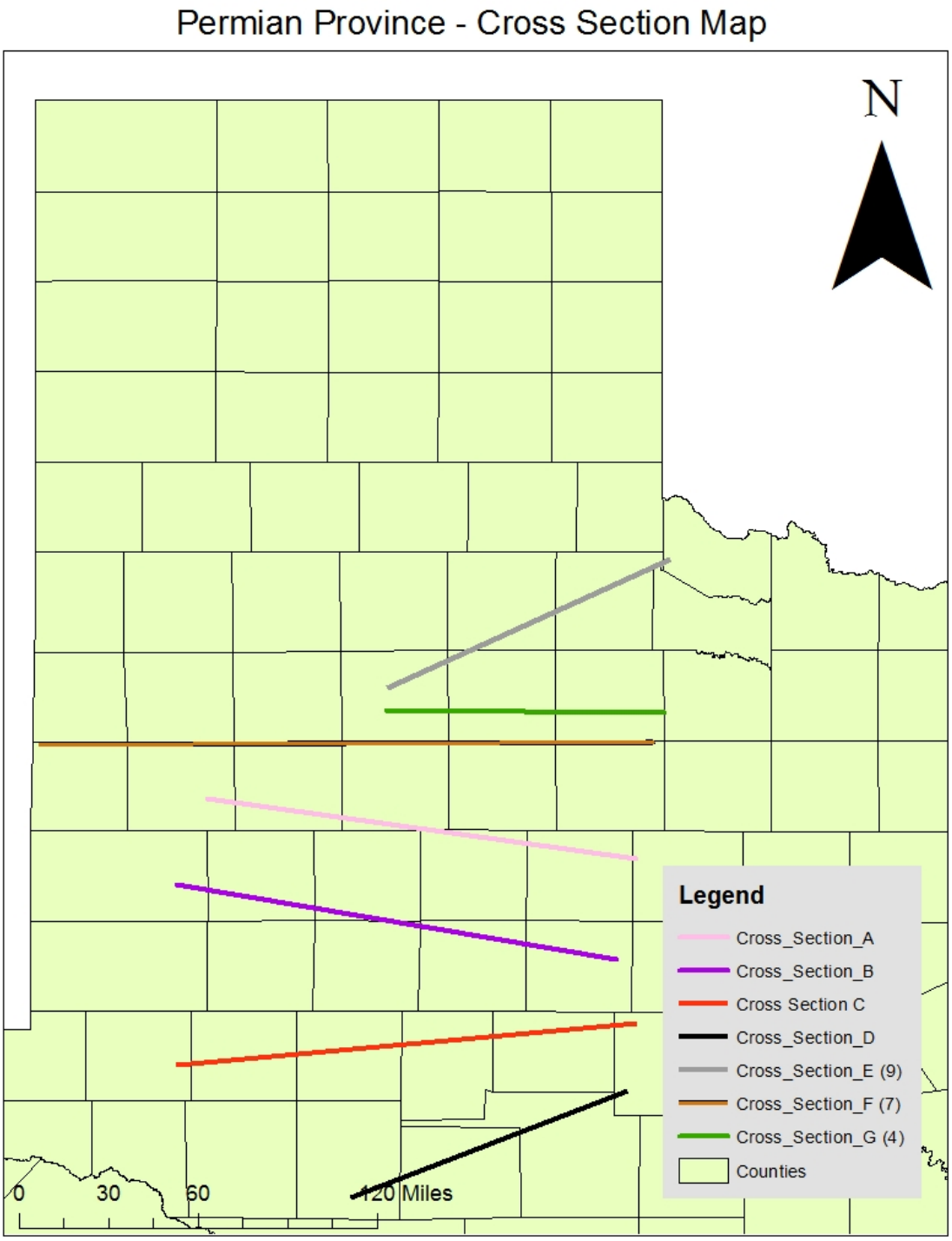


Figure 3.1. The locations of cross sections along the eastern Midland Basin. The cross sections span a North to South distance of 275 kilometers.

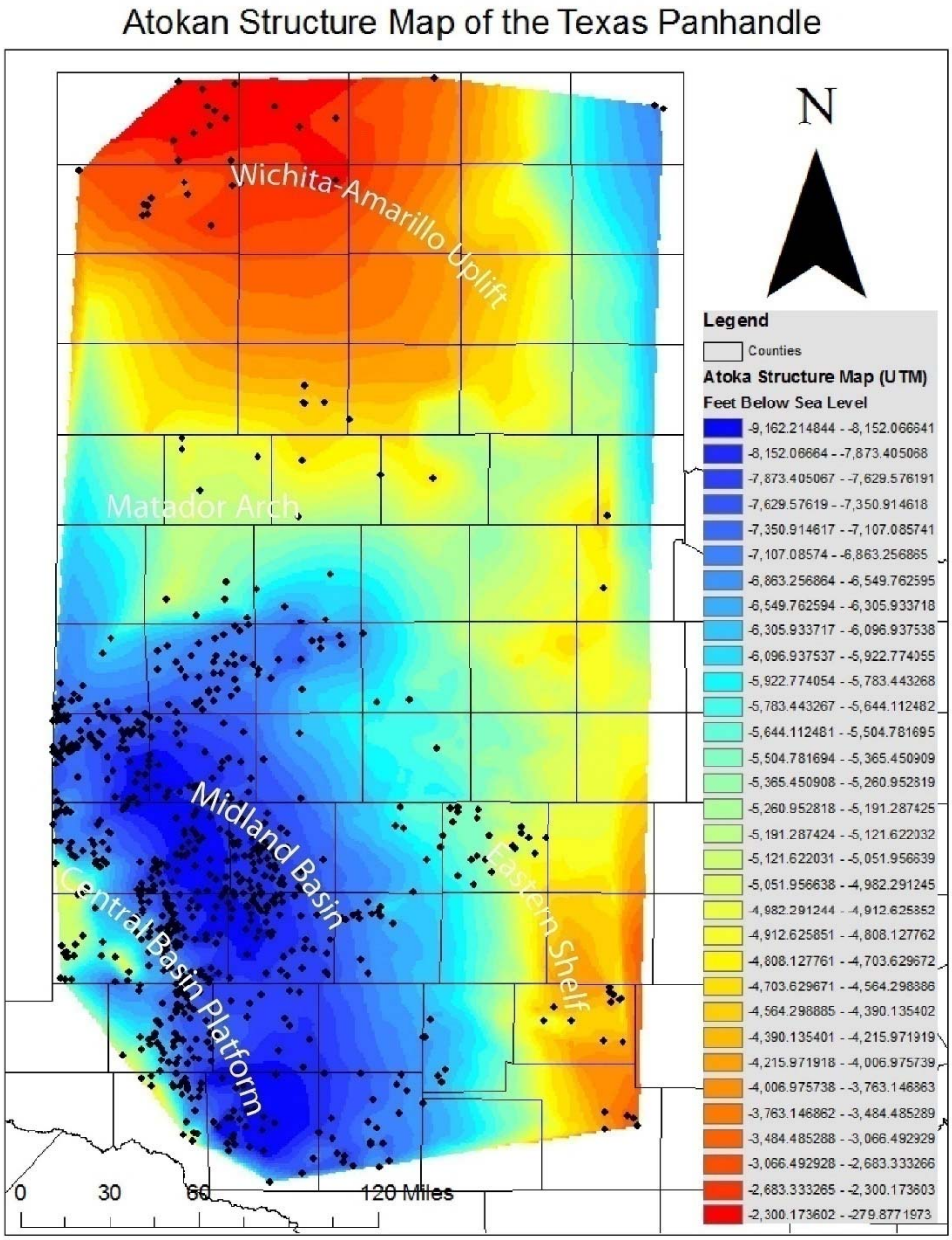


Figure 3.2. Figure 3.2 shows a map of Atokan paleogeography in the Midland Basin derived from fusulinid biostratigraphy. The red and yellow colors represent shallow sub-sea depths, and the blues and greens represent deeper sub-sea values. Significant structural features are noted, including the Central Basin platform to the West, the Matador Arch to the North, and the Wichita-Amarillo Uplift to the far North.

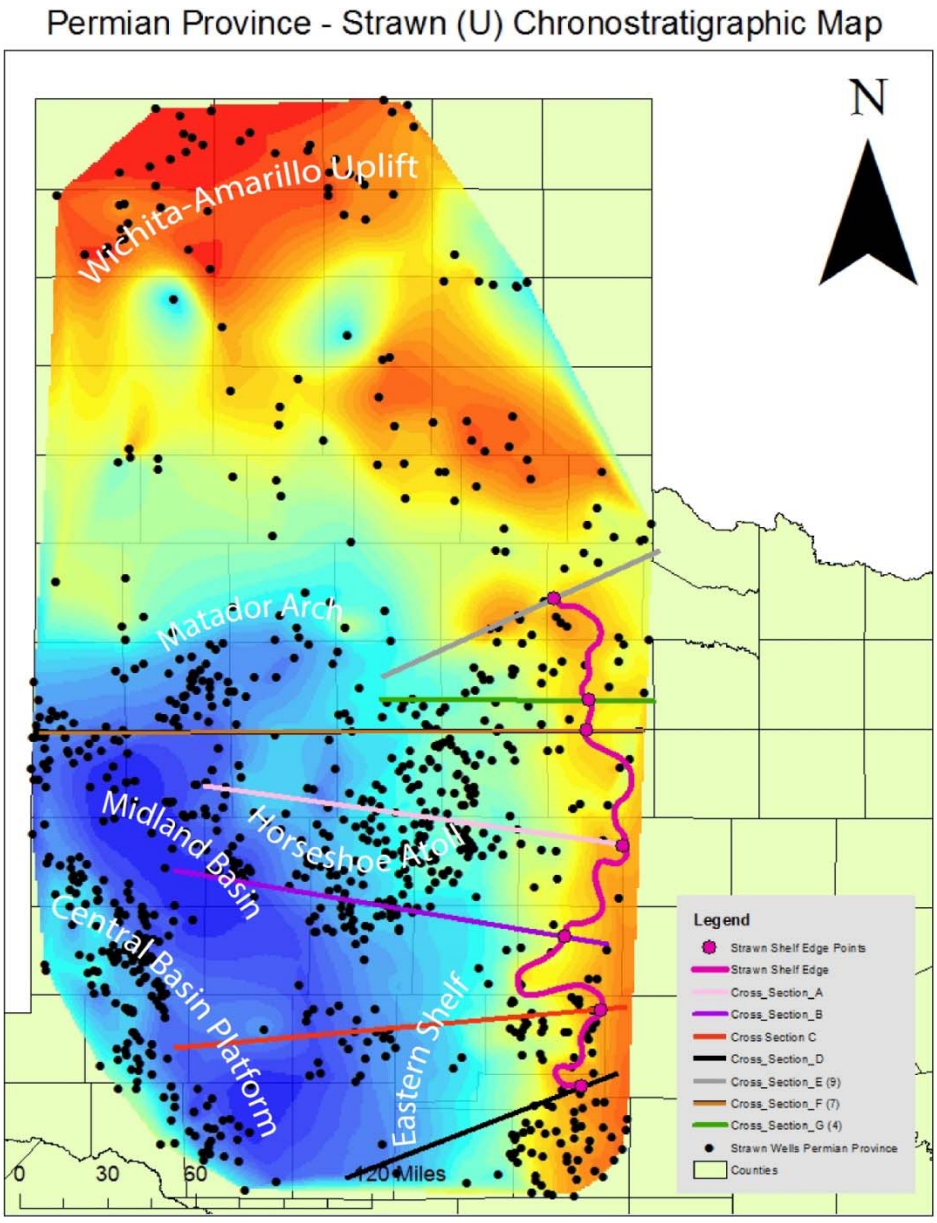


Figure 3.3. Figure 3.3 shows a map of Strawn paleogeography in the Midland Basin derived from fusulinid biostratigraphy. The red and yellow colors represent shallow sub-sea depths, and the blues and greens represent deeper sub-sea values. The Palo Duro Basin has begun to appear on subsurface maps during this point in the Permian Province.

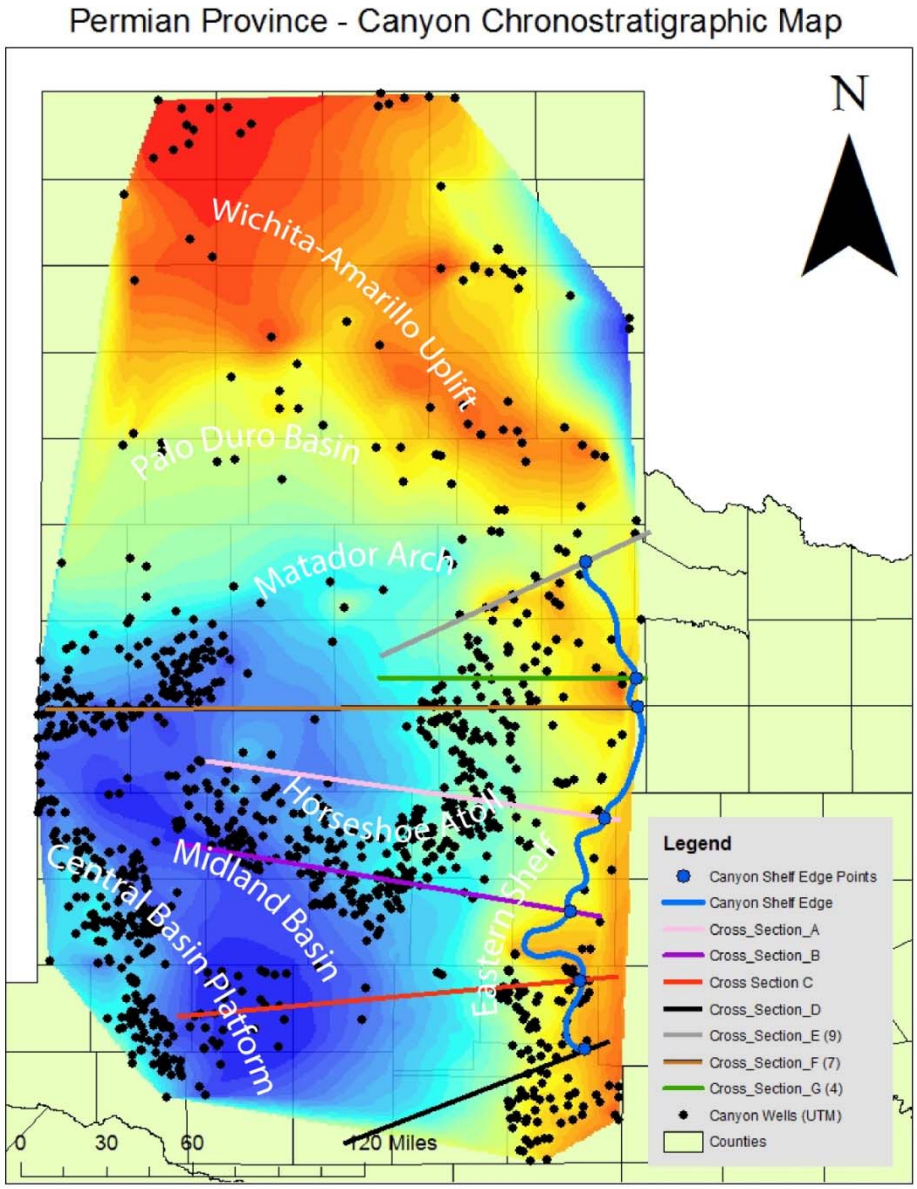


Figure 3.4. Figure 3.4 shows a map of Canyon paleogeography in the Midland Basin. The red and yellow colors represent shallow sub-sea depths, and the blues and greens represent deeper sub-sea values. The Horseshoe Atoll is developing at this time in the Midland Basin.

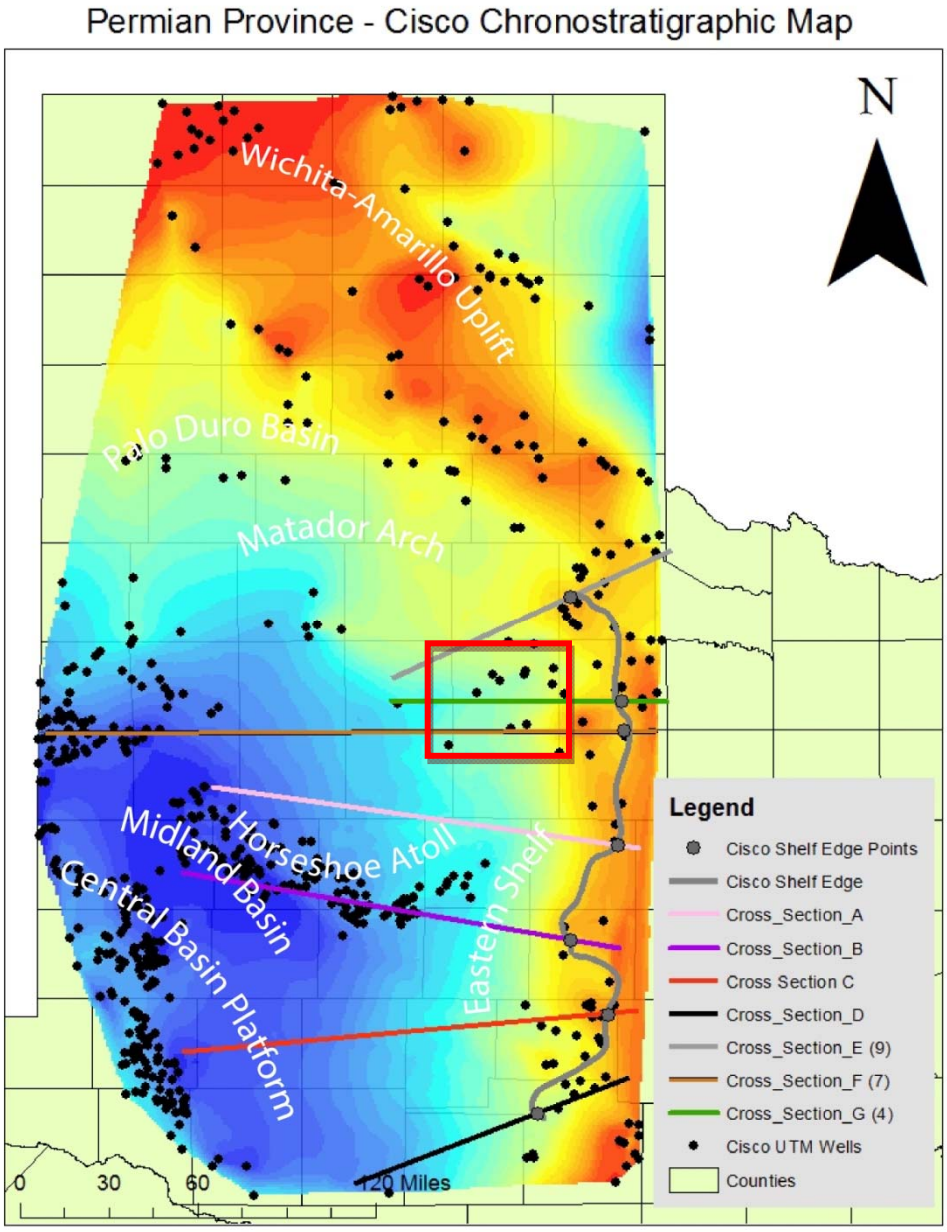


Figure 3.5. Figure 3.5 shows a map of Cisco paleogeography in the Midland Basin derived from fusulinid biostratigraphy. The red and yellow colors represent shallow sub-sea depths, and the blues and greens represent deeper sub-sea values. The Horseshoe Atoll has reached maturity at this point in the Midland Basin. The red box highlights a sediment funnel discussed later.

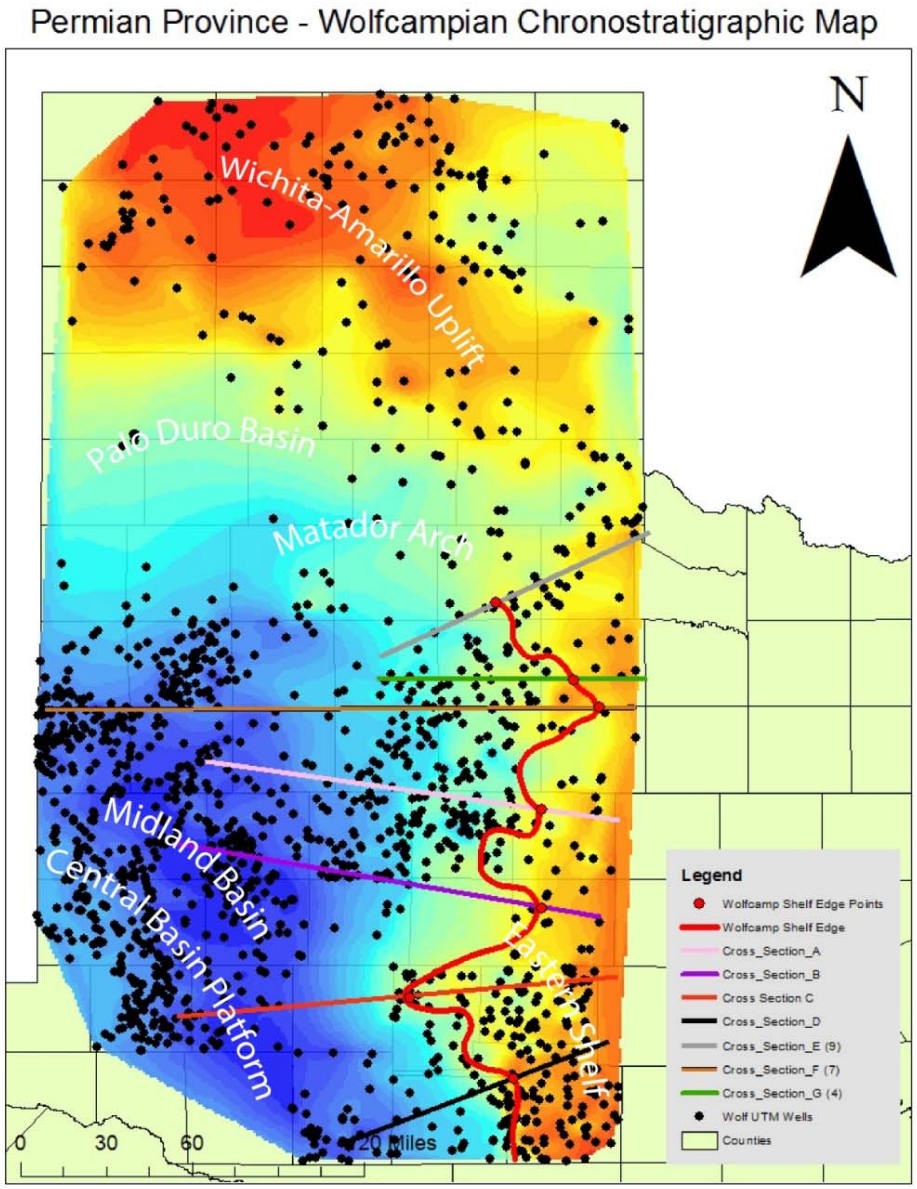


Figure 3.6. Figure 3.6 shows a map of Wolfcampian paleogeography in the Midland Basin derived from fusulinid biostratigraphy. The red and yellow colors represent shallow sub-sea depths, and the blues and greens represent deeper sub-sea values.

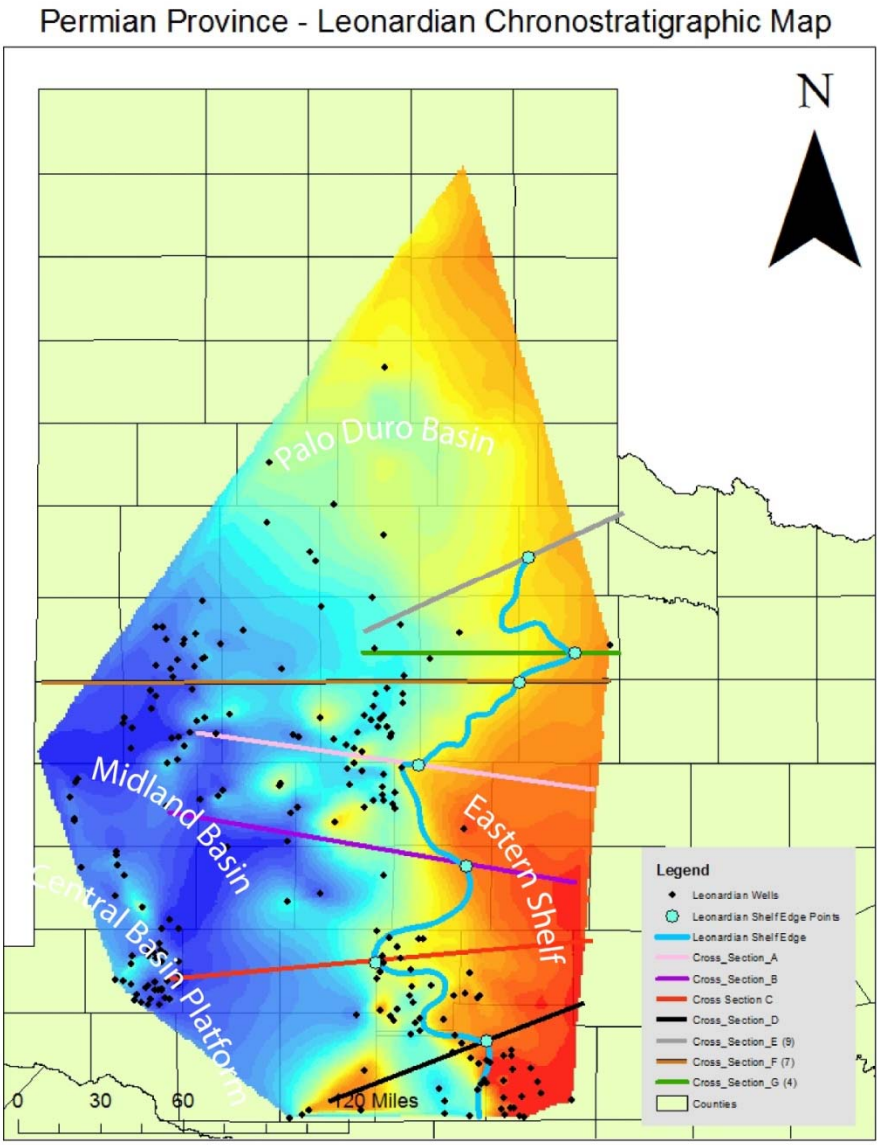


Figure 3.7. Figure 3.7 shows a map of Leonardian paleogeography in the Midland Basin derived from fusulinid biostratigraphy. The red and yellow colors represent shallow sub-sea depths, and the blues and greens represent deeper sub-sea values. The infilling of the Palo Duro Basin has already occurred at this point in time in the Permian Province.

# CHAPTER IV

# DISCUSSION OF RATIOS AND TREND COMPARISONS

## DATA ANALYSIS

The section discusses the methods for geospatially referencing the Midland Basin eastern shelf edges from existing literature, which are then compared against the surfaces derived from the biostratigraphic data in the PABZT project.

### *Quantitative construction of shelf-edge breaks from geometry of chronostratigraphic surfaces*

Seven cross sections are constructed along the eastern shelf to geometrically reconstruct the shelf edge break during late Pennsylvanian to Early Permian (Fig. 3.1). Cross-sections intersect the shelf edge perpendicularly, and at these locations, topographic profiles of each of the surfaces (Atokan-Leonardian) are constructed (Appendix 1). The cross sections are labeled A-G (Fig. 3.1), and span a combined distance north to south of 275 kilometers along the eastern shelf. On the profiles, the point of maximum flexure in the outer shelf position is denoted as the shelf edge. Connecting these flexure points estimates the shelf-edge position on each chronostratigraphic horizon. Connecting shelf edges requires some interpretation in the spaces between the cross section shelf picks, but mimic the existing structural trends seen on the map surfaces.

$$\frac{[Literature\ Shelf Edge\ Position\ (km)]}{[PABZT\ Edge\ Position\ (km)]} = Comparison\ ratio\ (dimensionless)$$

| | Canyon Shelf edge | | Cisco Shelf edge | | Wolfcampian Shelf edge | | Leonardian Shelf edge | |
|---|---|---|---|---|---|---|---|---|
| | Comparison ratio | Distance apart | Comparison ratio | Distance apart | Comparison ratio | Distance apart | Comparison ratio | Distance apart |
| **Cross Section A** | | | | | | | | |
| BEG | 0.98 | 4.21 km | 1.07 | 12.33 km | | | 1.15 | 14.8 km |
| Baumgardner et al (2016) | | | | | 1.47 | 51.43 km | | |
| Fu (2011) | | | | | 1.39 | 45.30 km | | |
| Montgomery (1996) | | | | | 1.28 | 36.02 km | | |
| **Cross Section B** | | | | | | | | |
| BEG | 0.97 | 5.00 km | 1.00 | 0 km | | | 1.26 | 31.56 km |
| Baumgardner et al (2016) | | | | | 1.4 | 51.31 km | | |
| Fu (2011) | | | | | 1.56 | 63.61 km | | |
| Montgomery (1996) | | | | | 1.32 | 24.32 km | | |
| **Cross Section C** | | | | | | | | |
| BEG | 1.35 | 52.82 km | 1.13 | 23.40 km | | | 1.12 | 11.62 km |
| Baumgardner et al (2016) | | | | | 1.00 | 0 km | | |
| Fu (2011) | | | | | 1.16 | 15.69 km | | |
| Montgomery (1996) | | | | | 1.03 | < 5 km | | |
| **Cross Section D** | | | | | | | | |
| BEG | 1.66 | 51.92 km | 1.08 | 6.62 km | | | 2.18 | 47.03 km |
| Baumgardner et al (2016) | | | | | 1.07 | 6.53 km | | |
| Fu (2011) | | | | | 1.14 | 11.41 km | | |
| Montgomery (1996) | | | | | 1.3 | 20.78 km | | |

Green indicates disagreement within 20%; Orange indicates disagreement larger than 20%

Table 4.2. A table of the comparison ratios from the shelf edge comparison analysis. Next to each comparison ratio is the difference in kilometers between the shelf edges along the cross sections. The green boxes indicate comparison values that fell within the 20% margin, indicating high values of similarity between the shelf edges; the orange values indicate ratios that fell outside the margin, and indicated low values of similarity.

## GENERAL TRENDS OF SHELF LOCATION AND ACCURACY

Comparison with PABZT constructed shelf-edge maps and those mined from existing literature produced a range of agreement (Table 4.2). This section aims to discuss some of the reasons for the observed north-south variation. Cross sections A and B represent the northern region of the eastern shelf of the Midland Basin, and cross sections C and D represent the southern region. The comparison ratios were designated into two categories, high and low similarity values, indicated by falling inside or outside of the 20% agreement, respectively (Table 4.2).

*Comparison Ratios and Paleogeographic Maps*

The Canyon paleogeographic matched well with the BEG's reconstructions of the Missourian shelf edge (Fig. 2.8, Fig. 4.1). In the northern region, the eastern shelf was portrayed in essentially the same location. However, to the south, the comparison ratio was > 20%, indicating that the BEG shelf edges were located ~ 50 kilometers farther inland than the PABZT data indicated. The southern region of the Midland Basin likely received a higher volume of sediment derived from the Llano Uplift during the Missourian (Wright, 2008b), which may explain the differences between the location on the maps. For example, a thicker unit of similar sediment would be more difficult to correlate to a thinner stratigraphic section located in the northern region.

The Cisco Series of paleogeographic maps matched well to the BEG reconstructions, which denoted the Flippen Limestone as the top of the Cisco Series (Fig. 2.9, Fig. 4.2). The northern region of the eastern shelf was nearly identical between the BEG shelf edges and constructed maps. The comparison ratios were 1.0 and 1.07, indicating that the shelf edges were in similar position along the cross sections. The southern region also exhibited high degrees of similarity. The comparison ratios were 1.13 and 1.08, and corresponded to ~ 24 kilometers between locations in the southern region. This comparison likely indicates that the Flippen Limestone represents minimal time diachroneity.

Three literature comparisons were made for the Wolfcampian Series (Fig. 2.10, Fig. 2.11, Fig. 2.12, Fig. 4.3). The northern portion of the Eastern Shelf exhibited poor correlation with each of the maps, whereas, the southern region had much better correlation with five of the six comparison ratios being within 20%. Reasons for discrepancy in the northern portion of the eastern shelf likely result from correlating to the regional Wolfcamp A well top, which in Lynn County conodont data demonstrates that this marker actually represents the top of the Leonardian (Kohn, 2016). Thus, while the Wolfcamp A marker top is a good subsurface lithostratigraphic marker, its use as a

Wolfcampian chronostratigraphic horizon is not warranted, and may be more useful as a comparison to Leonardian data instead.

Comparisons of Leonardian shelf edges produced the widest variance of correlation, with two cross sections within the 20% threshold and two greater than 20% (Fig. 2.13, Fig. 4.4). Moreover, there is no discernible trend in comparison from north-south. Although this wide disparity could reflect lithologic versus biostratigraphic data as inferred for the previous time periods, the limited number of fusulinid biostratigraphic reports in the PABZT database could also have an effect.

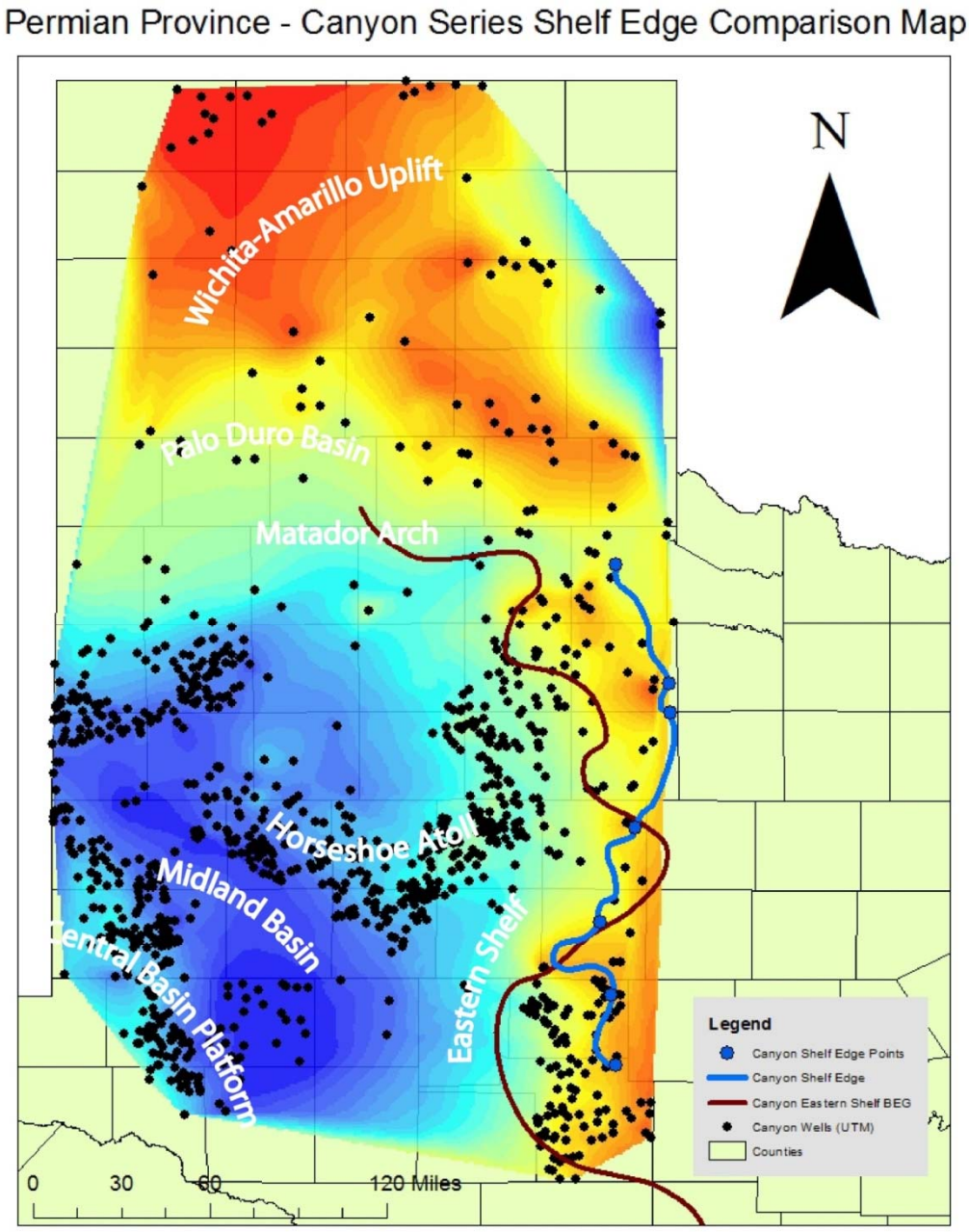


Figure 4.1. A map detailing the comparison of the constructed Canyon series shelf edge against the BEG's paleogeographic shelf edge from their 2008 Permian Basin Synthesis Project maps.

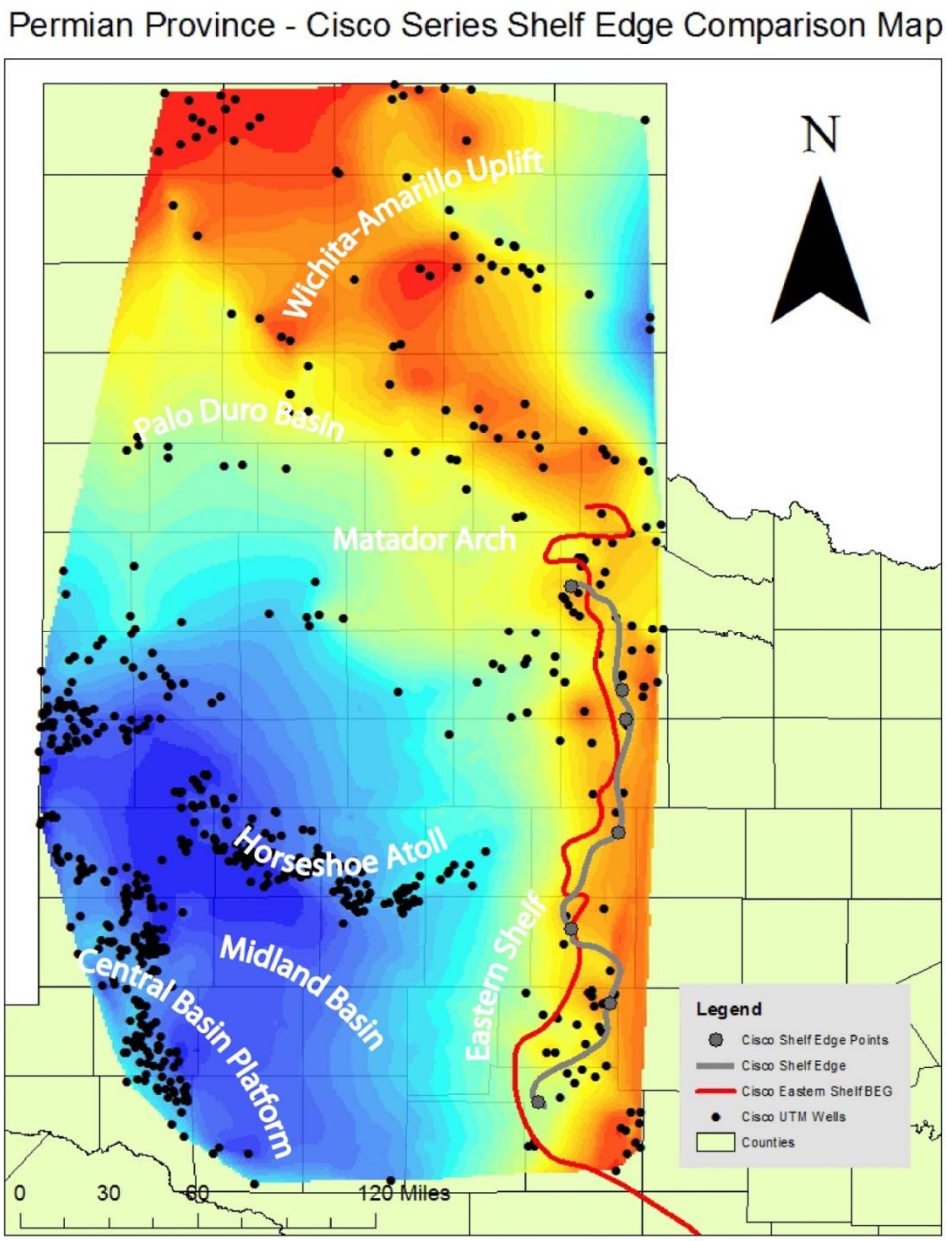


Figure 4.2. A map detailing the comparison of the constructed Canyon series shelf edge against the BEG's paleogeographic shelf edge from their 2008 Permian Basin Synthesis Project maps.

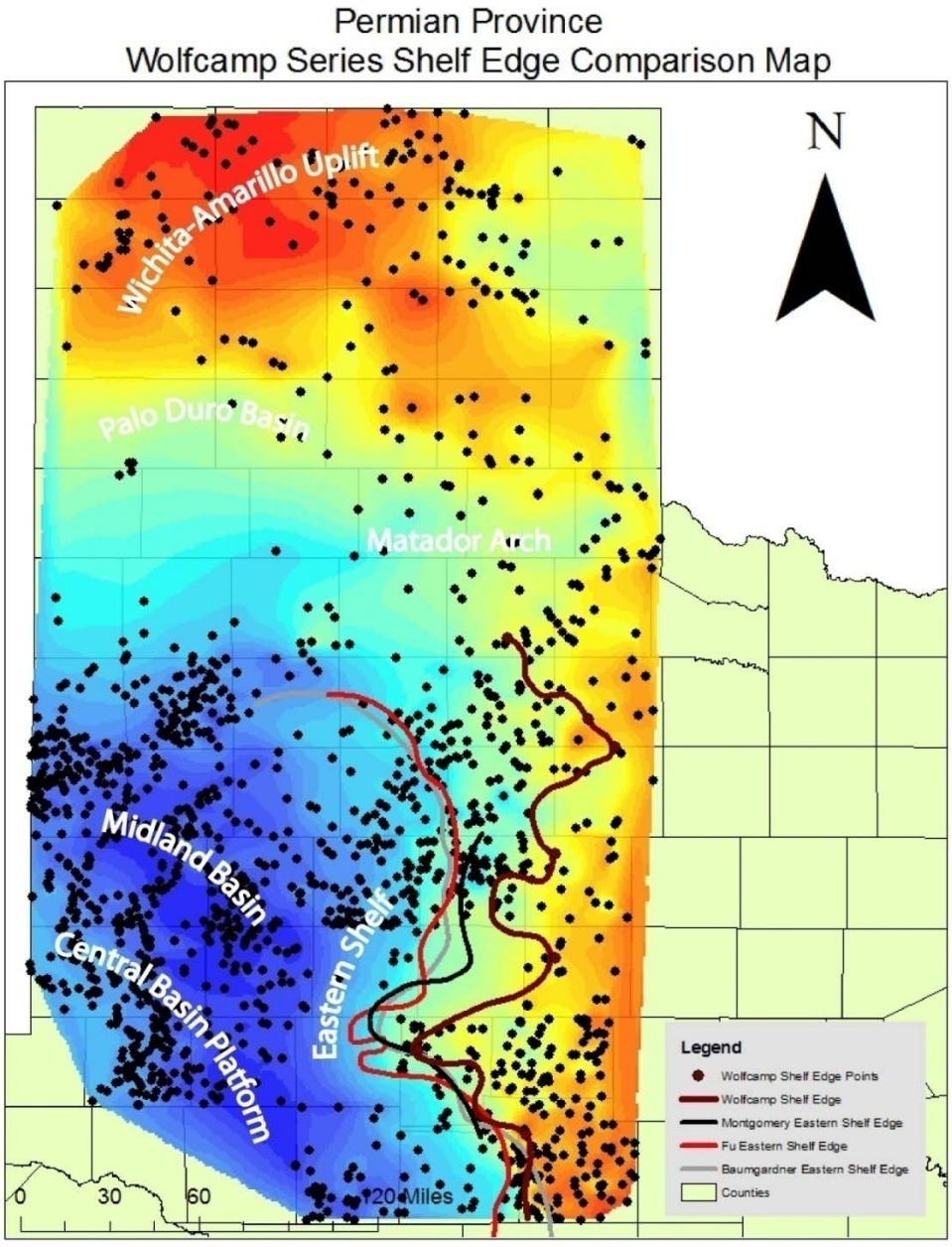


Figure 4.3. A map detailing the comparisons of the constructed Wolfcamp shelf against the shelf edges from literature by Montgomery (1996) in black, Fu (2011) in red, and Baumgardner (2016) in grey.

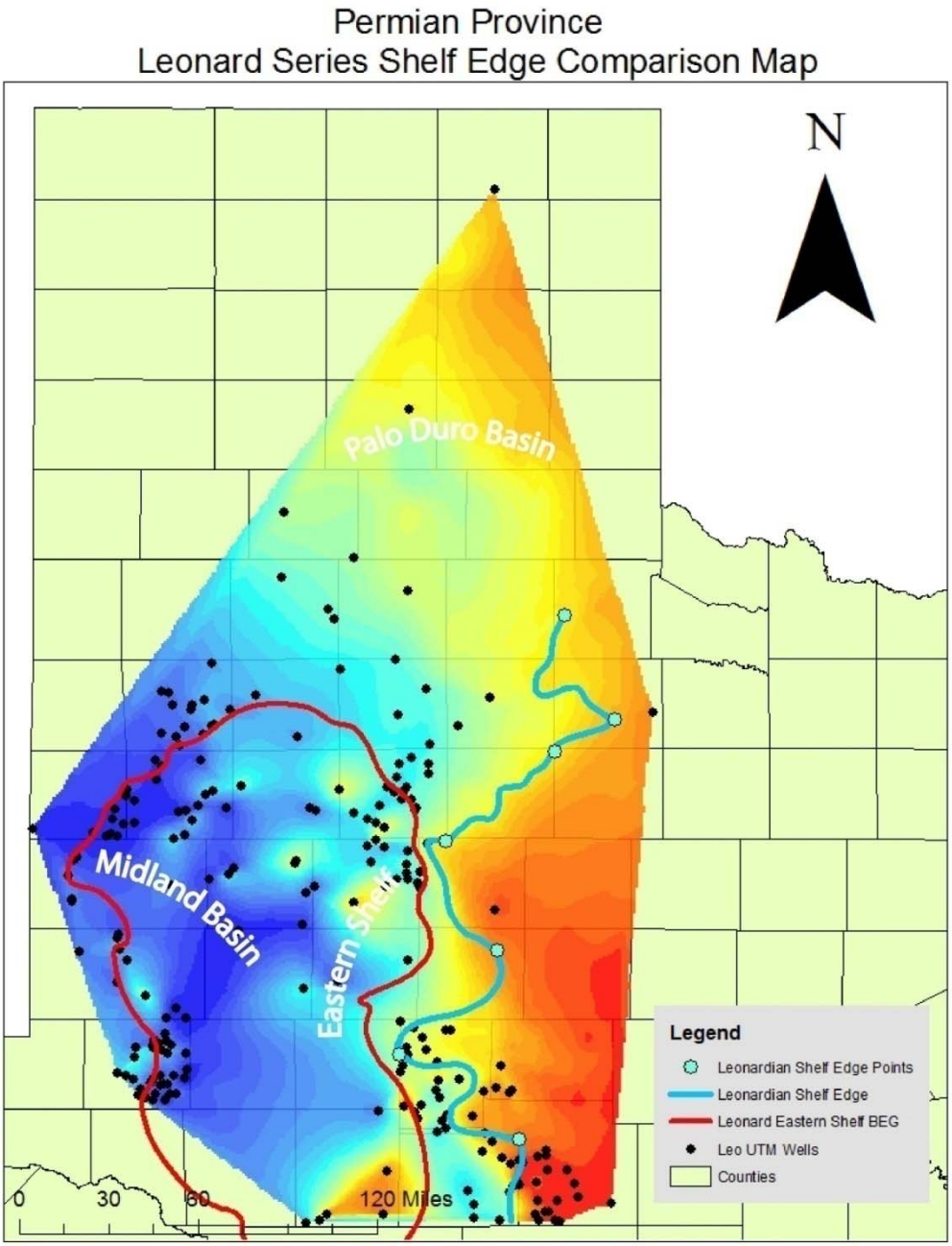


Figure 4.4. A map detailing the comparison of the constructed Canyon series shelf edge against the BEG's paleogeographic shelf edge from their 2008 Permian Basin Synthesis Project maps.

*Comparison Summary*

Creating a map from lithological data does not take into account the potential time transgressive character of facies, while use of fusulinid correlation does. Consistent across all comparisons is that the literature shelf-edge location almost always produces an comparison ratio greater than one, indicating that the PABZT shelf edge is nearly always in a more westward position. The reason for this is not clear. However, there also appears to be some differences from the northern to southern portions of eastern shelf, as well as variance between Pennsylvanian and Permian paleogeographic maps. The Pennsylvanian-aged paleogeographic maps matched better than the Permian-aged paleogeographic maps, which is likely a result of incorporating the lithologically based Wolfcamp well markers that reside outside of the biostratigraphically defined Wolfcampian series. Variance from north-to-south may occur due to the loss of chronostratigraphic significance when lithologically correlating thicker packages of strata in the south to thinner northern strata.

## PROGRADATION/AGGRADATIONAL CONTROLS ON THE EASTERN SHELF

Plotting the location of the shelf edge through time allows assessment of the basin filling history. In this section, the position of the shelf edge on each cross section is noted and cross plotted versus its corresponding age. The datum that all distances were measured from was the position of the Leonardian shelf edge along each cross section. Cross sections E, G, and A are denoted as the northern region of the eastern shelf of the Midland Basin. Cross sections B, C, and D are denoted as the southern region of the Eastern Shelf.

In the Pennsylvanian, the northern region largely reflected aggradation of the shelf with a minor Late Pennsylvanian backstepping event recorded in the northern most area (Fig. 4.5, Fig. 4.9, Fig. 4.10). This shelf-stacking pattern indicates that rate of accommodation creation via subsidence and eustasy was similar to the rate of sediment

supply. However, in the early Permian, the shelf edge at all locations in the northern region moved 65-78 kilometers westward, indicating that sediment supply greatly outpaced the rate of accommodation creation.

In the Pennsylvanian, the southern region exhibited aggradation with a very minor backstepping event observed at cross section B (Fig. 4.6). This reflects that the rate of accommodation creation was in pace with the rate of sediment supply for the time period. Cross section C is the only locale to record a significant shift of the shelf edge position, beginning during the Virgilian. In the early Permian, the shelf edge prograded 80 kilometers landward throughout the entire region. Comparing these values to the northern region, cross sections C and A had similar large-scale events during the Virgilian, both recording magnitudes of 78-80 kilometers of shelf movement.

The controls on accommodation are a combination of sediment supply, eustasy, and subsidence. Across both the north and south regions, large-scale progradation occurred in the in the very late Pennsylvanian and early Permian. Eustatic curves produced for the early Permian suggest that sea level was fairly stable (Haq, 2005) or rising (Vail et al. 1977). Thus, a sea level forced regression is not a viable mechanism for the large magnitude of progradation observed in the early Permian. A scenario invoking a large increase in the rate of sediment supply as the mechanism for progradation seems unlikely given that the Wichita-Amarillo uplift was buried in the Wolfcampian (Soreghan et al. 2012) and climate was significantly drying (e.g. Tabor and Poulsen, 2008). A drier climate and reduced upland regions should result in a lower rate of sediment supply, yet progradation of the shelf indicates that even with a reduced sediment supply rate still outpaced accommodation. Thus, it is likely that the progradation was driven by a reduction in the rate of subsidence, indicating that early Permian subsidence was minimal. Elsewhere in western equatorial Pangaea, subsidence in basins was waning at the Pennsylvanian-Permian boundary (Soreghan et al. 2012), which if applied to the Midland Basin would result in decreased accommodation and the resultant large-scale progradation of the shelf. Other workers have also proposed decreased tectonic activity during the Late Pennsylvanian (Silver and Todd, 1969; Wright, 2008a) such that by the Leonardian times tectonism had ceased completely (Handford, 1981).

Further evidence for the aggradation during the Pennsylvanian and the progradation in the Permian is highlighted in isopach maps of the Permian Region. Figure 4.11 shows that during the upper Pennsylvanian, the center of the basin was starved, as indicated by the warm colors in the center of the image, showing thin sediment deposition. In the Upper Pennsylvanian-early Permian map, (Fig. 4.12) the center of the basin exhibits darker blue colors, indicating an increase in thickness of strata in that location, most likely from the progradation and sediment that was forced into the center of the basin from the subsidence shut-off. So, the thickness patterns during the late Pennsylvanian and early Permian correlate with the shelf edge patterns observed thus far.

Some other factors that influenced general aggradation in the Midland Basin were "structural downwarping" events during the late Desmoinesian (Wright, 2008a). This tectonic activity resulted in the creation of a deep-water region in the Midland Basin, between 500 and 2,000 feet, which increased accommodation space and allowed for aggradation of existing sediments (Wright, 2008a). Some sediment troughs were also created as a result of this downwarping, and may have funneled more material from the eastern shelf towards the center of the Midland Basin, from Knox and Baylor counties to Mitchell, Fisher, and Lubbock counties, which can be seen in the boxed area on Figure 3.5 (Wright, 2008a). This continued subsidence also assisted with the creation of the Horseshoe Atoll near Hockley County. Increased subsidence rates played a major role in the Permian Province during the Missourian and the Virgilian, but decreased in frequency during the beginning of the Permian (Wright, 2008b).

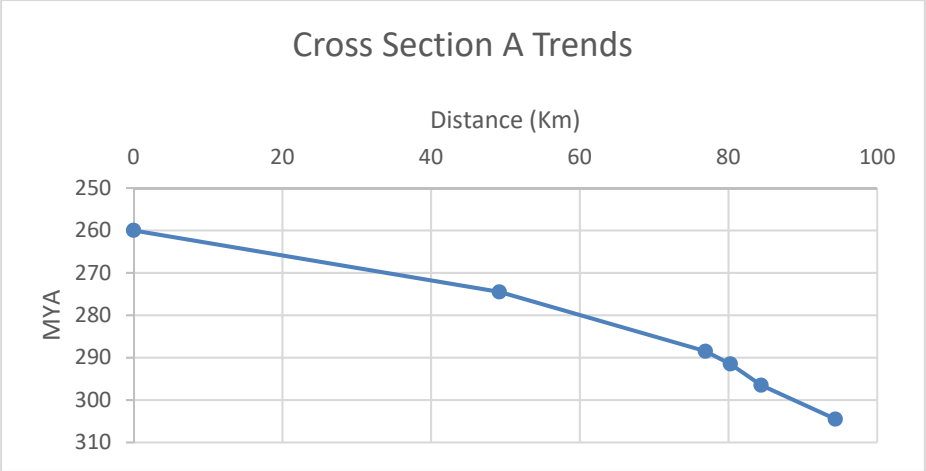


Figure 4.5. Figure 4.5 shows progradational and aggradational trends of the eastern shelf of the Midland Basin along cross section A, which is along the northern end of the shelf. The x-axis represents the distance the shelf edge moved compared against the surface (Atokan-Leonardian). The y-axis represents millions of years, with the bottom of the axis representing the oldest time (end of Atokan), and the top of the axis being the youngest time (end of Leonardian).

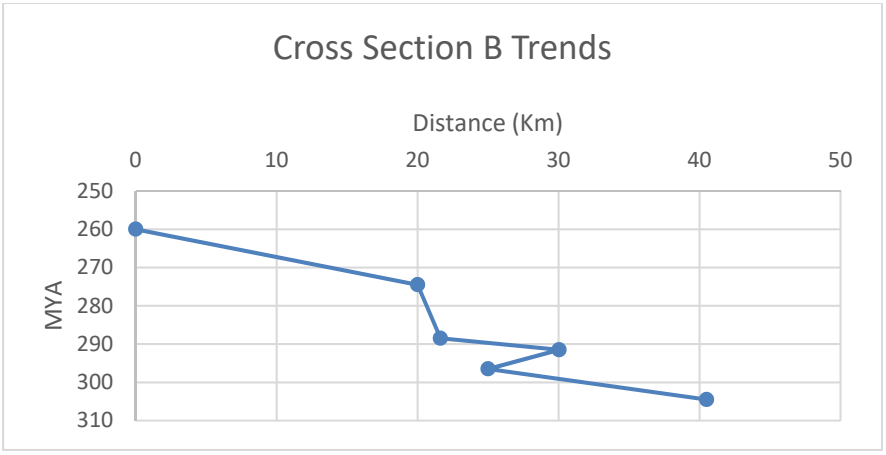


Figure 4.6. Figure 4.6 shows the progradational and aggradational trends of the eastern shelf of the Midland Basin along cross section B, which is 52 kilometers away from cross section A, and located in the middle of the eastern shelf. The axis represents the distance the shelf edge moved compared against the surface (Atokan-Leonardian). The y-axis represents millions of years, with the bottom of the axis representing the oldest time (end of Atokan), and the top of the axis being the youngest time (end of Leonardian).

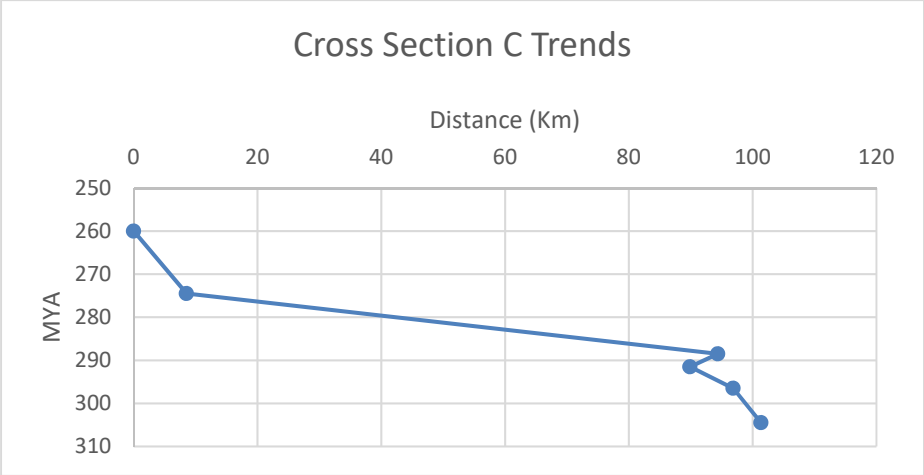


Figure 4.7. Figure 4.7 shows the progradational and aggradational trends of the eastern shelf of the Midland Basin along cross section C, which is 50 kilometers away from cross section B, and located in the southern portion of the eastern shelf. The axis represents the distance the shelf edge moved compared against the surface (Atokan-Leonardian). The y-axis represents millions of years, with the bottom of the axis representing the oldest time (end of Atokan), and the top of the axis being the youngest time (end of Leonardian).

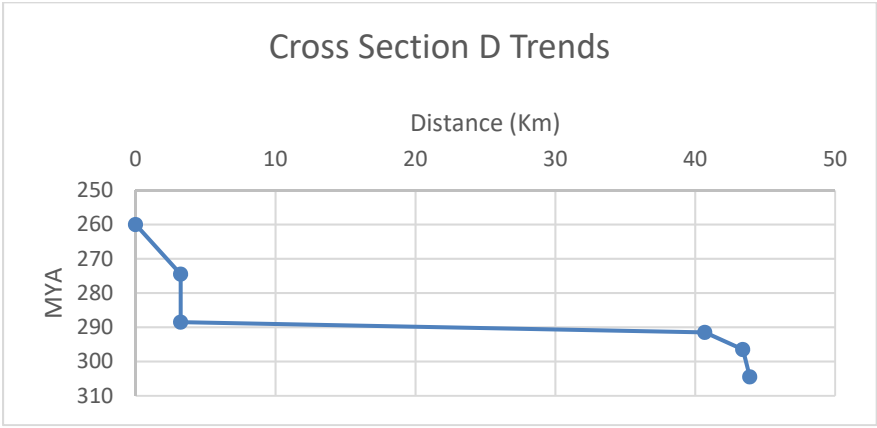


Figure 4.8. Figure 4.8 shows the progradational and aggradational trends of the eastern shelf of the Midland Basin along cross section D, which is 57 kilometers away from cross section C, and located in the southern portion of the eastern shelf. The axis represents the distance the shelf edge moved compared against the surface (Atokan-Leonardian). The y-axis represents millions of years, with the bottom of the axis representing the oldest time (end of Atokan), and the top of the axis being the youngest time (end of Leonardian).

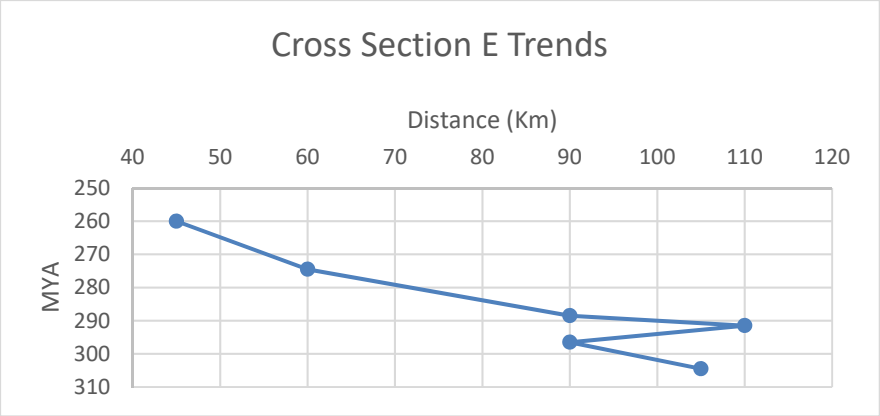


Figure 4.9. Figure 4.9 shows the progradational and aggradational trends of the eastern shelf of the Midland Basin along cross section E, which is 60 kilometers away from cross section F, and located in the southern portion of the eastern shelf. The axis represents the distance the shelf edge moved compared against the surface (Atokan-Leonardian). The y-axis represents millions of years, with the bottom of the axis representing the oldest time (end of Atokan), and the top of the axis being the youngest time (end of Leonardian).

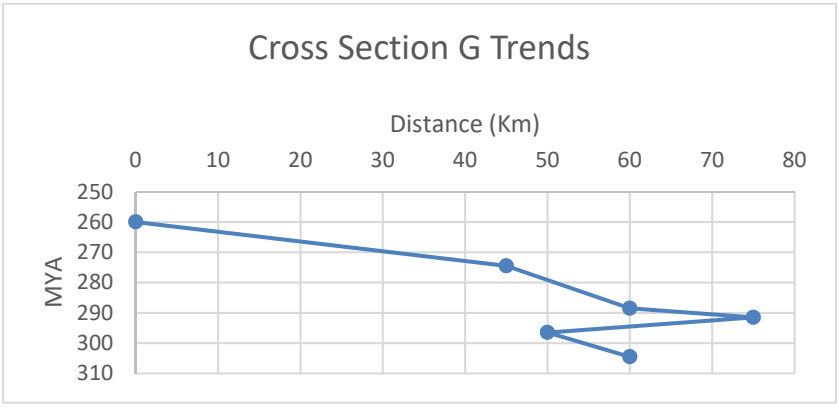


Figure 4.10. Figure 4.10 shows the progradational and aggradational trends of the eastern shelf of the Midland Basin along cross section G, which is 54 kilometers away from cross section A, and located in the southern portion of the eastern shelf. The axis represents the distance the shelf edge moved compared against the surface (Atokan-Leonardian). The y-axis represents millions of years, with the bottom of the axis representing the oldest time end of Atokan), and the top of the axis being the youngest time (end of Leonardian).

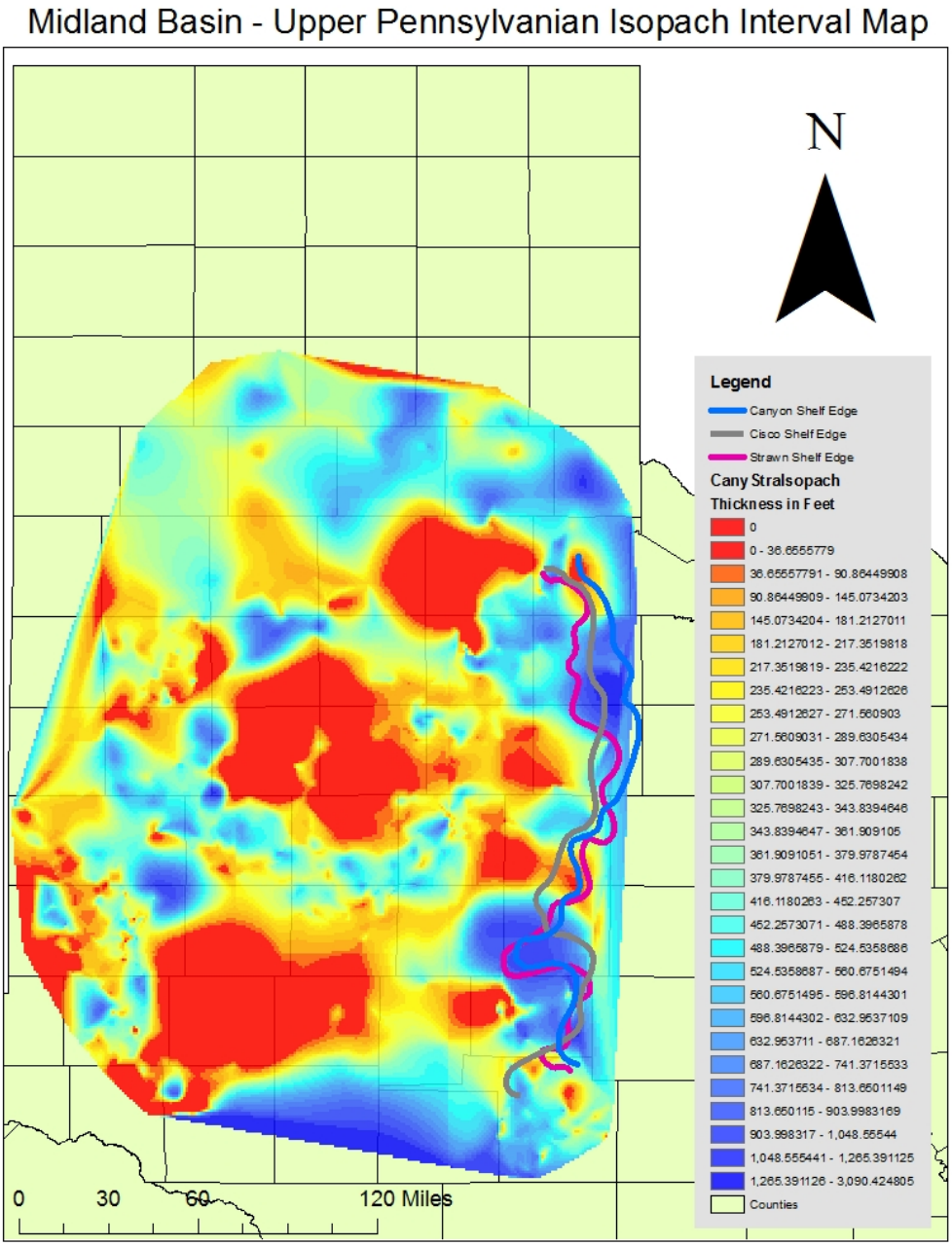


Figure 4.11. An isopach map of the Upper Strawn to the Canyon Series in the Midland Basin. The red and yellow colors indicate thin areas of sediment deposition, while the blue and green colors represent the thick areas of sediment deposition.

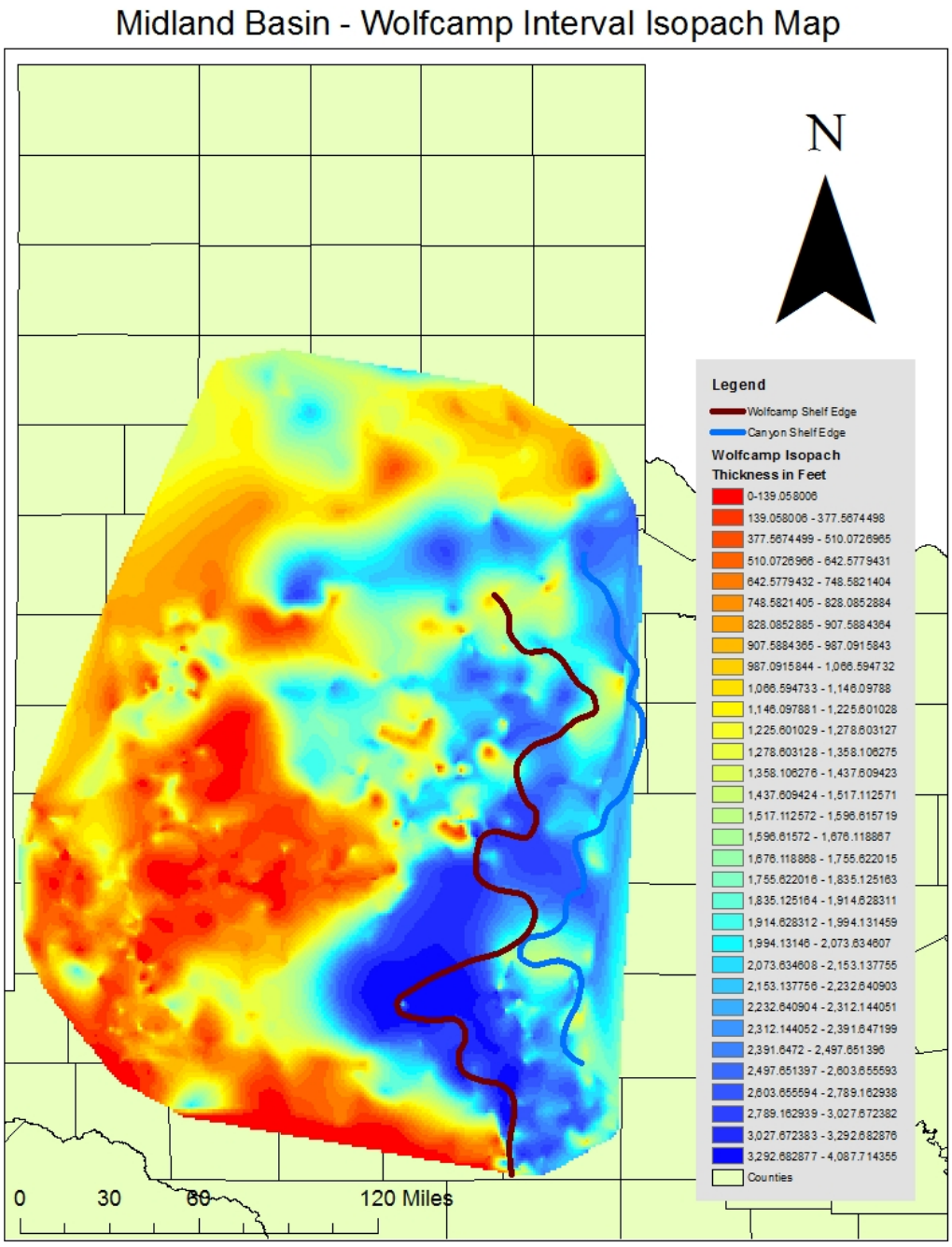


Figure 4.12. An isopach map of the Upper Pennsylvanian to Lower Permian Series in the Midland Basin. The red and yellow colors indicate thin areas of sediment deposition, while the blue and green colors represent the thick areas of sediment deposition.

# CHAPTER V

# CONCLUSIONS

This project aimed to create a set of paleogeographic maps of the Permian Province and Midland Basin through fusulinid occurrences at well sites, and hang those values a sea-level datum. From these maps, the goal was to identify where the shelf edge was along the eastern shelf of the Midland Basin, and observe its progression through the Pennsylvanian and Permian. The other major goal of this project was to compare shelf edges to other positions developed by lithologically based maps, and contrast the accuracy of biostratigraphy versus lithology for tracking shelf edge growth.

The chronostratigraphic framework developed as a result of constructed paleogeographic maps indicates that biostratigraphy matches with previous literature only up to a point. The comparison ratios showed that the Pennsylvanian reconstructions (Cisco and Canyon) matched well to the BEG's literature on the Permian Province, while the Permian reconstructions (Wolfcamp and Leonard) did not. Some reasons for this may be due to the thicknesses of the stratal units during the Pennsylvanian, and the ease at correlation between the northern and southern regions. The Permian reconstructions correlated poorly with the existing literature, including Fu (2011), Baumgardner (2016), and Montgomery (1996), and this may be due to the correlation of Wolfcamp A, which has been revealed as representing the top of the Leonardian section instead. The reason for the poor Leonardian correlation may have been due to the sparse amount of well locations documented on the eastern shelf, which influenced the lacking correlation between the reconstruction and the literature.

During the Pennsylvanian, several large aggradational events were recorded in both locations, and included ~ 80 kilometers of shelf movement. During the late Pennsylvanian to early Permian, the shelf edge prograded significantly more in the northern and southern regions, and moved between 65-78 kilometers, indicating that a significant progradational event across the study area. The increased subsidence around the eastern region of the Midland Basin majorly influenced the aggradational trends seen

along the southern region of the shelf. Other controls on the basin were structural downwarping, paleo-climate, and sediment supply from highlands outside of the shelf.

## ERROR DISCUSSION

There were several aspects of this research that bear discussion regarding error, as they play a pivotal role in shaping the data produced from the biostratigraphic reports, the chronostratigraphic intervals, and the topographic profiles. Some human error that resulted from the methodology of this research included the measuring of the well locations through Google Earth, the selection of the flexure points along the topographic profiles, and the discernment of the fusulinid genera that composed the biostratigraphic reports. These errors could have potentially skewed the location of the wells, as well as the distribution of the chronostratigraphic intervals throughout the Texas Panhandle.

## FURTHER RESEARCH

Further research could investigate why the Leonardian and Wolfcampian surfaces diverged with the established literature to such a degree, and how fusulinid occurrences may have influenced the conservative values of the position of the eastern shelf. Some further projects that could develop after this research include developing an interactive database with the biostratigraphic reports hyperlinked to every well location in the Permian Province, which would prove invaluable to those in the oil industry and other academic institutions.

# BIBLIOGRAPHY

Algeo, T. J. (1992). Continent-scale wrenching of southwestern Laurussia during the Ouachita Marathon orogeny and tectonic escape of the Llano block, in Lindsay, R. F., and Reed, L. R., eds., Sequence stratigraphy applied to Permian basin reservoirs: outcrop analogs in the Caballo and Sacramento Mountains of New Mexico: *West Texas Geological Society, Field Seminar Guidebook*, 92, 115-131.

Baumgardner, R. (2012). Wolfberry Play, Midland Basin, West Texas: Regional Stratigraphy. Lecture presented at Forth Worth Geological Society in Fort Worth, Texas. Retrieved from http://www.searchanddiscovery.com/pdfz/documents/2012/10419hamlin/ndx_hamlin.pdf.html.

Baumgardner, R. (2014). High Resolution Core Studies of Wolfcamp/Leonard Basinal Facies, Southern Midland Basin, Texas. Poster presented at West Texas Geological Society in Midland, Texas. Retrieved from http://www.searchanddiscovery.com/documents/2014/10607baumgardner/ndx_baumgardner.pdf

Baumgardner, R. (2016). An early Permian coastal flora dominated by *Germaropteris martinsii* from basinal sediments in the Midland Basin, West Texas. *Palaeogeography, Palaeoclimatology, Palaeoecology,* 459, 409-422.

BEG, (2008). Permian Basin Synthesis Project; The University of Austin, Bureau of Economic Geology. Retrieved from http://www.beg.utexas.edu/research/areas/permian-basin-synthesis.

Blakey, R. (2011). North American Paleogeographic Maps: Late Pennsylvanian (300Ma). Retrieved from https://www2.nau.edu/rcb7/nam.html.

Boring, T. H. (1993). Upper Strawn (Desmoinesian) carbonate and clastic depositional environments, Southeast King County, Texas, in Johnson, K. S., and Campbell, J. A., eds*., Petroleum-reservoir geology in the southern Midcontinent, 1991 symposium: University of Oklahoma*, p. 195–198.

Brown, Jr. L.F., A.W. Cleaves II, and A.W. Erxleben. (1973). Pennsylvanian depositional systems in North-Central Texas: A guide for interpreting terrigenous clastic facies in a cratonic basin: The University of Texas at Austin, Bureau of Economic Geology, Guidebook, 14, 122 p.

Candelaria, M. P. (1990). "Atoka" detrital a subtle stratigraphic trap in the Midland Basin, in Flis, J. E., and Price, R. C., eds., *Permian Basin oil and gas fields; innovative ideas in exploration and development: West Texas Geological Society*, 90-87, 104–106.

Cleaves, A. W. (2000). Sequence stratigraphy and reciprocal sedimentation in Middle and Late Pennsylvanian carbonate-bank systems, eastern shelf of the Midland Basin, north-central

Texas, in Johnson, K. S., ed., *Platform carbonates in the southern Midcontinent, 1996 symposium: University of Oklahoma*, 101, 227–257.

Dunbar, C. (1942). Pennsylvanian Fusulinidae of Illinois. *State of Illinois Registration and Education Bulletin*, 67, 218 p.

Dutton, S. P., Kim, E. M., Broadhead, R. F., Raatz, W. D., Breton, C. L., Ruppel, S. C., & Kerans, C. (2005). Play analysis and leading-edge oil-reservoir development methods in the Permian basin: Increased recovery through advanced technologies. *AAPG Bulletin*, *89*(5), 553-576.

Flamm, D. (2008*). Wolfcampian Development of the Nose of the Eastern Shelf of the Midland Basin, Glasscock, Sterling, and Reagan Counties, Texas* (Unpublished master's thesis). Brigham Young University, 64 p.

Fu, Q. (2011, March 08). A synthesis of the Wolfcampian platform carbonate system in the Permian Basin region. Lecture presented at West Texas Geological Society in Midland, Texas. Retrieved from http://www.wtgs.org/media/files/None/Synthesis-of-the-Wolfcampian-Platform.pdf.

Galley, J. E. (1958). Oil and geology in the Permian Basin of Texas and New Mexico, in Weeks, L. G., ed., Habitat of oil: *American Association of Petroleum Geologists Special Publication*, 395–446.

Handford, C.R. (1981). Sedimentology and genetic stratigraphy of Dean and Spraberry formations (Permian), Midland Basin, Texas: *AAPG Bulletin*, 65/9, 1602-1616.

Hamlin, H. S., & Baumgardner, R. W. (2012). Wolfberry (Wolfcampian-Leonardian) Deep-water Depositional Systems in the Midland Basin: Stratigraphy, Lithofacies, Reservoirs, and Source Rocks. Report of Investigations, *Bureau of Economic Geology, University of Texas at Austin*, 277, 1-61.

Haq, B.U. and Schutter, S.R. (2008). A Chronology of Paleozoic Sea Level Changes, *Science*, 5898, 64-68. Retrieved from http://science.sciencemag.org/content/322/5898/64.

Hentz, T. et. al. (2016). Upper Pennsylvanian and Lower Permian Shelf-to-Basin Facies Architecture and Trends, Eastern Shelf of the Southern Midland Basin, West Texas. Poster presented to AAPG Southwest Section Convention in Abilene, Texas. Retrieved from http://www.searchanddiscovery.com/documents/2016/10847hentz/ndx_hentz.pdf.

Hillier, R. (2015). *Formation Evaluation of Leonardian Strata within the Northern Spraberry Trend, West Texas* (Unpublished master's thesis). Montana State University, 191 p.

Hopkins, K. W., and Ahr, W. M. (1985). Reconstruction of the paleoenvironments of Jameson (Strawn) Reef Field, Coke County, Texas, in *Transactions of the 35th annual meeting of the Gulf Coast Association of Geological Societies AAPG regional meeting and the 32nd annual meeting of the Gulf Coast Section of the Society of Economic Paleontologists and Mineralogists*, 35,117–124.

Janson, X., and Kerans, C. (2007). Day 4: Deeper water mud mounds and crinoidal turbidites—Mississippian Lake Valley Formation, Sacramento Mountains—analog for Cisco reservoir in SACROC and Cogdell, in Kerans, C., Janson, X., and Bellian, J., Linking depositional, diagenetic, facies, stratal geometries and cycle architecture: examples for Paleozoic carbonate systems of West Texas and southern New Mexico: The University of Texas at Austin, Bureau of Economic Geology, RCRL Spring Field Course Guide, 111–161.

Kluth, C.F., and Coney, P.J. (1981). Plate tectonics of the Ancestral Rocky Mountains: *Geology*, 9,10–15,

Kluth, C.F. (1986). Plate tectonics of the Ancestral Rocky Mountains, in J.A. Peterson, ed., *Paleotectonics and sedimentation in the Rocky Mountain region*: *AAPG Memoir* 41, 353-369.

Kohn, J. (2016). *Late Pennsylvanian (Virgilian) to Early Permian (Leonardian) conodont biostratigraphy of the "Wolfcamp Shale," northern Midland Basin, Texas* (Unpublished Master's Thesis). Texas Tech University.

Landreth, R. (1977*). Depositional Environments and Diagenesis of the Lower Clear Fork Group, Mitchell County, Texas* (Unpublished Master's Thesis).Texas Tech University.

Marshall, J. (1952). Spraberry reservoir of West Texas. AAPG Bulletin, 35, 4, 899-915. Retrieved from http://archives.datapages.com/data/bulletns/1949-52/data/pg/0036/0011/2150/2189.htm.

Mazzullo, S. J., and Reid, A. M. (1989). Lower Permian platform and depositional systems, Northern Midland Basin, Texas: *in* Crevello, Paul D., Wilson, J. J., Sarg, J. F., and Read, J. F., (eds.), Controls on carbonate platform and basin development: *Society of Economic Paleontologists and Mineralogists Special Publication*, 44, 305-320.

Midland Subsurface Library, (2017). Permian Basin Map. Retrieved from http://www.subsurface.info/Permian_Basin_Map.html.

Mongtomery, S.L. (1996). Permian "Wolfcamp" Limestone Reservoirs: Powell Ranch Field, Eastern Midland Basin. *AAPG Bulletin*, 80, 9, 1349-1365.

Myers, D. A. (1982). Stratigraphic summary of Pennsylvanian and Lower Permian rocks, Manzano Mountains, New Mexico. *Albuquerque country II: New Mexico Geological Society, Guidebook*, *33*, 233-237.

Reid, A.M., et al. (1989). "Refined Fusulinid Biostratigraphic Zonations of Wolfcampian and Lower Leonardian Strata in Permian Basin". *AAPG Southwest Section Meeting*, San Angelo, Texas.

Ruppel, S. C., W. B. Ward, E. E. Ariza, and J. W. Jennings, Jr. (2000). Cycle and sequence stratigraphy of Clear Fork reservoir-equivalent outcrops: Victorio Peak Formation, Sierra Diablo, Texas, in R. Lindsay, R. Trentham, R. F. Ward, and A. H. Smith, eds., *Classic Permian geology of West Texas and Southeastern New Mexico, 75 years of Permian*

*Basin oil & gas exploration & development: West Texas Geological Society Publication* 00-108, 109–130.

Ruppel, S. C., and Jones, R. H. (2004). Facies, sequence stratigraphy and porosity development in the Fullerton Clear Fork reservoir, in Ruppel, S. C., ed., 7 Multidisciplinary imaging of rock properties in carbonate reservoirs for flowunit targeting: *The University of Texas at Austin, Bureau of Economic Geology, final technical report prepared for U.S. Department of Energy,*120 p.

Saller, A. H., Dickson, J. A. D., and Boyd, S. A. (1994). Cycle stratigraphy and porosity in Pennsylvanian and Lower Permian shelf limestones, eastern Central Basin Platform, Texas: *American Association of Petroleum Geologists Bulletin*, v. 78, no. 12, p. 1820-1842.

Saller, A. (2014). Late Pennsylvanian and Early Permian Sedimentation on the Central Basin Platform and Implications to the Wolfberry Deposition in the Western Midland Basin. *AAPG 2014 Southwest Section Annual Convention. Midland, Texas*. Retrieved from http://www.searchanddiscovery.com/documents/2014/10606saller/ndx_saller.pdf.

Schatzinger, R. A. (1987). Depositional environments and diagenesis of the eastern portion of the Horseshoe Atoll, West Texas (unpublished master's thesis). The University of Texas at Austin, Department of Geological Sciences, 340 p.

Silver, B., Todd, R. (1969). Permian Cyclic Strata, Northern Midland and Delaware Basins, West Texas and Southeastern New Mexico. *The American Association of Petroleum Geologists Bulletin*. Retrieved from http://rockfractureandstress.com/BurnettRanchPermianCyclicStrataNorthernMidlandandDelawareBasins,WestTexasandSoutheasternNewMexico.pdf.

Soreghan, G. S., Keller, G. R., Gilbert, M. C., Chase, C. G., & Sweet, D. E. (2012). Load-induced subsidence of the Ancestral Rocky Mountains recorded by preservation of Permian landscapes. *Geosphere*, 8(3), 654-668.

Tabor, N.J, Poulson, C.J. (2008). Late Paleozoic tropical climate and atmospheric circulation: A review of paleoclimate indicators and models: *Palaeogeography, Palaeoclimatology, Palaeoecology*, 268, 181–192.

Tai, P. -C, and Dorobek, S. L. (2000). Tectonic model for late Paleozoic deformation of the Central Basin Platform, Permian Basin region, West Texas, in DeMis, W. D., Nelis, M. K., and Trentham, R. C., eds*., The Permian Basin: proving ground for tomorrow's technologies: West Texas Geological Society*, 109, 157–176.

Thompson, M.L. (1948). *Protozoa, Article 1*. University of Kansas Publications, 184 p.

Thompson, M. L. (1950). Pennsylvanian Fusulinids of the South-Central Wasatch Mountains, Utah. *Journal of Paleontology,* 24(4): 35 p.

Troschinetz, J., and Loucks, R. G. (1991). Reservoir quality distribution in the Pennsylvanian Bend Conglomerate fan-delta system off the southeastern Central Basin Platform, in

Candelaria, M. P., ed., Permian Basin plays; tomorrow's technology today: *West Texas Geological Society Bulletin*, 1, 163 p.

Vail, P.R., et. al. (1977). Seismic stratigraphy and global changes of sea level, *Seismic Stratigraphy -- applications to hydrocarbon exploration: AAPG Memoir* 26, 49-212.

Vest, E. L. (1970). Oil fields of Pennsylvanian-Permian Horseshoe Atoll, west Texas, in M. Halbouty, ed., Geology of giant petroleum fields: *AAPG Memoir* 14, 185–203.

Wahlman, G. P. (1998). Fusulinid biostratigraphy of the new Pennsylvanian-Permian boundary in the southwest and midcontinent USA. Geological Society of America, South-central Section Meeting. In *Abstracts with Programs*, 30, 3, 34.

Wahlman, G.P. (2013). Pennsylvanian to Lower Permian (Desmoinesian-Wolfcampian) fusulinid biostratigraphy of Midcontinent North America. *Stratigraphy* v. 10, 73-104p.

Ward, R., Kendall, C. G. and Harris P. M. (1986). Upper Permian (Guadalupian) facies and their association with hydrocarbons Permian Basin, West Texas and New Mexico: *American Association of Petroleum Geologists Bulletin*, 70, 239–262.

Wilde, G. (2004). Practical Fusulinid Zonation; the species concept; with the Permian Basin emphasis. *WTGS Bulletin*. V. 44, 1,5-23.

Wright, W. (2008a). Depositional History of the Atokan Succession (Lower Pennsylvanian) in the Permian Basin. *Bureau of Economic Geology, the University of Texas at Austin*, 67 p.

# APPENDIX 1

TOPOGRAPHIC CROSS SECTION PROFILES

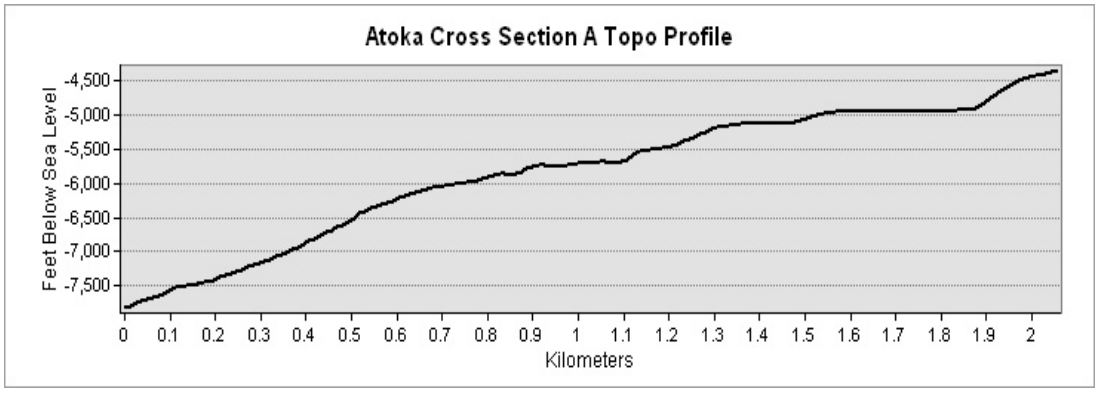


Description: -- The topographic profile of the Atoka Chronostratigraphic map along cross section A. Note that is it difficult to define the point of flexure to represent the shelf edge, and subsequently no quantitative shelf edge was mapped for this surface and time interval. The x-axis distance along the cross section is measured in tens of kilometers, e.g. .20=20 kilometers. The y-axis represents thousands of feet below sea level. Shallower sub-sea depths represent the top of the y-axis, and deeper sub-sea depths represent the bottom of the y-axis.

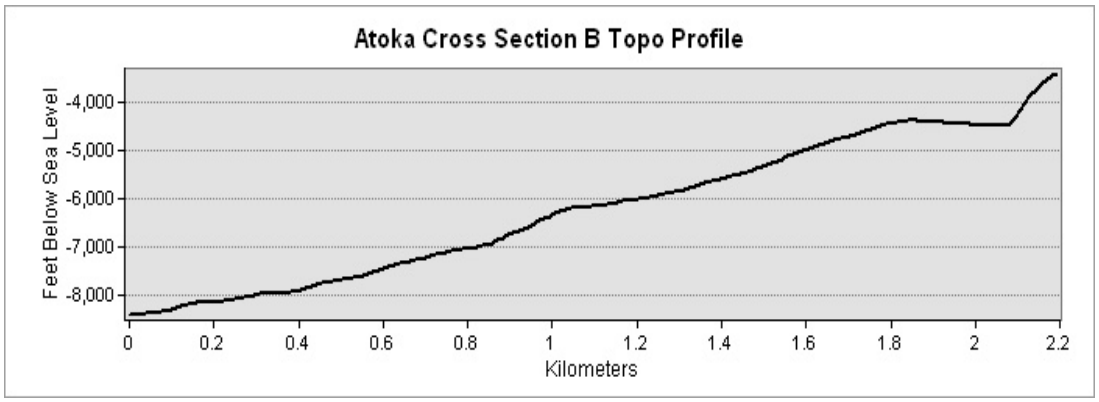


Description: -- The topographic profile of the Atoka Chronostratigraphic map along cross section B. Note that is it difficult to define the point of flexure to represent the shelf edge, and subsequently no quantitative shelf edge was mapped for this surface and time interval. The x-axis distance along the cross section is measured in tens of kilometers, e.g. .20=20 kilometers. The y-axis represents thousands of feet below sea level. Shallower sub-sea depths represent the top of the y-axis, and deeper sub-sea depths represent the bottom of the y-axis.

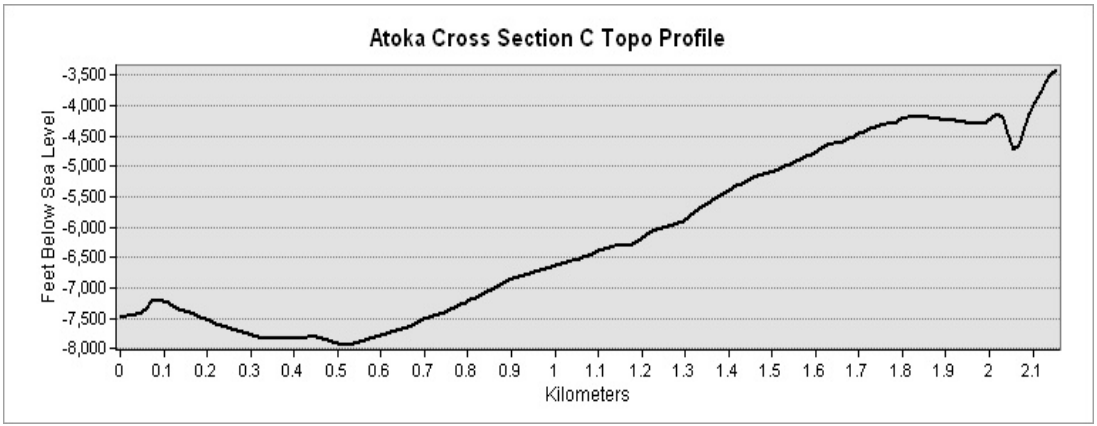


Description: -- The topographic profile of the Atoka Chronostratigraphic map along cross section C. Note that is it difficult to define the point of flexure to represent the shelf edge, and subsequently no quantitative shelf edge was mapped for this surface and time interval. The x-axis distance along the cross section is measured in tens of kilometers, e.g. .20=20 kilometers. The y-axis represents thousands of feet below sea level. Shallower sub-sea depths represent the top of the y-axis, and deeper sub-sea depths represent the bottom of the y-axis.

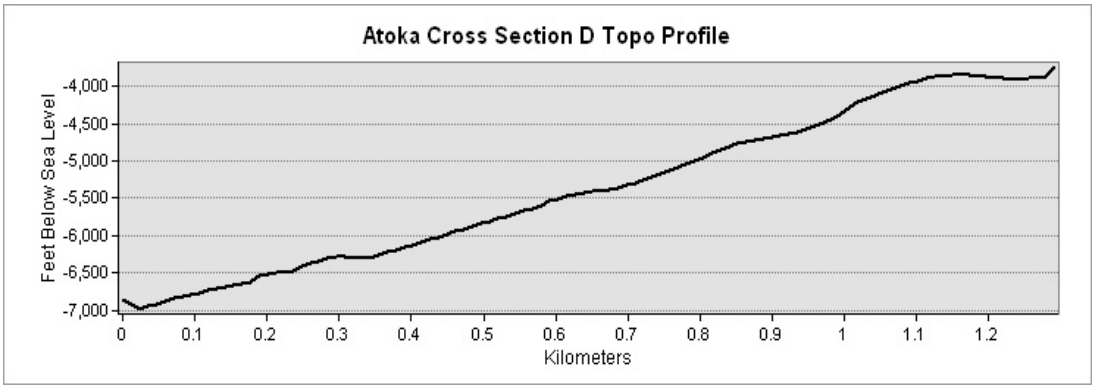


Description: -- The topographic profile of the Atoka Chronostratigraphic map along cross section D. Note that is it difficult to define the point of flexure to represent the shelf edge, and subsequently no quantitative shelf edge was mapped for this surface and time interval. The x-axis distance along the cross section is measured in tens of kilometers, e.g. .20=20 kilometers. The y-axis represents thousands of feet below sea level. Shallower sub-sea depths represent the top of the y-axis, and deeper sub-sea depths represent the bottom of the y-axis.

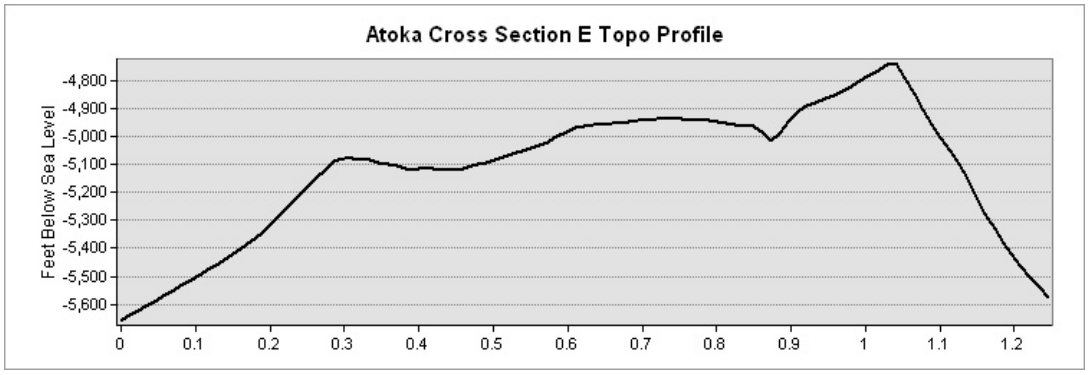


Description: -- The topographic profile of the Atoka Chronostratigraphic map along cross section E. Note that is it difficult to define the point of flexure to represent the shelf edge, and subsequently no quantitative shelf edge was mapped for this surface and time interval. This cross section was drawn along the width of the Midland Basin, and looks to illustrate the rough eastern and western edges of the basin. The x-axis distance along the cross section is measured in tens of kilometers, e.g. .20=20 kilometers. The y-axis represents thousands of feet below sea level. Shallower sub-sea depths represent the top of the y-axis, and deeper sub-sea depths represent the bottom of the y-axis.

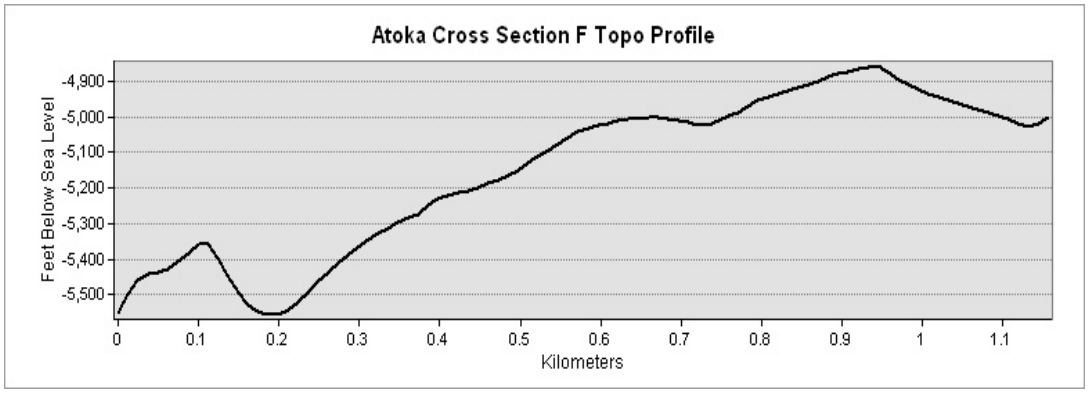


Description: -- The topographic profile of the Atoka Chronostratigraphic map along cross section F. Note that is it difficult to define the point of flexure to represent the shelf edge, and subsequently no quantitative shelf edge was mapped for this surface and time interval. The x-axis distance along the cross section is measured in tens of kilometers, e.g. .20=20 kilometers. The y-axis represents thousands of feet below sea level. Shallower sub-sea depths represent the top of the y-axis, and deeper sub-sea depths represent the bottom of the y-axis.

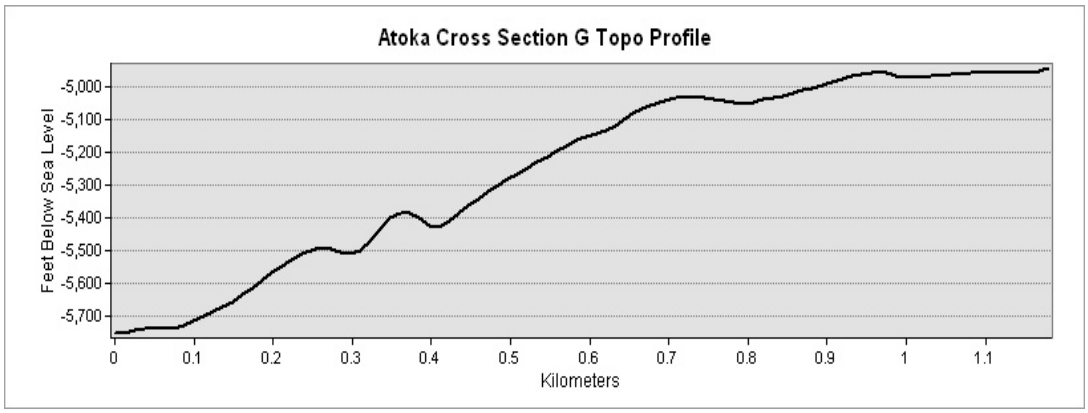


Description: -- The topographic profile of the Atoka Chronostratigraphic map along cross section G. Note that is it difficult to define the point of flexure to represent the shelf edge, and subsequently no quantitative shelf edge was mapped for this surface and time interval. The x-axis distance along the cross section is measured in tens of kilometers, e.g. .20=20 kilometers. The y-axis represents thousands of feet below sea level. Shallower sub-sea depths represent the top of the y-axis, and deeper sub-sea depths represent the bottom of the y-axis.

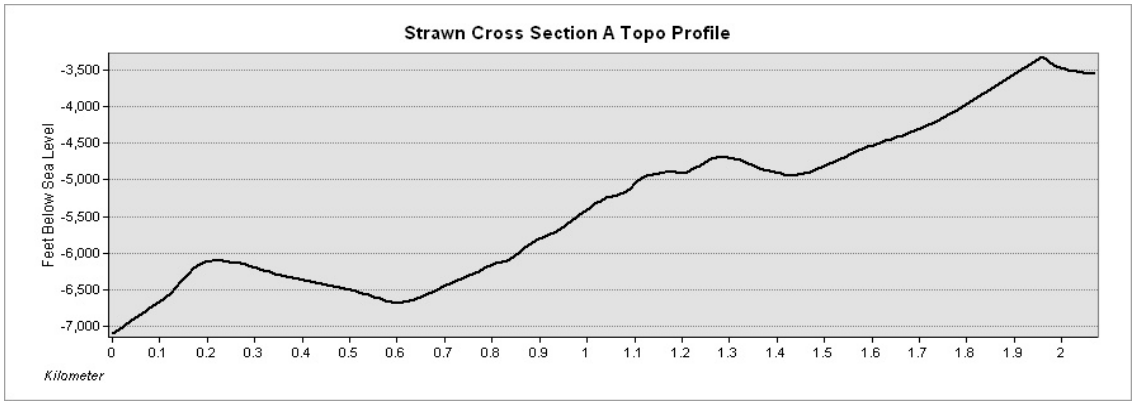


Description: -- The topographic profile of the Strawn Chronostratigraphic map along cross section A. The points of flexure on the Strawn surface were easier to identify, and therefore use to construct a quantitative shelf edge. The x-axis distance along the cross section is measured in tens of kilometers, e.g. .20=20 kilometers. The y-axis represents thousands of feet below sea level. Shallower sub-sea depths represent the top of the y-axis, and deeper sub-sea depths represent the bottom of the y-axis.

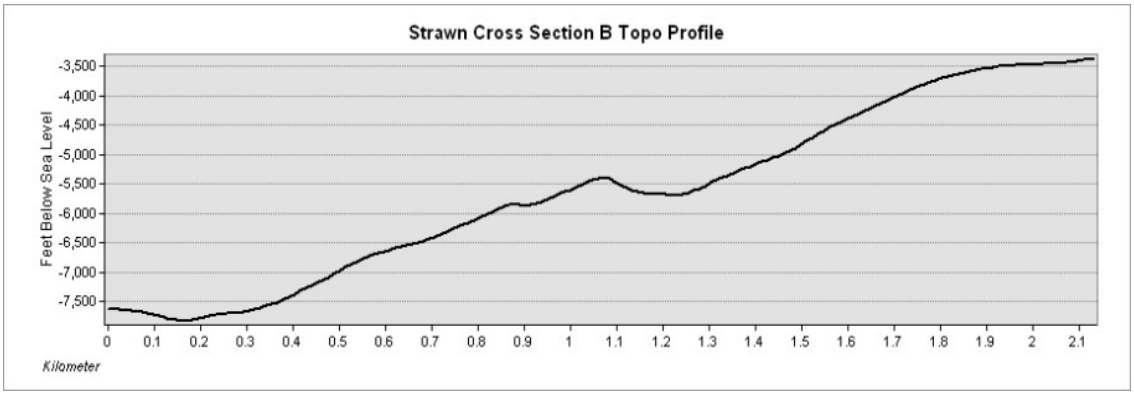


Description: -- The topographic profile of the Strawn Chronostratigraphic map along cross section B. The points of flexure on the Strawn surface were easier to identify, and therefore use to construct a quantitative shelf edge. The x-axis distance along the cross section is measured in tens of kilometers, e.g. .20=20 kilometers. The y-axis represents thousands of feet below sea level. Shallower sub-sea depths represent the top of the y-axis, and deeper sub-sea depths represent the bottom of the y-axis.

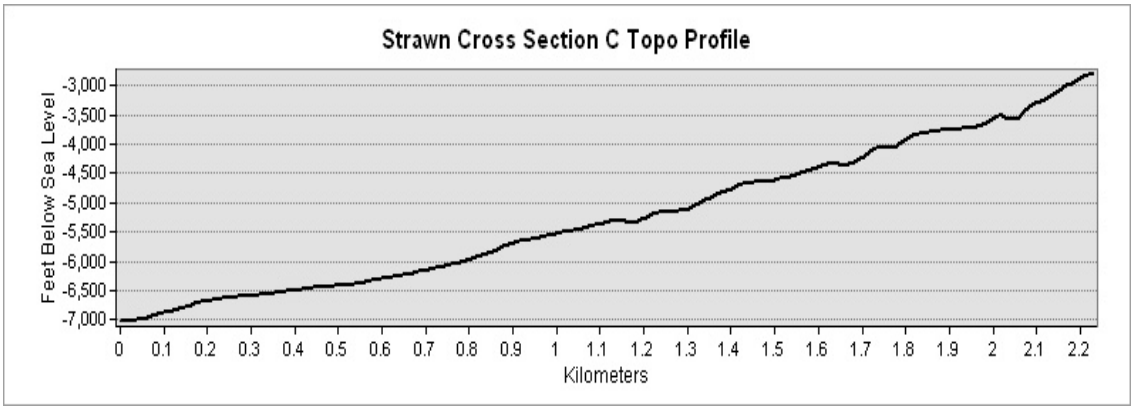


Description: -- The topographic profile of the Strawn Chronostratigraphic map along cross section C. The points of flexure on the Strawn surface were easier to identify, and therefore use to construct a quantitative shelf edge. The x-axis distance along the cross section is measured in tens of kilometers, e.g. .20=20 kilometers. The y-axis represents thousands of feet below sea level. Shallower sub-sea depths represent the top of the y-axis, and deeper sub-sea depths represent the bottom of the y-axis.

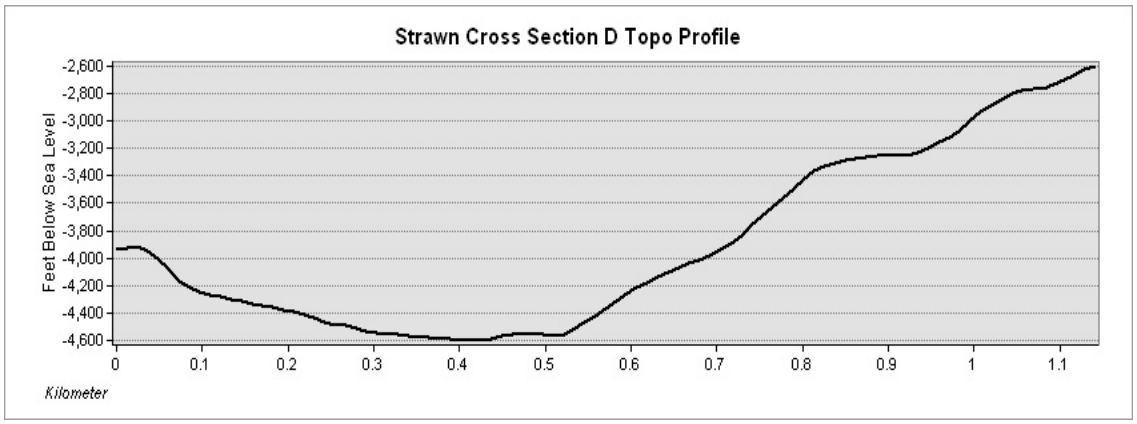


Description: -- The topographic profile of the Strawn Chronostratigraphic map along cross section D. The points of flexure on the Strawn surface were easier to identify, and therefore use to construct a quantitative shelf edge. The x-axis distance along the cross section is measured in tens of kilometers, e.g. .20=20 kilometers. The y-axis represents thousands of feet below sea level. Shallower sub-sea depths represent the top of the y-axis, and deeper sub-sea depths represent the bottom of the y-axis.

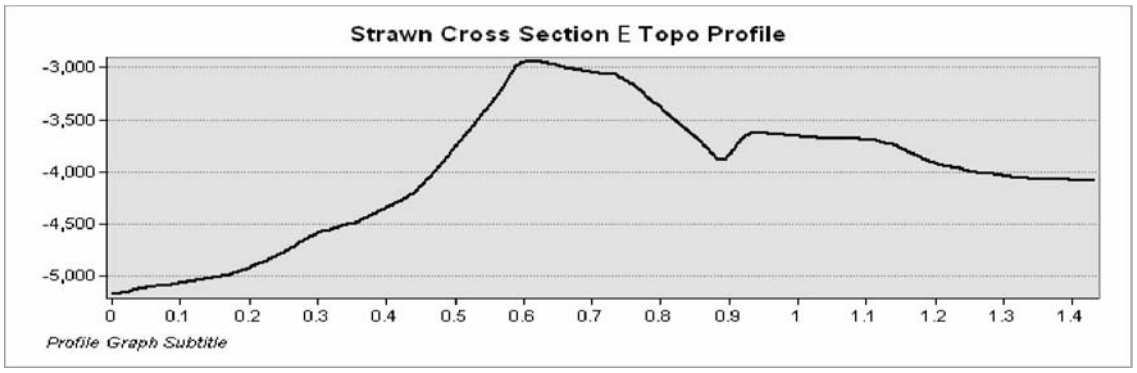


Description: -- The topographic profile of the Strawn Chronostratigraphic map along cross section E. The points of flexure on the Strawn surface were easier to identify, and therefore use to construct a quantitative shelf edge. The x-axis distance along the cross section is measured in tens of kilometers, e.g. .20=20 kilometers. The y-axis represents thousands of feet below sea level. Shallower sub-sea depths represent the top of the y-axis, and deeper sub-sea depths represent the bottom of the y-axis.

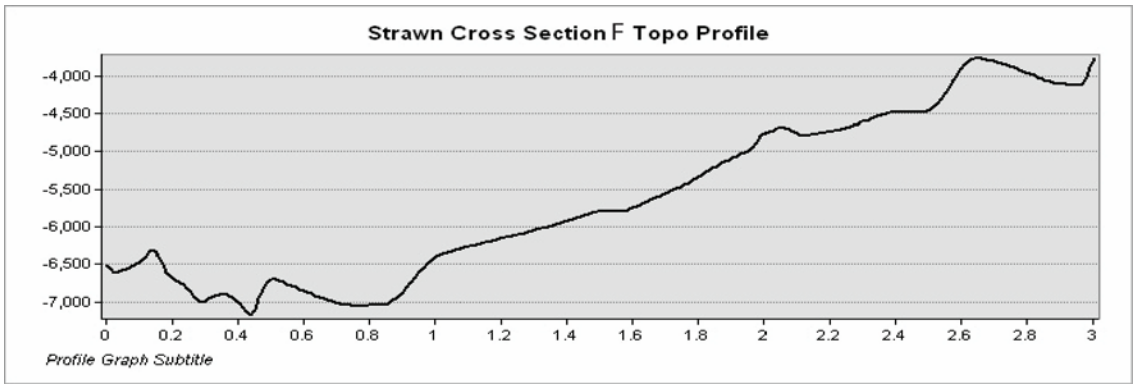


Description: -- The topographic profile of the Strawn Chronostratigraphic map along cross section F. The points of flexure on the Strawn surface were easier to identify, and therefore use to construct a quantitative shelf edge. The x-axis distance along the cross section is measured in tens of kilometers, e.g. .20=20 kilometers. The y-axis represents thousands of feet below sea level. Shallower sub-sea depths represent the top of the y-axis, and deeper sub-sea depths represent the bottom of the y-axis.

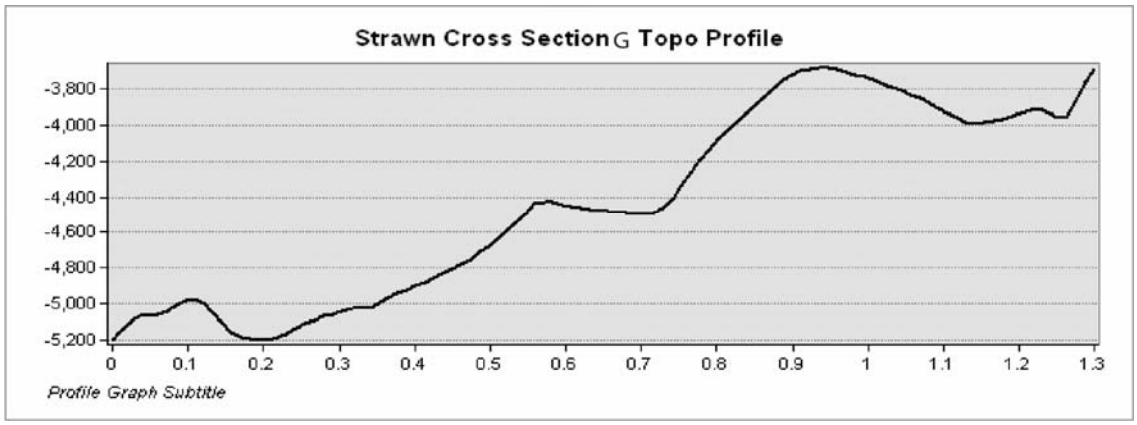


Description: -- The topographic profile of the Strawn Chronostratigraphic map along cross section G. The points of flexure on the Strawn surface were easier to identify, and therefore use to construct a quantitative shelf edge. The x-axis distance along the cross section is measured in tens of kilometers, e.g. .20=20 kilometers. The y-axis represents thousands of feet below sea level. Shallower sub-sea depths represent the top of the y-axis, and deeper sub-sea depths represent the bottom of the y-axis.

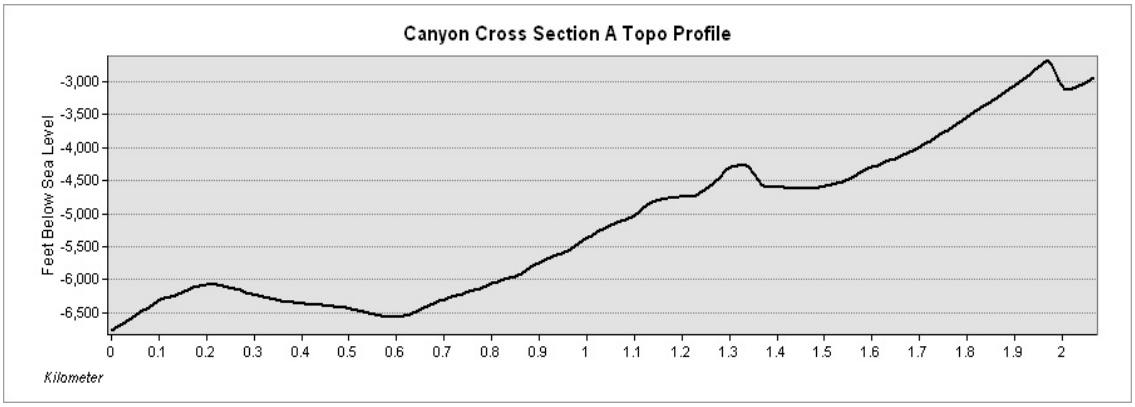


Description: -- The topographic profile of the Canyon Chronostratigraphic map along cross section A. The points of flexure on the Canyon surface were easier to identify, and therefore use to construct a quantitative shelf edge. The x-axis distance along the cross section is measured in tens of kilometers, e.g. .20=20 kilometers. The y-axis represents thousands of feet below sea level. Shallower sub-sea depths represent the top of the y-axis, and deeper sub-sea depths represent the bottom of the y-axis.

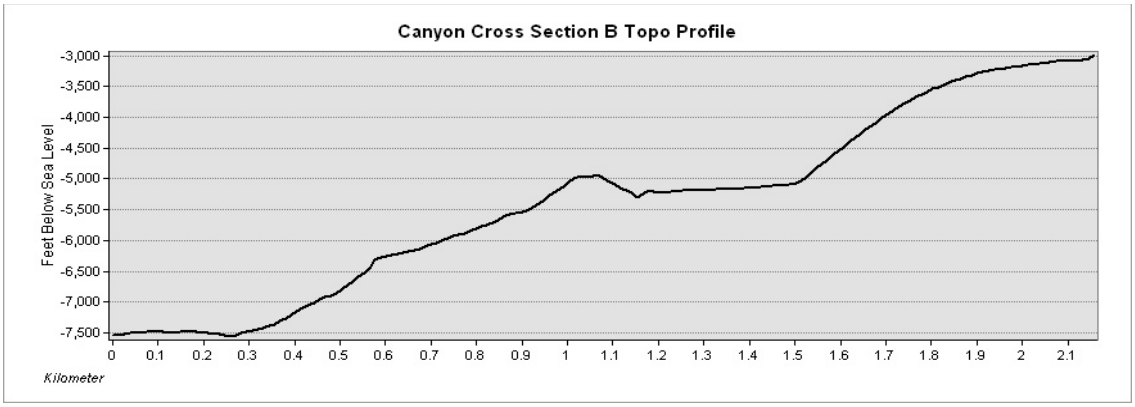


Description: -- The topographic profile of the Canyon Chronostratigraphic map along cross section B. The points of flexure on the Canyon surface were easier to identify, and therefore use to construct a quantitative shelf edge. The x-axis distance along the cross section is measured in tens of kilometers, e.g. .20=20 kilometers. The y-axis represents thousands of feet below sea level. Shallower sub-sea depths represent the top of the y-axis, and deeper sub-sea depths represent the bottom of the y-axis.

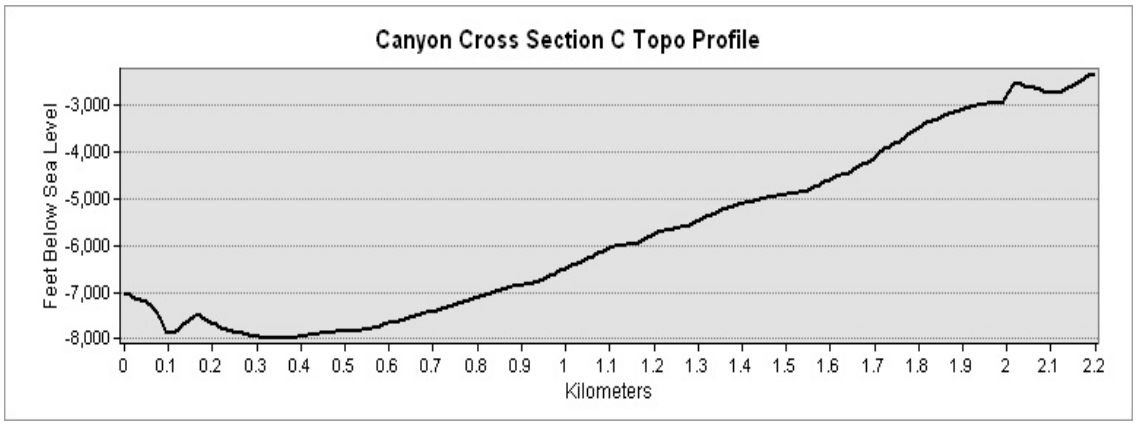


Description: -- The topographic profile of the Canyon Chronostratigraphic map along cross section C. The points of flexure on the Canyon surface were easier to identify, and therefore use to construct a quantitative shelf edge. The x-axis distance along the cross section is measured in tens of kilometers, e.g. .20=20 kilometers. The y-axis represents thousands of feet below sea level. Shallower sub-sea depths represent the top of the y-axis, and deeper sub-sea depths represent the bottom of the y-axis.

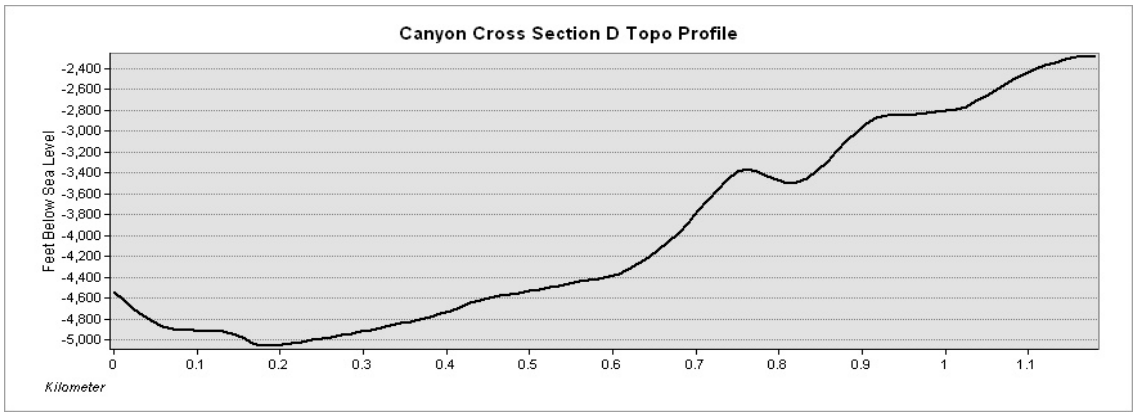


Description: -- The topographic profile of the Canyon Chronostratigraphic map along cross section D. The points of flexure on the Canyon surface were easier to identify, and therefore use to construct a quantitative shelf edge. The x-axis distance along the cross section is measured in tens of kilometers, e.g. .20=20 kilometers. The y-axis represents thousands of feet below sea level. Shallower sub-sea depths represent the top of the y-axis, and deeper sub-sea depths represent the bottom of the y-axis.

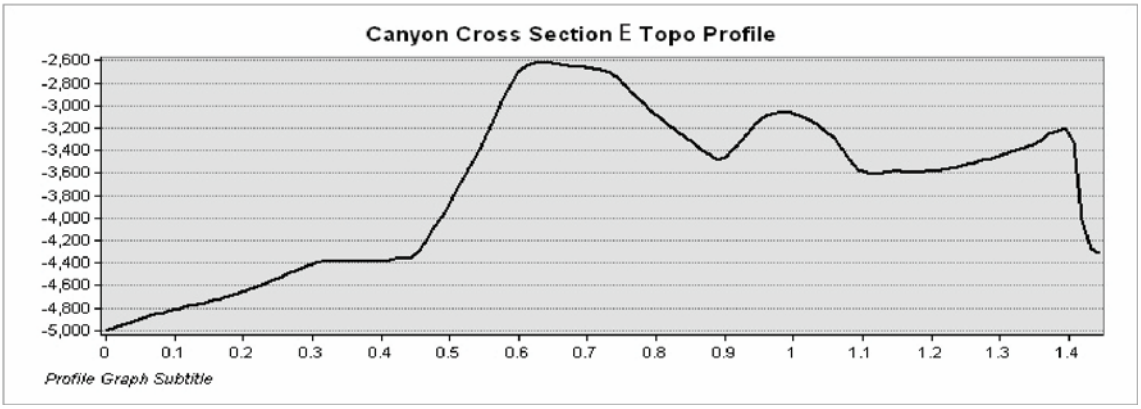


Description: -- The topographic profile of the Canyon Chronostratigraphic map along cross section E. The points of flexure on the Canyon surface were easier to identify, and therefore use to construct a quantitative shelf edge. The x-axis distance along the cross section is measured in tens of kilometers, e.g. .20=20 kilometers. The y-axis represents thousands of feet below sea level. Shallower sub-sea depths represent the top of the y-axis, and deeper sub-sea depths represent the bottom of the y-axis.

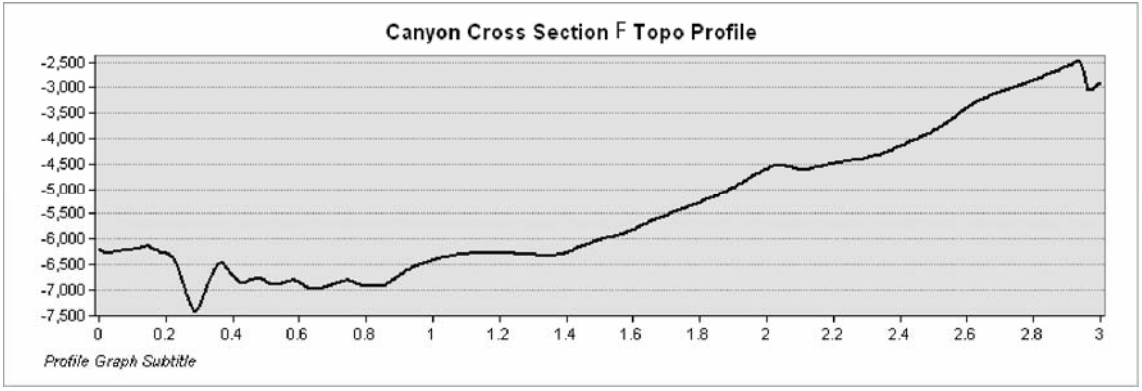


Description: -- The topographic profile of the Canyon Chronostratigraphic map along cross section F. The points of flexure on the Canyon surface were easier to identify, and therefore use to construct a quantitative shelf edge. The x-axis distance along the cross section is measured in tens of kilometers, e.g. .20=20 kilometers. The y-axis represents thousands of feet below sea level. Shallower sub-sea depths represent the top of the y-axis, and deeper sub-sea depths represent the bottom of the y-axis.

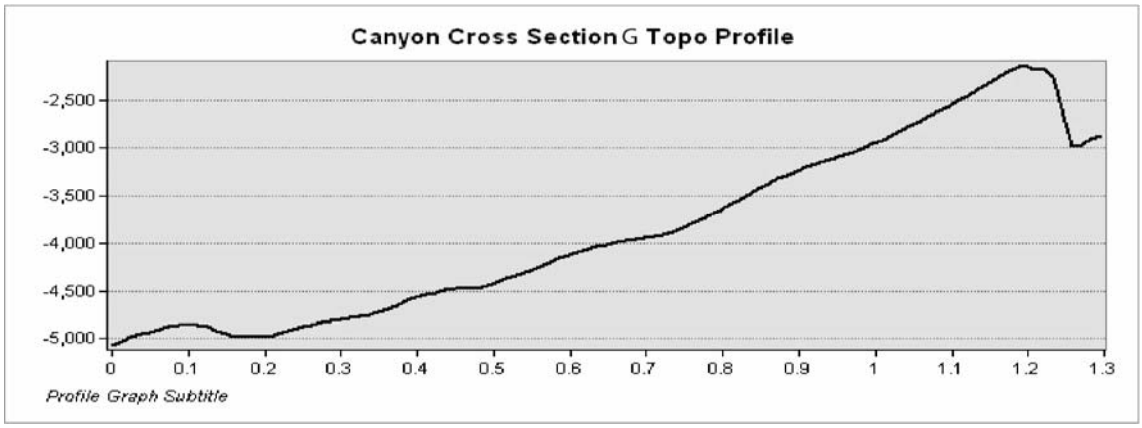


Description: -- The topographic profile of the Canyon Chronostratigraphic map along cross section G. The points of flexure on the Canyon surface were easier to identify, and therefore use to construct a quantitative shelf edge. The x-axis distance along the cross section is measured in tens of kilometers, e.g. .20=20 kilometers. The y-axis represents thousands of feet below sea level. Shallower sub-sea depths represent the top of the y-axis, and deeper sub-sea depths represent the bottom of the y-axis.

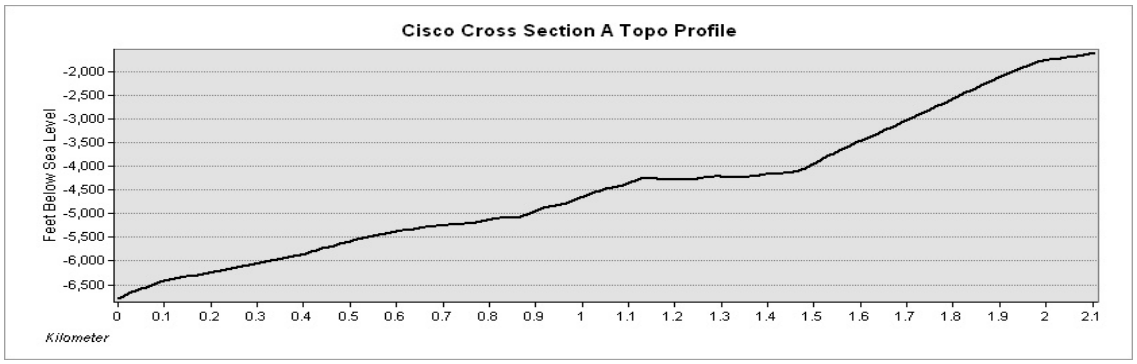


Description: -- The topographic profile of the Cisco Chronostratigraphic map along cross section A. The points of flexure on the Cisco surface were easier to identify, and therefore use to construct a quantitative shelf edge. The x-axis distance along the cross section is measured in tens of kilometers, e.g. .20=20 kilometers. The y-axis represents thousands of feet below sea level. Shallower sub-sea depths represent the top of the y-axis, and deeper sub-sea depths represent the bottom of the y-axis.

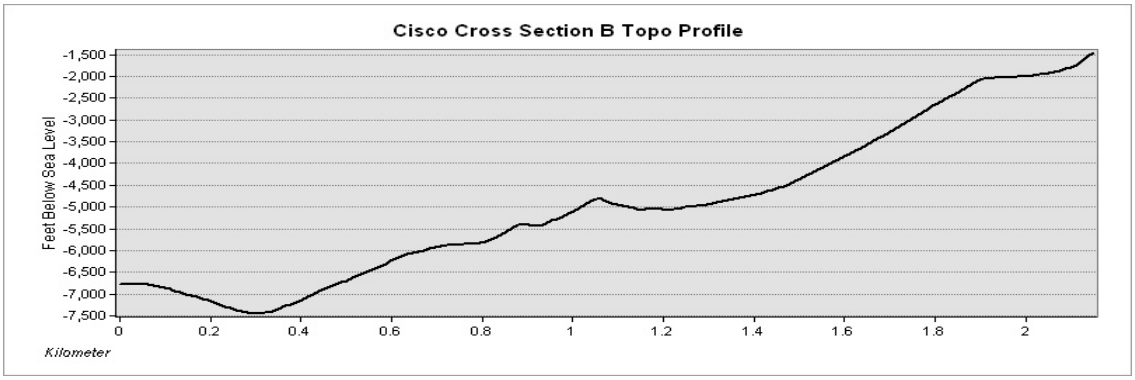


Description: -- The topographic profile of the Cisco Chronostratigraphic map along cross section B. The points of flexure on the Cisco surface were easier to identify, and therefore use to construct a quantitative shelf edge. The x-axis distance along the cross section is measured in tens of kilometers, e.g. .20=20 kilometers. The y-axis represents thousands of feet below sea level. Shallower sub-sea depths represent the top of the y-axis, and deeper sub-sea depths represent the bottom of the y-axis.

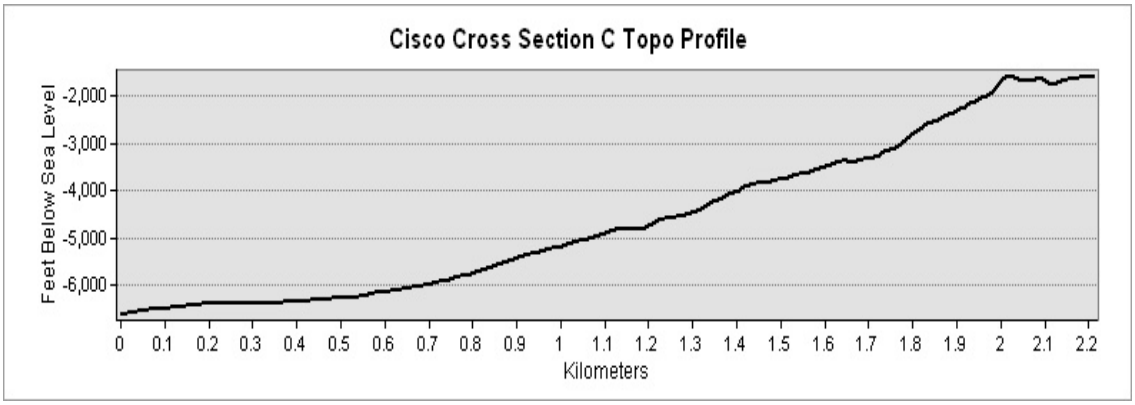


Description: -- The topographic profile of the Cisco Chronostratigraphic map along cross section C. The points of flexure on the Cisco surface were easier to identify, and therefore use to construct a quantitative shelf edge. The x-axis distance along the cross section is measured in tens of kilometers, e.g. .20=20 kilometers. The y-axis represents thousands of feet below sea level. Shallower sub-sea depths represent the top of the y-axis, and deeper sub-sea depths represent the bottom of the y-axis.

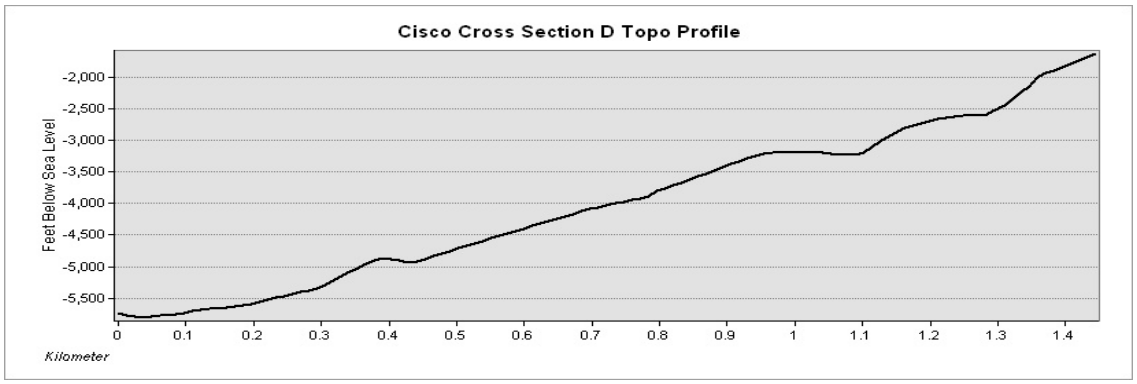


Description: -- The topographic profile of the Cisco Chronostratigraphic map along cross section D. The points of flexure on the Cisco surface were easier to identify, and therefore use to construct a quantitative shelf edge. The x-axis distance along the cross section is measured in tens of kilometers, e.g. .20=20 kilometers. The y-axis represents thousands of feet below sea level. Shallower sub-sea depths represent the top of the y-axis, and deeper sub-sea depths represent the bottom of the y-axis.

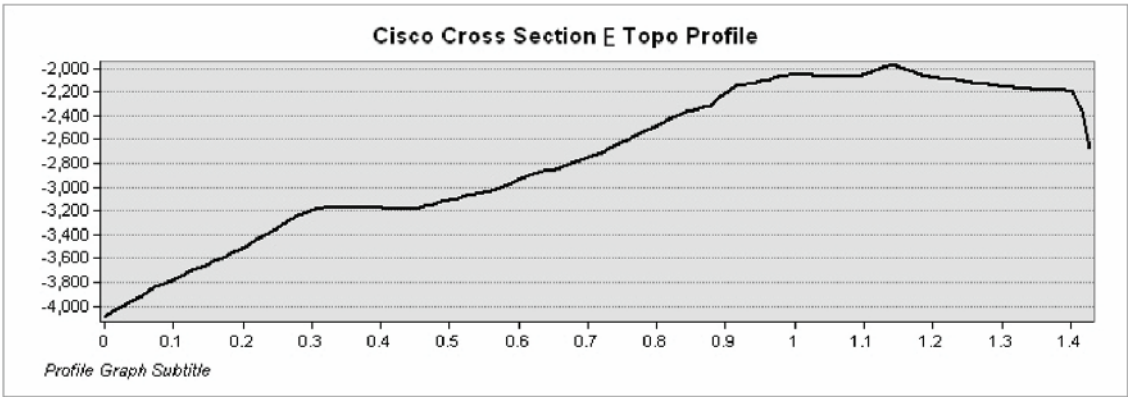


Description: -- The topographic profile of the Cisco Chronostratigraphic map along cross section E. The points of flexure on the Cisco surface were easier to identify, and therefore use to construct a quantitative shelf edge. The x-axis distance along the cross section is measured in tens of kilometers, e.g. .20=20 kilometers. The y-axis represents thousands of feet below sea level. Shallower sub-sea depths represent the top of the y-axis, and deeper sub-sea depths represent the bottom of the y-axis.

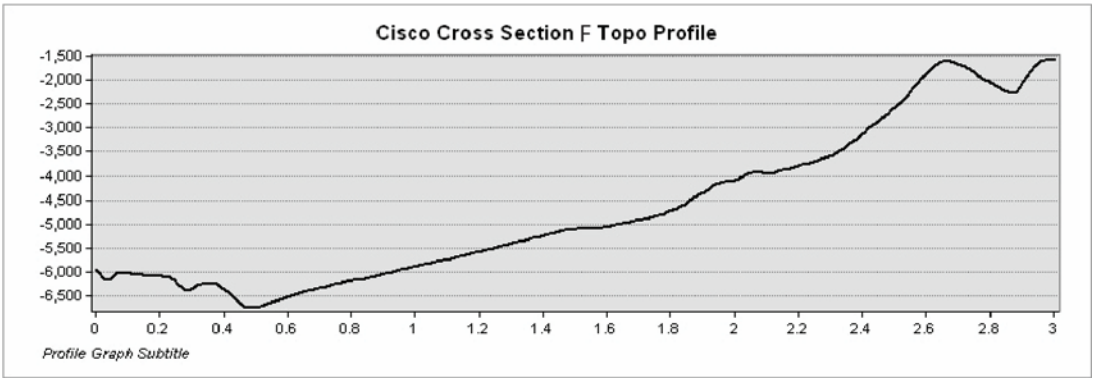


Description: -- The topographic profile of the Cisco Chronostratigraphic map along cross section F. The points of flexure on the Cisco surface were easier to identify, and therefore use to construct a quantitative shelf edge. The x-axis distance along the cross section is measured in tens of kilometers, e.g. .20=20 kilometers. The y-axis represents thousands of feet below sea level. Shallower sub-sea depths represent the top of the y-axis, and deeper sub-sea depths represent the bottom of the y-axis.

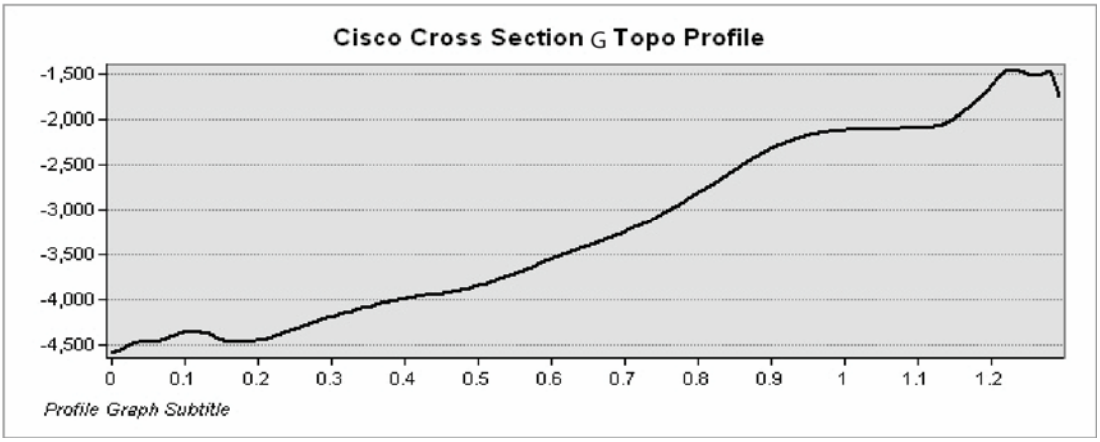


Description: -- The topographic profile of the Cisco Chronostratigraphic map along cross section G. The points of flexure on the Cisco surface were easier to identify, and therefore use to construct a quantitative shelf edge. The x-axis distance along the cross section is measured in tens of kilometers, e.g. .20=20 kilometers. The y-axis represents thousands of feet below sea level. Shallower sub-sea depths represent the top of the y-axis, and deeper sub-sea depths represent the bottom of the y-axis.

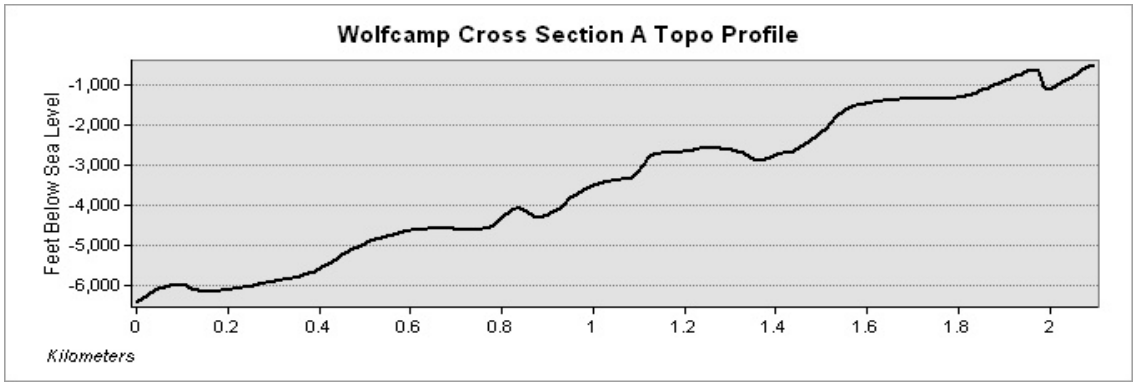


Description: -- The topographic profile of the Wolfcamp Chronostratigraphic map along cross section A. The points of flexure on the Wolfcamp surface were easier to identify, and therefore use to construct a quantitative shelf edge. The x-axis distance along the cross section is measured in tens of kilometers, e.g. .20=20 kilometers. The y-axis represents thousands of feet below sea level. Shallower sub-sea depths represent the top of the y-axis, and deeper sub-sea depths represent the bottom of the y-axis.

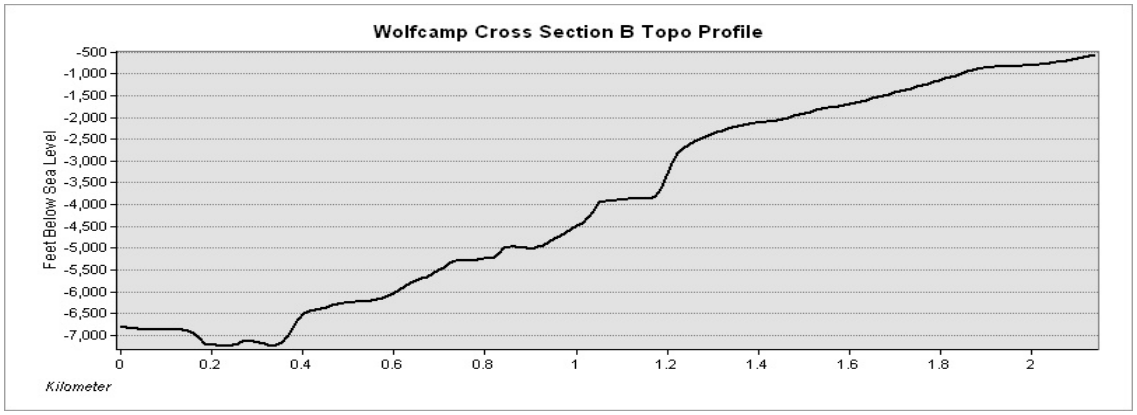


Description: -- The topographic profile of the Wolfcamp Chronostratigraphic map along cross section B. The points of flexure on the Wolfcamp surface were easier to identify, and therefore use to construct a quantitative shelf edge. The x-axis distance along the cross section is measured in tens of kilometers, e.g. .20=20 kilometers. The y-axis represents thousands of feet below sea level. Shallower sub-sea depths represent the top of the y-axis, and deeper sub-sea depths represent the bottom of the y-axis.

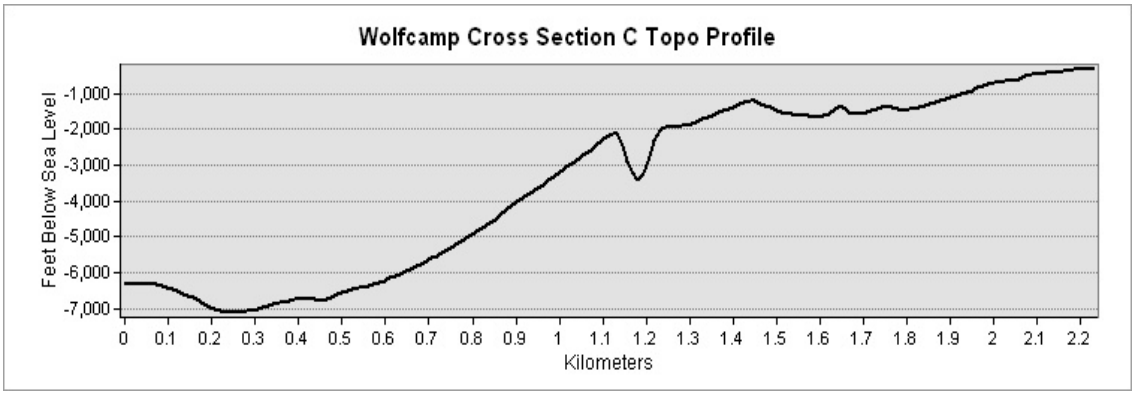


Description: -- The topographic profile of the Wolfcamp Chronostratigraphic map along cross section C. The points of flexure on the Wolfcamp surface were easier to identify, and therefore use to construct a quantitative shelf edge. The x-axis distance along the cross section is measured in tens of kilometers, e.g. .20=20 kilometers. The y-axis represents thousands of feet below sea level. Shallower sub-sea depths represent the top of the y-axis, and deeper sub-sea depths represent the bottom of the y-axis.

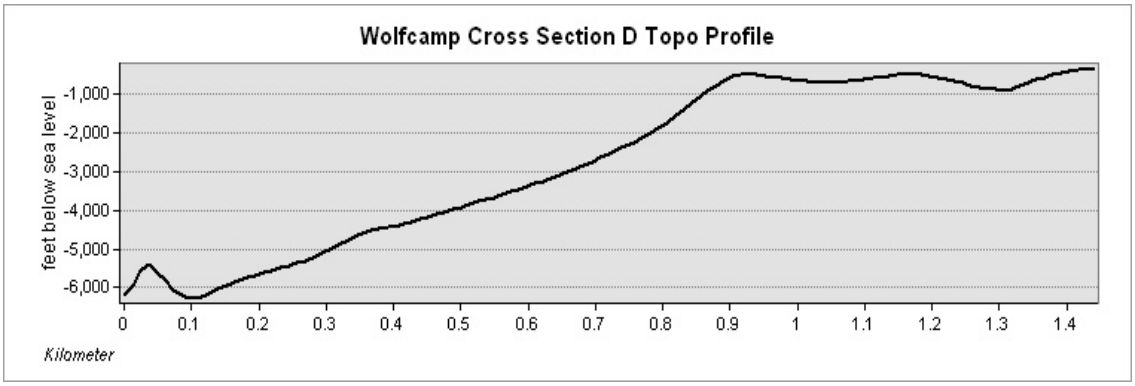


Description: -- The topographic profile of the Wolfcamp Chronostratigraphic map along cross section D. The points of flexure on the Wolfcamp surface were easier to identify, and therefore use to construct a quantitative shelf edge. The x-axis distance along the cross section is measured in tens of kilometers, e.g. .20=20 kilometers. The y-axis represents thousands of feet below sea level. Shallower sub-sea depths represent the top of the y-axis, and deeper sub-sea depths represent the bottom of the y-axis.

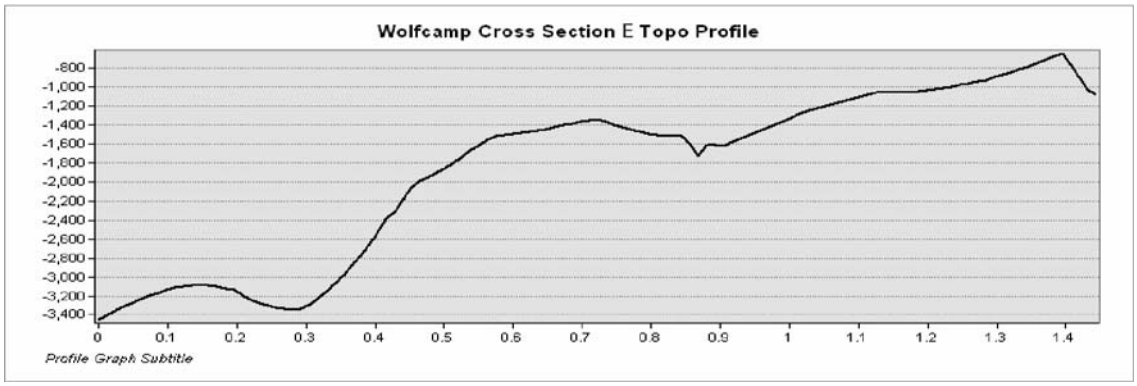


Description: -- The topographic profile of the Wolfcamp Chronostratigraphic map along cross section E. The points of flexure on the Wolfcamp surface were easier to identify, and therefore use to construct a quantitative shelf edge. The x-axis distance along the cross section is measured in tens of kilometers, e.g. .20=20 kilometers. The y-axis represents thousands of feet below sea level. Shallower sub-sea depths represent the top of the y-axis, and deeper sub-sea depths represent the bottom of the y-axis.

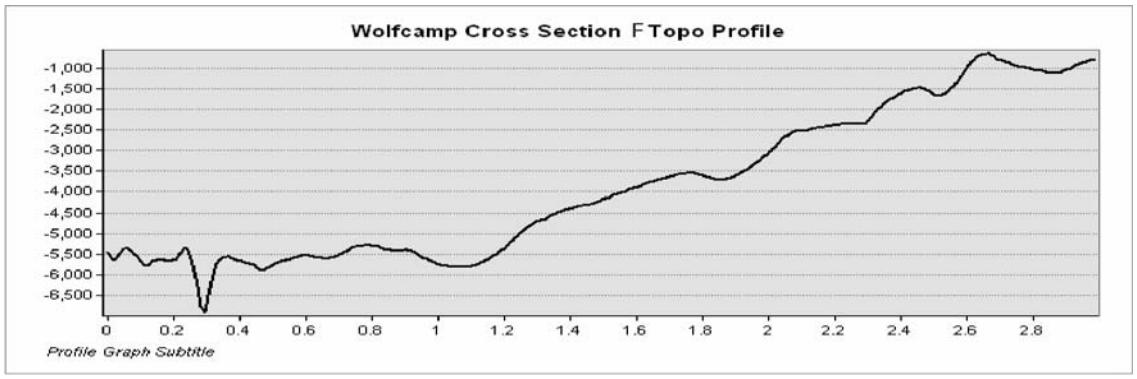


Description: -- The topographic profile of the Wolfcamp Chronostratigraphic map along cross section F. The points of flexure on the Wolfcamp surface were easier to identify, and therefore use to construct a quantitative shelf edge. The x-axis distance along the cross section is measured in tens of kilometers, e.g. .20=20 kilometers. The y-axis represents thousands of feet below sea level. Shallower sub-sea depths represent the top of the y-axis, and deeper sub-sea depths represent the bottom of the y-axis.

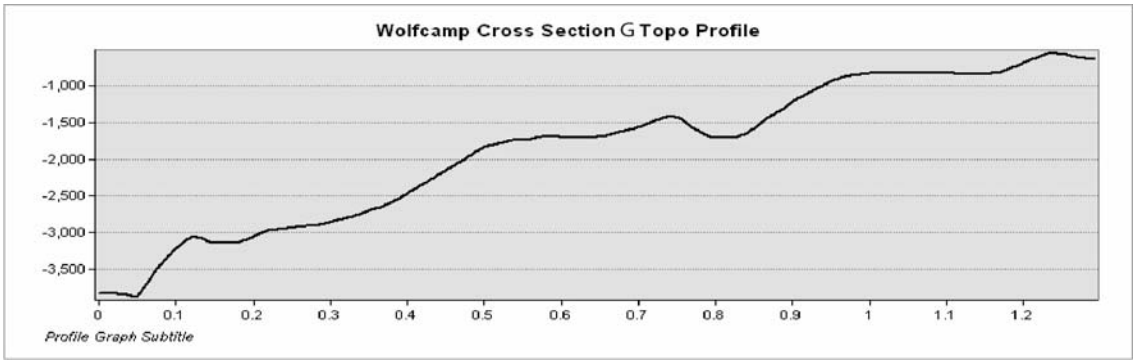


Description: -- The topographic profile of the Wolfcamp Chronostratigraphic map along cross section G. The points of flexure on the Wolfcamp surface were easier to identify, and therefore use to construct a quantitative shelf edge. The x-axis distance along the cross section is measured in tens of kilometers, e.g. .20=20 kilometers. The y-axis represents thousands of feet below sea level. Shallower sub-sea depths represent the top of the y-axis, and deeper sub-sea depths represent the bottom of the y-axis.

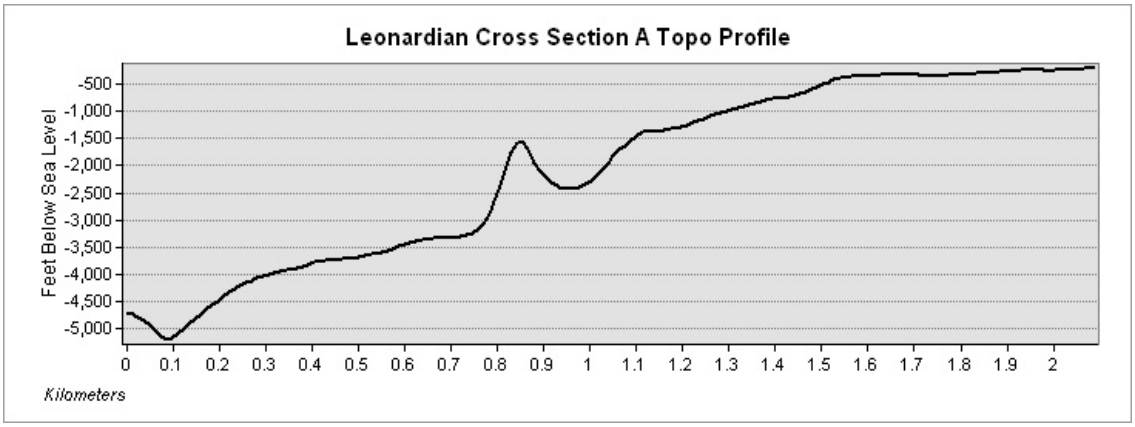


Description: -- The topographic profile of the Leonard Chronostratigraphic map along cross section A. The points of flexure on the Leonard surface were easier to identify, and therefore use to construct a quantitative shelf edge. The x-axis distance along the cross section is measured in tens of kilometers, e.g. .20=20 kilometers. The y-axis represents thousands of feet below sea level. Shallower sub-sea depths represent the top of the y-axis, and deeper sub-sea depths represent the bottom of the y-axis.

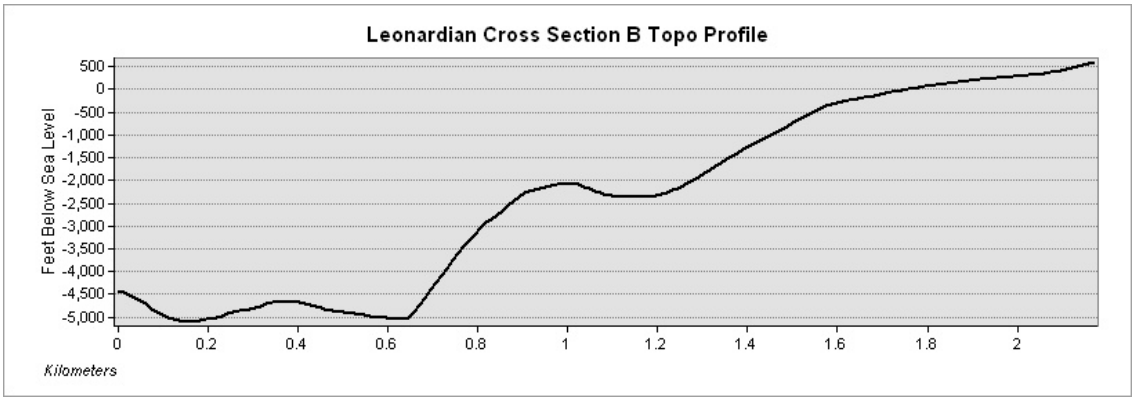


Description: -- The topographic profile of the Leonard Chronostratigraphic map along cross section B. The points of flexure on the Leonard surface were easier to identify, and therefore use to construct a quantitative shelf edge. The x-axis distance along the cross section is measured in tens of kilometers, e.g. .20=20 kilometers. The y-axis represents thousands of feet below sea level. Shallower sub-sea depths represent the top of the y-axis, and deeper sub-sea depths represent the bottom of the y-axis.

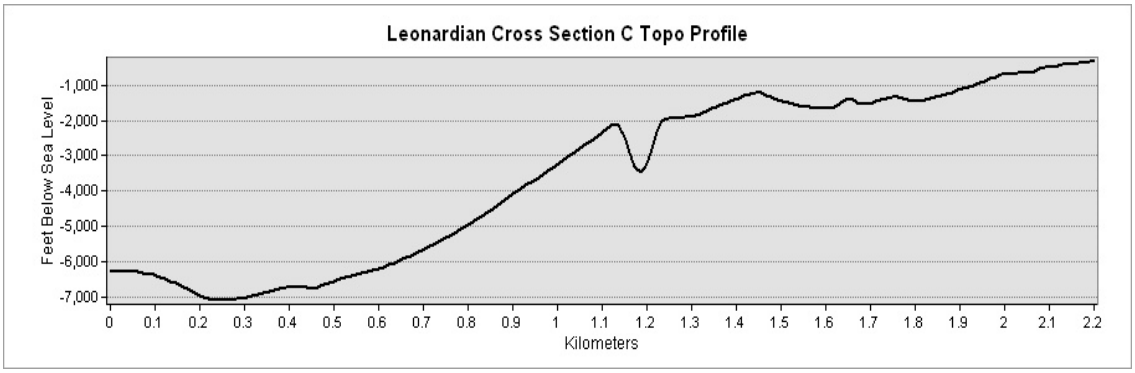


Description: -- The topographic profile of the Leonard Chronostratigraphic map along cross section C. The points of flexure on the Leonard surface were easier to identify, and therefore use to construct a quantitative shelf edge. The x-axis distance along the cross section is measured in tens of kilometers, e.g. .20=20 kilometers. The y-axis represents thousands of feet below sea level. Shallower sub-sea depths represent the top of the y-axis, and deeper sub-sea depths represent the bottom of the y-axis.

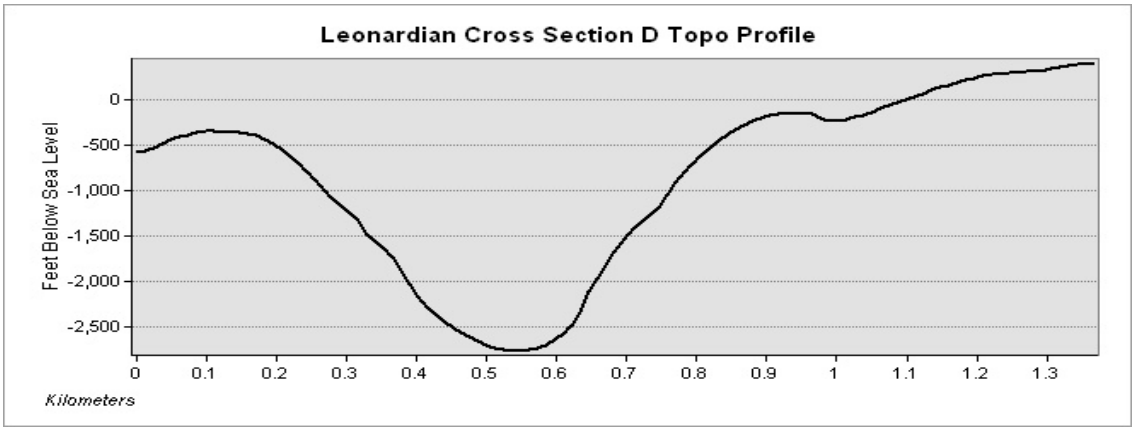


Description: -- The topographic profile of the Leonard Chronostratigraphic map along cross section D. The points of flexure on the Leonard surface were easier to identify, and therefore use to construct a quantitative shelf edge. The x-axis distance along the cross section is measured in tens of kilometers, e.g. .20=20 kilometers. The y-axis represents thousands of feet below sea level. Shallower sub-sea depths represent the top of the y-axis, and deeper sub-sea depths represent the bottom of the y-axis.

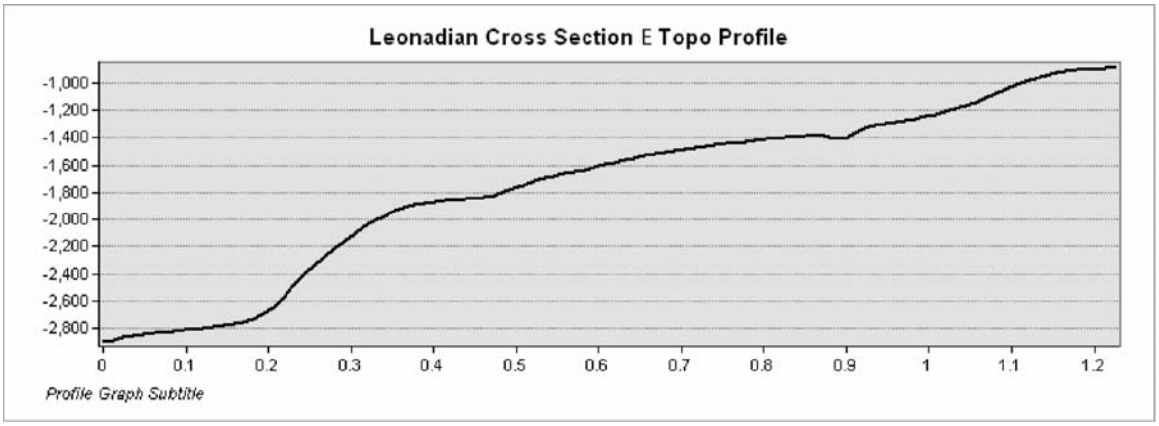


Description: -- The topographic profile of the Leonard Chronostratigraphic map along cross section E. The points of flexure on the Leonard surface were easier to identify, and therefore use to construct a quantitative shelf edge. The x-axis distance along the cross section is measured in tens of kilometers, e.g. .20=20 kilometers. The y-axis represents thousands of feet below sea level. Shallower sub-sea depths represent the top of the y-axis, and deeper sub-sea depths represent the bottom of the y-axis.

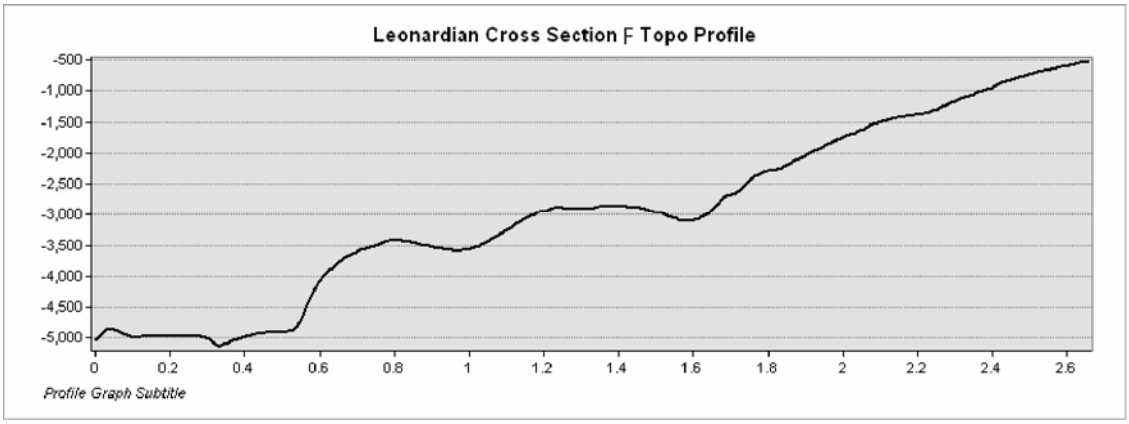


Description: -- The topographic profile of the Leonard Chronostratigraphic map along cross section F. The points of flexure on the Leonard surface were easier to identify, and therefore use to construct a quantitative shelf edge. The x-axis distance along the cross section is measured in tens of kilometers, e.g. .20=20 kilometers. The y-axis represents thousands of feet below sea level. Shallower sub-sea depths represent the top of the y-axis, and deeper sub-sea depths represent the bottom of the y-axis.

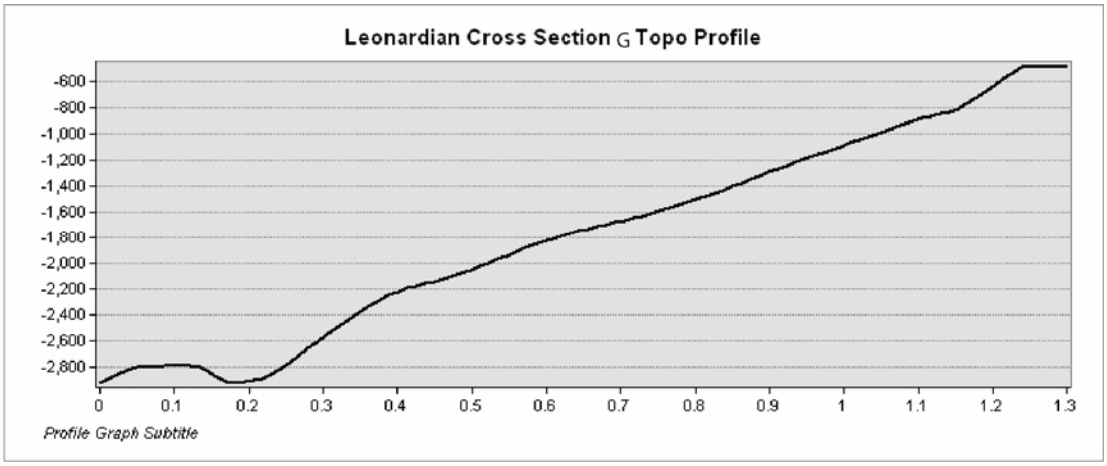


Description: -- The topographic profile of the Leonard Chronostratigraphic map along cross section G. The points of flexure on the Leonard surface were easier to identify, and therefore use to construct a quantitative shelf edge. The x-axis distance along the cross section is measured in tens of kilometers, e.g. .20=20 kilometers. The y-axis represents thousands of feet below sea level. Shallower sub-sea depths represent the top of the y-axis, and deeper sub-sea depths represent the bottom of the y-axis.